Development of a Numerical Model of Piston Secondary Motion for Internal Combustion Engines

by

Conor P. McNally

B.E. Mechanical Engineering
University College Dublin, Ireland
(1998)

Submitted to the Department of Mechanical Engineering
in Partial Fulfillment of the Requirements for the Degree of
Master of Science in Mechanical Engineering

at the

MASSACHUSETTS INSTITUTE OF TECHNOLOGY

May 2000
[June 2000]

Signature of Author _____
Department of Mechanical Engineering
May 2000

Certified by _____
Dr. Tian Tian
Lecturer, Department of Mechanical Engineering
Thesis Supervisor

Accepted by _____
Ain A. Sonin
Chairman, Department Committee on Graduate Studies
Department of Mechanical Engineering

Development of a Numerical Model of Piston Secondary Motion for Internal Combustion Engines

By
Conor McNally

Submitted to the Department of Mechanical Engineering on
May 19th, 2000 in Partial Fulfillment of the Requirements
for the Degree of Master of Science in Mechanical Engineering

The reciprocating motion of the piston of an internal combustion engine in the vertical plane is referred to as its *primary* motion, and it is this primary motion that produces power in the engine. Due to the fact that there is a clearance between the piston and the liner, and that certain forces on the piston have components in the horizontal direction, there exists some lateral motion of the piston and also some rotational motion about the wrist pin axis. This motion is referred to as *secondary* motion. Secondary motion has significant implications for oil transport past the piston ring-pack, engine friction and engine noise. For these reasons a comprehensive numerical model of secondary motion is a valuable tool for engine designers and development engineers.

This work involves the development of a comprehensive and robust computer model of piston secondary motion, which can be easily run on a desktop computer. The model is applicable to both conventional mono-piston assemblies and also to articulated piston assemblies.

The modeling approach involves treating the piston assembly as a set of independent rigid bodies, and formulating and solving the equations of motion for each body. The hydrodynamic skirt-liner interaction force is computed by solving the Reynolds equation for the oil film and integrating the computed pressure. This essentially one dimensional calculation is performed at several circumfrential locations on the piston, and the results are integrated to yield a single force in the main thrust-anti thrust direction. The model is first developed with a basic form of this hydrodynamic calculation, which is later improved to include a solution for the wetted region and a complete pressure distribution on the piston. Results using both forms of the model are compared and analyzed, and the final model is used to perform several parametric studies involving various engine operating parameters.

Thesis Supervisors :

Dr. Tian Tian
Lecturer, Department of Mechanical Engineering

Dr. Victor W. Wong
Lecturer, Department of Mechanical Engineering

Acknowledgements

First and foremost I would like to thank my thesis supervisor Dr. Tian Tian. I consider myself extremely fortunate to have had Tian as my supervisor during my time here at MIT. His keen understanding of physical and mathematical modeling and his enthusiasm have been the driving forces behind this project. But perhaps more importantly, Tian has seemed more like a friend than a supervisor throughout the time we have worked together. He has always been approachable and willing to give up his time to help me deal with the various problems encountered along the way. I have the utmost respect and admiration for Tian, both personally and professionally. Further thanks are due to the members of the Consortium on Lubrication in Internal Combustion Engines who have funded this project : Volvo, PSA (Peugeot Citroen), Renault, Dana Perfect Circle and Mahle.

I would like to thank Dr. Victor Wong for his help throughout the project and for bringing me to MIT in the first place. Leslie Regan also deserves a special thanks for her continued support and help dealing with the M.E. department. I would also like to thank Benoist Thirouard for his help and advice with various aspects of the model. Both Ertan Yilmaz and Gerald Chamarre provided valuable input data for the model, as well as very helpful advice. Chris O'Brien was a continual source of help with programming issues, and his input was greatly appreciated. I would further like to thank my friends Rik Waero and Cornelius O'Sullivan at the Sloan lab for their help, advice and encouragement. Indeed, all my colleagues at the Sloan Lab need to be thanked for making my time here both enjoyable and fulfilling - they include ; Matt Rublewski, Jim Cowart, Brian Hallgren, Gary Landsberg, Brigette Castaing, Ioannis Kitsopanidis, Ferran Ayala and Martin Kostom

Finally I would like to thank my family and especially my parents for their continued encouragement and support , without which I would never have made it to MIT let alone managed to graduate.

Table of Contents

List of Figures

List of Tables

Chapter 1

Introduction

1.1 Background

The motion of the piston in an internal combustion engine can be separated into two distinct components - *primary* motion and *secondary* motion. Primary motion refers to the reciprocating motion of the piston in the vertical plane, and this motion is uniquely determined by the design data of the engine, i.e. the stroke, connecting rod length and the engine speed. Piston secondary motion consists of a translational motion perpendicular to the cylinder axis and a rotation about the wrist pin axis. During the operating cycle of the engine certain moments and lateral forces are generated which act on the piston. It is these forces and moments, coupled with the fact that there is a small clearance between the piston and the cylinder, that result in secondary motion.

1.1.1 Motivation and Applications

Oil Consumption Modeling

The major motivation for this study is the effect that secondary motion has on the dynamics of the piston ring/liner (PRL) system. Complex models have been developed at the Sloan Automotive Laboratory which model the dynamics of the PRL system in an effort to predict engine oil consumption. In order to model the dynamics of the piston ring-pack, it is essential to have complete data on the dynamics of the piston itself, as it is the piston that houses the rings. In addition to this, the tilt of the piston greatly affects the nature of the interface between the rings and the liner, and this has a great impact on both the sealing ability of the rings and the wear patterns generated. Thus, a complete dynamic model of piston secondary motion is an essential input to the ring dynamics/oil consumption model, and it is for this reason that the current work was undertaken.

Engine Noise

Piston secondary motion has also been identified as the primary source of engine noise [1-2]*. As the piston moves through the combustion top dead center (TDC) position, the side force acting on the piston changes direction and increases in magnitude due the rise in cylinder pressure. This accelerates the piston laterally across the cylinder and it impacts against the liner wall. This phenomenon is known as "piston slap" and it excites the cylinder block, causing a large portion of the engine's audible noise. There are several approaches used to minimize piston slap by varying engine geometry and operating parameters. In order for these approaches to be successful, a good understanding of the dynamics behind the phenomenon is necessary, and hence a piston secondary motion model is a valuable tool for controlling and minimizing piston noise.

Engine Friction

It has been shown that a significant amount of engine frictional losses (20-30% of total engine friction) comes from the interaction between the skirt and the liner [3]. The skirt-liner axial friction force is one of the main outputs generated by a secondary motion model that incorporates a skirt hydrodynamic calculation. Thus, such a model will aid greatly in understanding and controlling this important component of engine friction.

1.1.2 Types of Automotive Piston

There are essentially two types of piston used in today's automotive engine that will be analyzed in this work.

Mono Piston

By far the most common, and the one used in all passenger car engines, is the *mono* piston. As the name suggests, the piston comprises one single component , which is

* Numbers in parentheses refer to references listed at the end of this report

usually made from aluminum. The upper part of the piston that supports the combustion force and holds the piston rings is called the *crown.* The lower part of the piston that supports the lateral forces against the liner walls is called the *skirt.* The piston is linked to the connecting rod via the *wrist pin* on which both components are hinged. An example of a mono piston assembly can be seen in Figure 1.1 below.

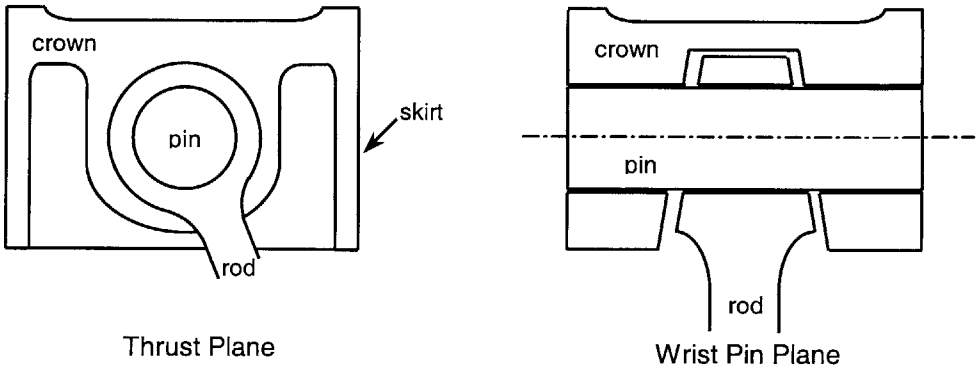

Figure 1.1 Schematic drawing of a Mono piston assembly

Articulated Piston

In some heavy duty diesel engines, due to the extremely high combustion temperatures and pressures, it is desirable to have a stainless steel crown section. However, an aluminum skirt is still preferable due to it's low weight and elasticity. Two components of different materials cannot be rigidly joined together in the piston, as their differing coefficients of expansion would lead to failure. Instead, articulated pistons comprise a stainless steel crown and an aluminum skirt which are separate components and are hinged separately on the wrist pin. An example of an articulated piston assembly can be seen in Figure 1.2 below.

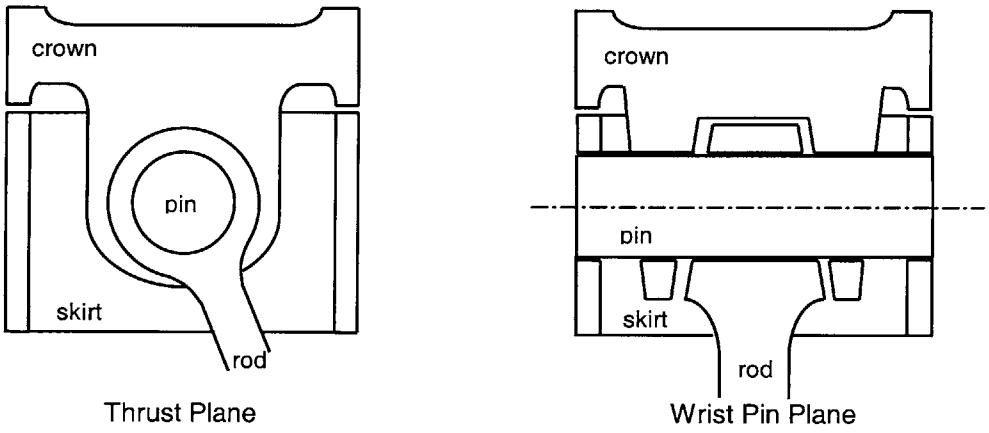

Figure 1.2 Schematic drawings of an articulated piston assembly

1.1.3 Characterization of Secondary motion

Secondary motion is most easily described in terms of the lateral displacement, ε, of the wrist pin axis from the center line of the cylinder, and the angular displacement, ϕ, of the piston from the vertical (for articulated pistons, there is a separate angular displacement variable for the skirt and the crown). The parameters ε and ϕ are shown in figure 1.3 .

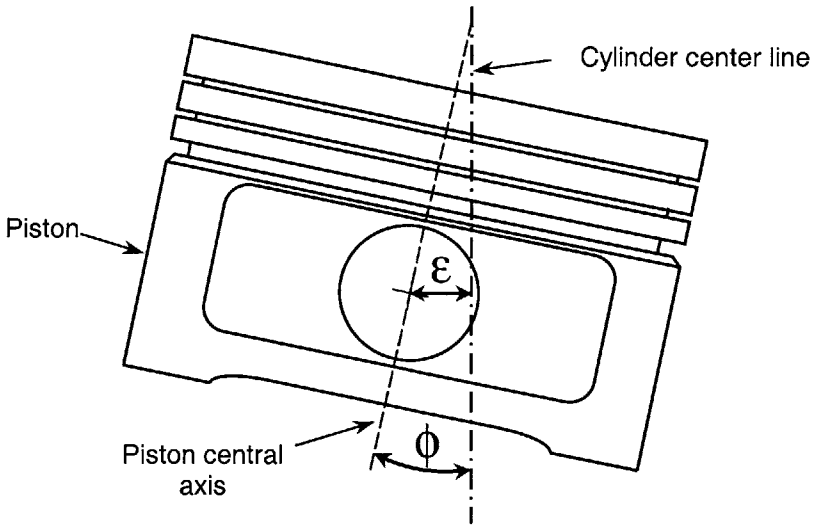

Figure 1.3 Parameters describing piston secondary motion

1.1.4 Factors Influencing Secondary Motion

The main factors influencing secondary motion can be divided into three categories, *forces*, *moments* and *geometry*.

Forces

The predominant driving force behind secondary motion is the lateral reaction force imparted on the skirt by the connecting rod (via the wrist pin). As the crankshaft rotates, and the orientation of the connecting rod moves away from the vertical, the reaction force between the rod and the pin develops a lateral component in addition to the pre-dominant vertical component. This lateral force component is transmitted through the wrist pin to the skirt, and tends to accelerate the skirt toward the liner. In opposition to this side force,

there is a retarding hydrodynamic force generated in the oil film between the skirt and the liner, and this force tends to decelerate the skirt. Lateral motion of the piston is thus driven by the side force from the connecting rod, and retarded or damped by the hydrodynamic force generated in the oil film.

Moments

There are several moments which influence the angular motion of the piston. When there is an offset between the c.g. of the piston and the bore centerline, the axial acceleration of the piston generates an inertial moment. A further moment is generated when the there is an offset between the pin axis center and the piston centerline (this is termed the "pin offset" and is often found in mono piston assemblies). In this situation, the gas pressure force acting down on the piston causes a moment about the pin axis. Due to the relative rotation of the piston (or both the crown and skirt in articulated pistons) and the wrist pin, a shear torque generated in the oil film which acts on the piston. In response to these driving moments, there is a hydrodynamic moment generated in the oil film between the skirt and the liner which tends to damp or retard the piston's angular motion. The magnitude of this moment is not only dependant on the hydrodynamic force in the oil film, but also on the distribution of this force. Since the majority of the hydrodynamic force is usually concentrated at the point of minimum oil film thickness, the location of this minimum point affects the hydrodynamic moment greatly.

Geometry

The motion of the piston is also greatly dependant on the geometry of the piston/liner system. The radial clearance between the skirt or crown and the liner determines how much lateral and angular motion can occur. The offsets of both the c.g. and the pin axis can cause moments to be generated on the system as described above. The profile of the skirt has a major impact on the distribution of the hydrodynamic forces in the oil film, and thus affects the magnitude of the hydrodynamic moments.

1.2 Previous Work on Modeling Secondary Motion

The first attempts at modeling piston secondary motion were made in the mid 1960's when Ungar and Ross [4] and Griffiths and Skorecki [5] published their work on the subject. These early models were relatively simple and looked only at the dynamics of the system, ignoring the hydrodynamic interaction between the skirt and liner. The first serious attempt at modeling secondary motion was by Li et al. [6] in 1982. This study treated the dynamics of the system in a relatively simple manner, combining the piston and wrist pin into a single lumped mass. The hydrodynamics of the skirt liner interface were considered, and the 1-D Reynolds equation was solved for the thrust and anti-thrust sides of the piston. The authors used the model to study the effects on the secondary dynamics of pin offset, clearance and oil viscosity. In 1982 Knoll and Peeken [7] took a more detailed look at the hydrodynamics of the skirt-liner interaction. They formulated and solved the full 2-D Reynolds equation for the oil film using a sophisticated finite element (FE) method. They assumed that the skirt was fully flooded with oil and didn't consider surface roughness or boundary lubrication. The model was limited to an analysis of the skirt-liner system and didn't attempt to model the dynamics. Another model that focused only on the skirt-liner hydrodynamics was presented by Oh, Li, and Goenka [8] in 1987. This model was significant in that it was the first to consider elastic deformation of the skirt. Such elastic deformation occurs on a scale comparable to the minimum oil film thickness and can greatly alter the hydrodynamics. The authors formulated and solved the full 2-D Reynolds equation in polar co-ordinates using a finite difference (FD) method. They assumed fully flooded conditions in the oil film. A finite element model of the piston was used to generate a deformation matrix. In order to solve the deformation and Reynolds equations simultaneously an iterative Newton-Raphson method was incorporated. A steady-state thermal deformation calculation was also included in the model. The authors concluded that elastic deformation of the skirt changed the operating profile considerably and had a significant effect on the hydrodynamic forces and moments produced.

A very complete model of secondary motion, including skirt hydrodynamics and deformation, was presented by Zhu et al. [9-10] in 1991. The authors used essentially the same formulation of the equations of motion as Li et al. [6]. They also presented a detailed analysis of the skirt elastohydrodynamics (hydrodynamics considering elastic deformation of the skirt), which took account of the detailed surface profiles of both the skirt and the liner. An 'averaged' Reynolds equation was formulated for the oil film which included several parameters determined by the surface roughness and waviness. This averaged Reynolds equation was solved concurrently with a deformation equation, again using an iterative Newton-Raphson technique. Similar to Oh, Li and Goenka [8], the authors found that elastic deformation of the skirt played a very important role in determining the hydrodynamic forces and moments, and went on to show the resulting effects on piston dynamics. A similar model was developed by Wong et al. [11] in 1994. In this model the authors used the 'averaged' Reynolds equation developed by Zhu et al. [9], and took the effects of skirt deformation into account. A finite difference method was used to solve the averaged Reynolds equation and the skirt was essentially considered to be fully flooded. The work in question focused at characterizing the relationship between piston slap and engine noise, and was accompanied by extensive secondary motion and vibration measurements on a single cylinder test engine [12].

The first attempt at modeling the dynamics of articulated pistons was presented by Keribar and Dursunkaya [13-14] in 1992. Each component of the articulated piston was treated as a separate component and the equations of motion developed for each. The resulting 10 degree of freedom system was solved in conjunction with the skirt elastohydrodynamic equations. The skirt hydrodynamics did not consider surface roughness and waviness parameters. While the skirt hydrodynamics were analyzed in detail, the hydrodynamics of the crown-liner interface was not considered. The authors determined that in order to fully solve the system equations, a hydrodynamic analysis of the various pin bearings was necessary.

1.3 Thesis Objectives

Of all the secondary motion models developed to date, only one has been applicable to articulated piston assemblies. This model failed to take the crown-liner hydrodynamics into account, and also used a complex and computationally intensive method of computing the skirt hydrodynamics. It is the objective of the present work to develop a complete model of piston secondary motion, for both mono and articulated pistons, that considers all the important physical phenomena, but that can be easily run on a desktop computer. To this end, the formulation of both the equations of motion and the skirt-liner and crown-liner hydrodynamics must be efficient, and lengthy and complex methods such as finite element and finite difference must be avoided. It is intended to formulate the model in such a way that the inclusion of skirt deformation and bore distortion can easily be incorporated at a later date.

Chapter 2

Model Development

2.1 Introduction

The general approach to modeling the dynamics of the system will be to treat each of the components as a separate rigid body. This multi-component approach recognizes the fact that the secondary motion of the piston (or skirt) is a result of the secondary motion of all the components in the system. The equations of motion are developed independently for each component in terms of the generalized degrees of freedom (axial, lateral and rotational). The side load on the assembly is not specified explicitly, rather it comes about as a result of the motion of the connecting rod and the gas pressure force. The only external variables specified as inputs are cylinder pressure and crank angle. The model is initially developed in this most general form to yield a flexible platform for future modifications and improvements. Simplifying assumptions are made along the way to yield a compact and efficient preliminary version of the model.

2.2 Equations of Motion

The equations of motion are developed for individual components in the system by considering inertia and all external forces and moments acting on each component. For conventional mono pistons the components comprise the piston, the pin and the rod. For articulated pistons the components are the crown, the skirt, the pin and the rod. As mentioned before, the degrees of freedom considered for secondary motion are lateral, axial and rotational. The axial component of secondary motion is not one that is considered in standard treatments of this subject, and indeed it is negligible compared to the primary axial motion. However, it is considered here to allow for the most generalized consideration of the motion, and it is necessary to formulate a comprehensive

set of motion equations. The symbol for the lateral component of the secondary motion is ε, and this is defined as the lateral displacement of the wrist pin bearing center of the component in question from the bore centerline. The axial component is represented by γ, and this is defined as the axial displacement of the wrist pin bearing center of the component in question from the *nominal wrist pin position.* This nominal wrist pin position is the position that the wrist pin center would occupy if there were no secondary motion of any of the components in the system. The symbol for the rotational component of secondary motion is ϕ, and this is defined as the angular displacement of the central axis of the component from the axial centerline of the bore. The equations of motion will be derived fully for the case of an articulated piston. A mono piston comprises a simpler version of the same system, and the derivation of the equations for such a piston will be omitted for the sake of brevity.

Crown Equations

Figure 2.1 shows the free body diagram for the crown indicating all the forces and moments acting on the component.

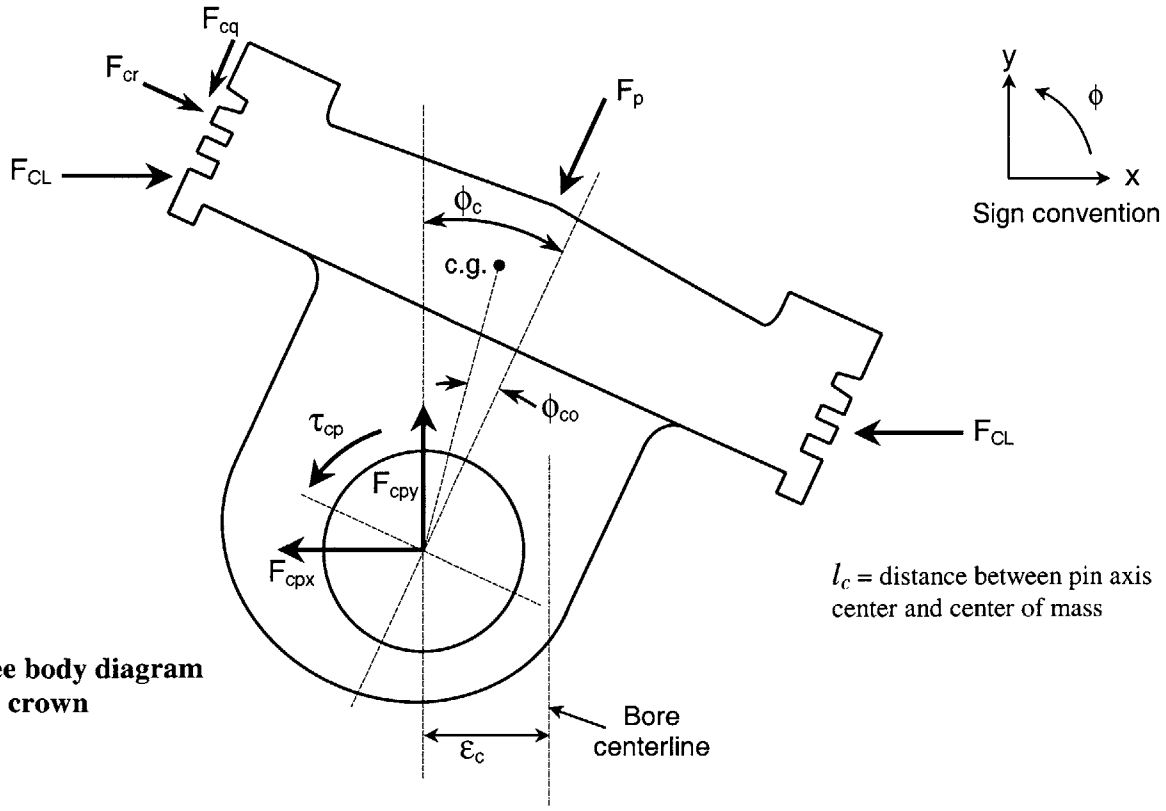

Figure 2.1 Free body diagram of the crown

The sign convention used for the lateral, axial and rotational directions are shown in the top right hand corner of figure 2.1. The only force that does not follow this convention is the gas pressure force acting on the crown. Since this is *always* acting towards the crankcase, the positive direction is set as downwards. Note that the angular and lateral displacements of the crown are greatly exaggerated in this diagram in order to display them clearly. A full description and explanation of each of the terms in figure 2.1 and all subsequent figures can be found in appendix A (nomenclature).

Force balance in the x-direction yields

$$m_c \ddot{\varepsilon}_{c,cm} = F_{cpx} + F_{cr} + F_{CL} \tag{2.1}$$

Force balance in the y-direction yields

$$m_c \left(a_p + \ddot{\gamma}_{c,cm}\right) = F_{cpy} + F_{cq} - F_p \tag{2.2}$$

Moment balance about the pin center yields

$$I_c \ddot{\phi}_c - m_c \left[l_c \sin(\phi_c + \phi_{co})(a_p + \ddot{\gamma}_c) + l_c \cos(\phi_c + \phi_{co}) \ddot{\varepsilon}_c \right] = \tau_{cp} + M_{CL} + M_{cr} + M_{cq} + M_p \tag{2.3}$$

Each moment term in equation 2.3 (denoted by a capital *M*) corresponds to one of the main forces shown in the free body diagram (figure 2.1). These moments refer to the moments about the wrist pin axis center caused by the force in question. The inertial terms in equations 2.1 and 2.2 are formulated in terms of the parameters $\ddot{\varepsilon}_{c,cm}$ and $\ddot{\gamma}_{c,cm}$ which refer to the lateral and axial accelerations of the center of mass of the crown. The lateral and axial displacements of the center of mass can easily be expressed in terms of the displacements of the pin axis center, as given by the following equations

$$\varepsilon_{c,cm} = \varepsilon_c + l_c \sin(\phi_c + \phi_{co}) \tag{2.4 a}$$

$$\gamma_{c,cm} = \gamma_c + l_c \cos(\phi_c + \phi_{co}) \tag{2.4 b}$$

Skirt Equations

Figure 2.2 shows the free body diagram for the skirt indicating all the forces and moments acting.

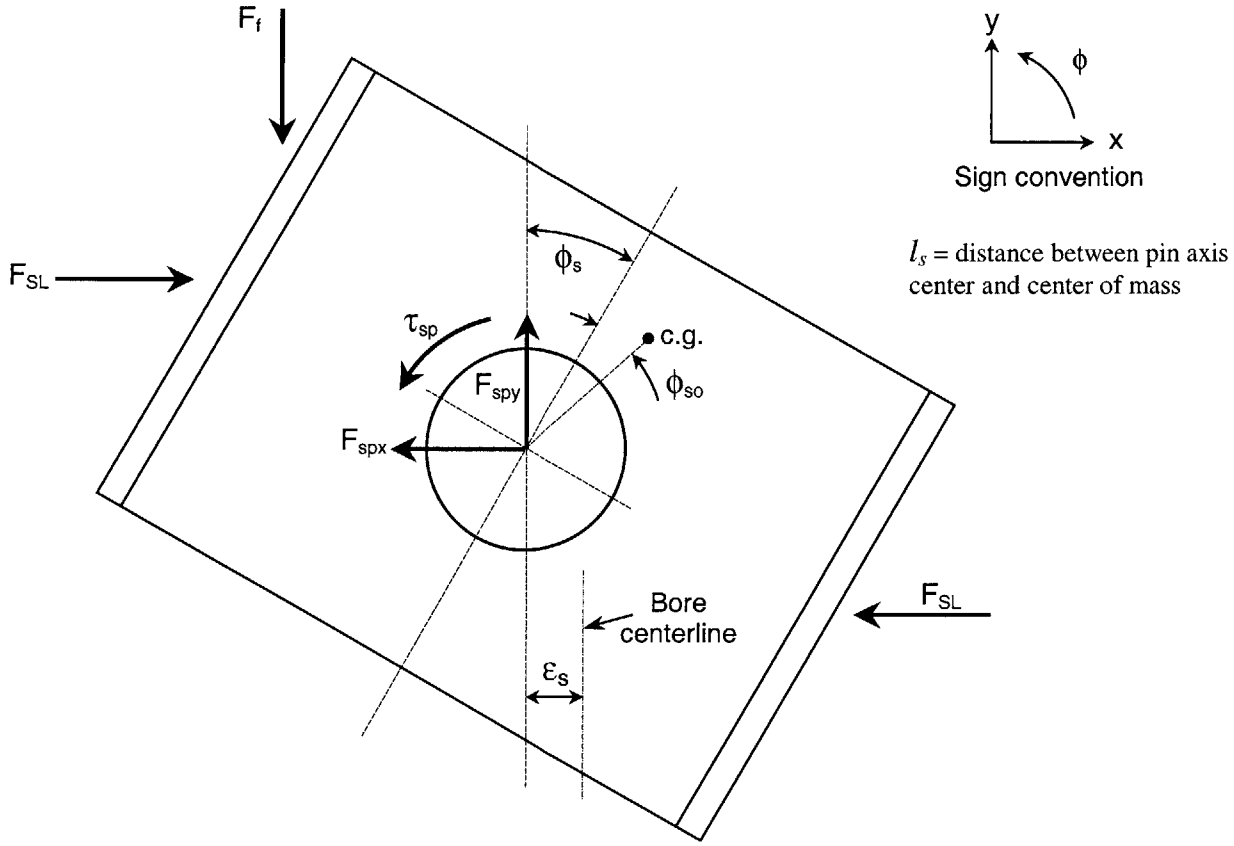

Figure 2.2 Free body diagram of the skirt

Force balance in the x-direction yields

$$m_s \ddot{\varepsilon}_{s,cm} = F_{spx} + F_{SL} \tag{2.5}$$

Force balance in the y-direction yields

$$m_s \left(a_p + \ddot{\gamma}_{s,cm}\right) = F_{spy} + F_f \tag{2.6}$$

Moment balance about the pin center yields

$$I_s \ddot{\phi}_s - m_s \left[l_s \sin(\phi_s + \phi_{so})(a_p + \ddot{\gamma}_s) + l_s \cos(\phi_s + \phi_{so})\ddot{\varepsilon}_s\right] = \tau_{sp} + M_{SL} + M_f \tag{2.7}$$

Again, the displacements of the center of mass can be expressed in terms of the pin axis displacements as follows,

$$\varepsilon_{s,cm} = \varepsilon_s + l_s \sin(\phi_s + \phi_{so}) \tag{2.8 a}$$

$$\gamma_{s,cm} = \gamma_s + l_s \cos(\phi_s + \phi_{so}) \tag{2.8 b}$$

Pin Equations

Figure 2.3 shows the free body diagram for the pin indicating all the forces and moments acting.

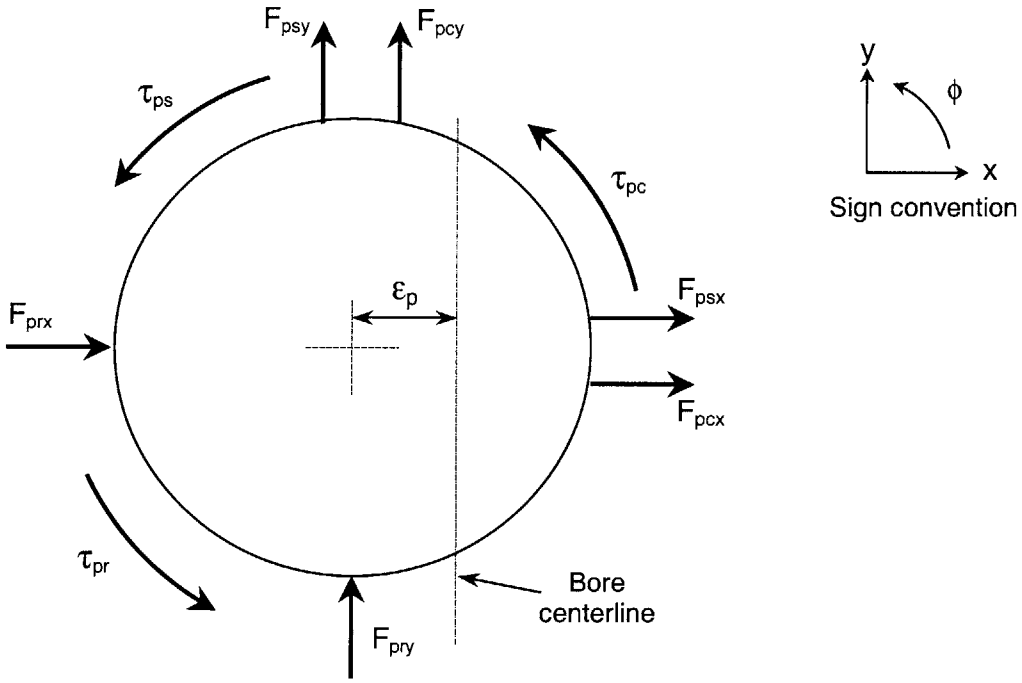

Figure 2.3 Free body diagram of the wrist pin

Force balance in the x-direction yields

$$m_p \ddot{\varepsilon}_{p,cm} = F_{pcx} + F_{psx} + F_{prx} \tag{2.9}$$

Force balance in the y-direction yields

$$m_p \left(a_p + \ddot{\gamma}_{p,cm}\right) = F_{pcy} + F_{psy} + F_{pry} \tag{2.10}$$

Moment balance about the pin center yields

$$I_p \ddot{\phi}_p = \tau_{pc} + \tau_{ps} + \tau_{pr} \tag{2.11}$$

Note that it has been assumed that the pin is perfectly symmetric, and hence the center of mass coincides with the pin axis center. Thus there is no moment due to the angular momentum, and the displacements of the pin center are exactly the same as those for the center of mass, i.e.

$$\varepsilon_{p,cm} = \varepsilon_p \qquad (2.12\ a)$$

$$\gamma_{p,cm} = \gamma_p \qquad (2.12\ b)$$

Rod Equations

Figure 2.4 shows the free body diagram for the pin indicating all the forces and moments acting.

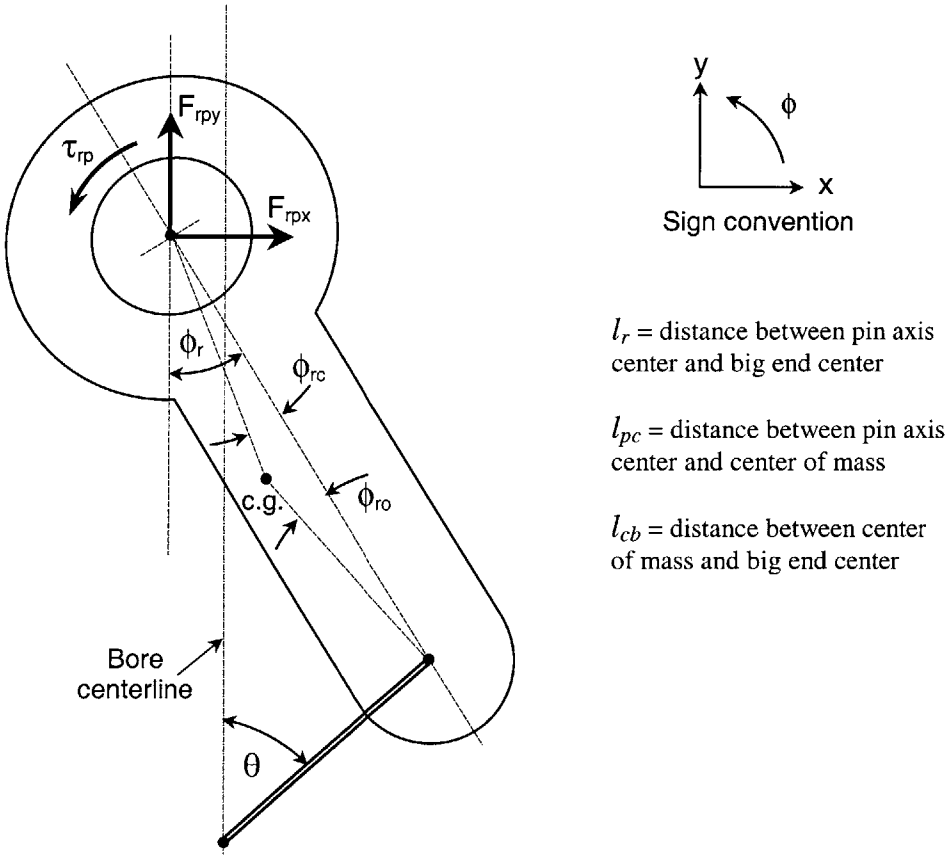

Figure 2.4 Free body diagram of connecting rod

For the connecting rod, the big end is assumed to have no secondary motion and trace a perfect circular path as dictated by ideal crank-slider kinematics. This means that the location of the small end (or wrist pin) bearing center is not independent of the rod rotation. The lateral and axial components of the pin axis' secondary motion can always be expressed as a function of the rod angle ϕ_r. For this reason, there is only one degree of freedom in the motion of the rod, and hence only one equation is required to solve the system. The moment equation will be used in this case.

Moment balance about the big end bearing center yields

$$I_r\ddot{\phi}_r + m_r l_{cb}\left[\sin(\phi_r + \phi_{ro})(a_p + \ddot{\gamma}_{r,b}) + \cos(\phi_r + \phi_{ro})\ddot{\varepsilon}_{r,b}\right] = \tau_{rp} - F_{rpy} l_r \sin\phi_r - F_{rpx} l_r \cos\phi_r \tag{2.13}$$

The displacements of the big end center can easily be expressed in terms of the rod angle ϕ_r and the geometry, as follows

$$\varepsilon_{r,b} = l_r \sin\phi_r \tag{2.14 a}$$

$$\gamma_{r,b} = l_r \cos\phi_r \tag{2.14 b}$$

Equations 2.1-2.3, 2.5-2.7, 2.9-2.11 and 2.13 constitute a system of ten second order differential equations representing the ten degrees of freedom in the system. In order to solve this system of equations, all the forces and moments must first be computed.

It was found that in order to fully determine the inter component reaction forces for this full degree of freedom model, a detailed analysis of the hydrodynamics in all of the wrist pin bearings would be required. In other words, the relative displacements of all the components would have to be used to compute the clearances in the wrist pin bearings, and these clearances used to compute the pressure distribution and subsequently the forces and moments in the oil film. Because of the non-symmetrical shape of the wrist pin bearings and the complex boundary conditions, standard bearing theory equations cannot be applied. A full 2-D solution of the Reynolds equation for the oil film would be

required in order to determine the forces and moments acting. It was felt that for the initial development of the model, this calculation was too complex and time consuming to incorporate, and hence certain simplifying assumptions were made to reduce the degrees of freedom in the system.

The first, and most obvious way of reducing the degrees of freedom in the system is to neglect the axial components of the secondary motion. Doing this will reduce the generality of the model, but will have no little or effect on the results, as the axial secondary motion is negligible when compared to the primary axial motion. This, however, does not remove the need to perform a full hydrodynamic analysis on the wrist pin bearings. In order to achieve this and to simplify the computation of the inter-component forces, it will be assumed that there is no relative lateral secondary motion between the various components. In other words it will be assumed that the lateral component of the secondary motion is the same for each component in the system. Given that the wrist pin bearing clearances are generally low compared to the skirt-liner clearances, this assumption should not have a great effect on the overall results.

With these assumptions in place, the system is reduced to four degrees of freedom. The four unknown variables to be solved for are now $\varepsilon, \phi_c, \phi_s$ and ϕ_p. The system of motion equations previously derived still apply, except for the fact that the axial secondary motion variables are removed, i.e.

$$\gamma_c = \gamma_s = \gamma_r = \gamma_p = 0$$

and the lateral component is the same for each component, i.e.

$$\varepsilon_c = \varepsilon_s = \varepsilon_r = \varepsilon_p = \varepsilon$$

These equations of motion can now be reduced to a system of four equations in the four system unknowns.

Reduction of the Equations of Motion

In reducing the equations of motion it will be assumed that the tilt angles and mass center offset angles of the crown and skirt (ϕ_c, ϕ_s, ϕ_{co} and ϕ_{so}) are small (these are generally of the order of 10 minutes) . Hence,

$$\sin(\phi_c + \phi_{co}) \approx \phi_c + \phi_{co}$$

$$\sin(\phi_s + \phi_{so}) \approx \phi_s + \phi_{so}$$

$$\cos(\phi_c + \phi_{co}) = \cos(\phi_s + \phi_{so}) \approx 1$$

From equation 2.4 (a), $\ddot{\varepsilon}_{c,cm}$ can be expressed as follows

$$\varepsilon_{c,cm} = \varepsilon + l_c(\phi_c + \phi_{co})$$

Differentiating this equation twice yields

$$\ddot{\varepsilon}_{c,cm} = \ddot{\varepsilon} - l_c\ddot{\phi}_c$$

Substituting this into equation 2.1 gives

$$m_c(\ddot{\varepsilon} - l_c\ddot{\phi}_c) = F_{cpx} + F_{cr} + F_{CL} \tag{2.15}$$

From equation 2.8 (a), $\ddot{\varepsilon}_{s,cm}$ can be expressed as follows

$$\varepsilon_{s,cm} = \varepsilon + l_s(\phi_s + \phi_{so})$$

Differentiating this equation twice yields

$$\ddot{\varepsilon}_{s,cm} = \ddot{\varepsilon} - l_s\ddot{\phi}_s$$

Substituting this into equation 2.5 gives

$$m_s(\ddot{\varepsilon} - l_s\ddot{\phi}_s) = F_{spx} + F_{SL} \tag{2.16}$$

Re-writing equation 2.9 noting that reaction forces between any two components are equal in magnitude but opposite in direction

$$m_p\ddot{\varepsilon} = -F_{cpx} - F_{spx} - F_{rpx} \tag{2.17}$$

Finally, combining equations 2.15, 2.16 and 2.17 allows for the inter-component reaction forces to be cancelled out, yielding the following equation

$$\ddot{\varepsilon}(m_c + m_s + m_p) - m_c l_c\ddot{\phi}_c - m_s l_s\ddot{\phi}_s = F_{cr} + F_{CL} + F_{SL} - F_{rpx} \tag{2.18}$$

Re-writing equation 2.3 making the small angle approximations and neglecting axial motion yields

$$\ddot{\phi}_c I_c - m_c l_c \ddot{\varepsilon} = m_c l_c (\phi_c + \phi_{co}) a_p + \tau_{cp} + M_{CL} + M_{cr} + M_{cq} + M_p \tag{2.19}$$

Similarly re-writing equation 2.7 gives

$$\ddot{\phi}_s I_s - m_s l_s \ddot{\varepsilon} = m_s l_s (\phi_s + \phi_{so}) a_p + \tau_{sp} + M_{SL} + M_f \tag{2.20}$$

Equations 2.11, 2.18, 2.19 and 2.20 constitute a new system of four differential equation of motion for the four main system variables $\varepsilon, \phi_c, \phi_s$ and ϕ_p. The inter component forces have been eliminated, and the remaining external forces and moments can all be determined. The only force still requiring attention is the rod to pin reaction force, F_{rpx}. This is the main driving side force in the system, and it must be computed from the moment equation for the rod (equation 2.13).

$$I_r \ddot{\phi}_r + m_r l_{cb} \left[\sin(\phi_r + \phi_{ro})(a_p + \ddot{\gamma}_{r,b}) + \cos(\phi_r + \phi_{ro}) \ddot{\varepsilon}_{r,b} \right] = \tau_{rp} - F_{rpy} l_r \sin\phi_r - F_{rpx} l_r \cos\phi_r$$

The tilt angle of the rod is independent of the main system variables and is only a function of the crank angle. The lateral motion of the wrist pin axis center can be expressed as a function of the rod tilt angle only. The only parameter in equation 2.13 that is a function of the system variables is the rod to pin shear torque, τ_{rp} (this shear torque depends on the relative angular velocities of the pin and the rod, thus is dependant on the system variable ϕ_p). However, we note that τ_{rp} is very much smaller than the other two moment terms on the right hand side of equation 2.13, and so it can easily be neglected. Re-writing equation 2.13 gives an expression for F_{rpx}

$$F_{rpx} = \left(\frac{1}{l_r \cos\phi_r} \right) \left\{ m_r l_{cb} \left[\sin(\phi_r + \phi_{ro}) a_p + \cos(\phi_r + \phi_{ro}) \ddot{\varepsilon}_{r,b} \right] - I_r \ddot{\phi}_r - F_{rpy} l_r \sin\phi_r \right\} \tag{2.21}$$

In order to fully determine the right hand side of equation 2.21, expressions must be derived for $\phi_r, \ddot{\phi}_r, \ddot{\varepsilon}_{r,b}$ and F_{rpy} in terms of known parameters (i.e. independent of the main system variables)

From the schematic of the connecting rod (figure 2.4) ϕ_r can written down as follows

$$\phi_r = \sin^{-1}\left(\frac{a\sin\theta}{l_r}\right)$$

where a is the crank radius and θ is the crank angle. Differentiating this equation twice and assuming that the engine is running at a constant speed ($\ddot{\theta} = 0$) yields an expression for the angular acceleration of the rod, $\ddot{\phi}_r$

$$\ddot{\phi}_r = \frac{\dot{\theta}^2 a\sin\theta}{l_r\sqrt{1-\left(\frac{a\sin\theta}{l_r}\right)^2}}\left[1-\frac{(a\cos\theta)^2}{l_r^2\left(1-\left(\frac{a\sin\theta}{l_r}\right)^2\right)}\right] \tag{2.22}$$

From equation 2.14 (a)

$$\varepsilon_{r,b} = l_r \sin\phi_r$$

Note that it is not reasonable to make small angle assumptions here, as the tilt angle of the rod is significantly higher than that of either the crown or the skirt. Differentiating the above equation twice yields

$$\ddot{\varepsilon}_{r,b} = \ddot{\phi}_r l_r \cos\phi - \dot{\phi}_r^2 l_r \sin\phi_r \tag{2.23}$$

An expression for F_{rpy} can be derived by summing equations 2.2, 2.6 and 2.10 (neglecting the axial component of the motion). Doing this cancels out the inter component reaction forces between the crown, skirt and pin.

$$F_{rpy} = F_{cq} - F_p + F_f - a_p(m_c + m_s + m_p) \tag{2.24}$$

Combining equations 2.22, 2.23 and 2.24 with equation 2.21 allows for the rod to pin reaction force to be accurately determined based solely on external parameters.

Equations 2.11, 2.18, 2.19 and 2.20 can now be re-arranged to give the final system of motion equations in the four system variables

System Equations – Articulated Piston

$$\ddot{\varepsilon} = \frac{c_1 + \left(\frac{m_c l_c}{I_c}\right)c_2 + \left(\frac{m_c l_c}{I_c}\right)c_3}{(m_s + m_c + m_p) - \left(\frac{m_c^2 l_c^2}{I_c}\right) - \left(\frac{m_s^2 l_s^2}{I_s}\right)} \qquad (2.25)$$

$$\ddot{\phi}_c = \frac{c_2 + m_c l_c \ddot{\varepsilon}}{I_c} \qquad (2.26)$$

$$\ddot{\phi}_s = \frac{c_3 + m_s l_s \ddot{\varepsilon}}{I_s} \qquad (2.27)$$

$$\ddot{\phi}_p = \frac{-1}{I_p}\left[\tau_{cp} + \tau_{sp} + \tau_{rp}\right] \qquad (2.28)$$

where,

$$c_1 = F_{cr} + F_{CL} + F_{SL} - F_{rpx}$$

$$c_2 = m_c l_c(\phi_c + \phi_{co})a_p + \tau_{cp} + M_{CL} + M_{cr} + M_{cq} + M_p$$

$$c_3 = m_s l_s(\phi_s + \phi_{so})a_p + \tau_{sp} + M_f + M_{SL}$$

This set of motion equations has been developed specifically for the case of an articulated piston. The derivation of the equations for a mono piston is essentially done in exactly the same way. The overall system for a mono piston has only three degrees of freedom, i.e. ε, ϕ_s and ϕ_p, and hence there are three final equations of motion. Exactly the same simplifying assumptions are made for the mono piston system , i.e. no axial secondary motion, small tilt angles and no relative lateral motion between the components. The final system of equations for the mono piston system is as follows ;

System Equations – Mono Piston

$$\ddot{\varepsilon} = \frac{c_1 + \dfrac{m_s l_s}{I_s}}{(m_s + m_p) - \left(\dfrac{m_s{}^2 l_s{}^2}{I_s}\right)} \qquad (2.29)$$

$$\ddot{\phi}_s = \frac{c_2 + m_s l_s \ddot{\varepsilon}}{I_s} \qquad (2.30)$$

$$\ddot{\phi}_p = \frac{-1}{I_p}\left(\tau_{sp} + \tau_{rp}\right) \qquad (2.31)$$

where,

$c_1 = F_{cr} + F_{SL} - F_{rpx}$

$c_2 = m_s l_s (\phi_s + \phi_{so}) a_p + \tau_{sp} + M_p + M_{cq} + M_{cr} + M_{SL} + M_f$

2.3 Force Modeling

2.3.1 Hydrodynamic Forces

The most important and also the most difficult forces to model in the piston system are the hydrodynamic forces generated the oil film between the piston and the liner. In a mono piston assembly hydrodynamic forces are generated between the skirt and the liner. These forces comprise a normal hydrodynamic force (F_{SL}), an axial friction force (F_f) and their corresponding moments (M_{SL}) and (M_f). In an articulated piston assembly the same forces and moments occur between the skirt and liner, but there are additional forces and moments due to the interaction of the crown and the liner (F_{CL} and M_{CL}). Articulated pistons are generally designed such that one of the crown lands protrudes past the others

and comes into contact with the oil film on the liner. It is this contact that produces the crown liner hydrodynamic forces and moments. When modeling the hydrodynamics, exactly the same analysis will be applied to the skirt/liner system as the crown/liner system, and a generalized model will be developed that will be used to compute both sets of forces and moments.

Modeling the hydrodynamics essentially involves solving the Reynolds equation for the oil film to yield a pressure distribution, and then integrating this pressure distribution to find the total forces and moments. In the most general form, the Reynolds equation must be solved in two dimensions, i.e. axial and circumfrential. Traditionally, secondary motion models have used either a finite element or a finite difference method to perform this calculation. However, these methods are both computationally intensive and difficult to implement due to the complex boundary conditions present. For the purpose of keeping the present model computationally efficient, a new approach to solving the hydrodynamics will be adopted.

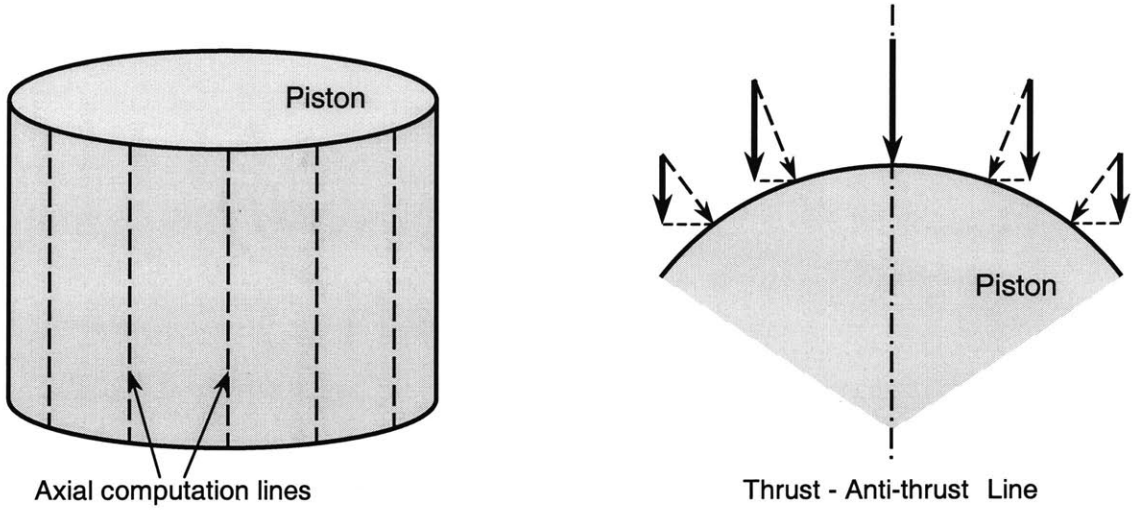

Figure 2.5 Pseudo 1-D treatment of Hydrodynamics

The essence of the new method will be to treat the oil film in a pseudo one dimensional fashion. That is, the 1-D Reynolds equation will be solved for several axial lines distributed circumfrentially around the piston. The local pressures will be integrated

axially to yield the normal force. These normal forces are then resolved into the thrust - anti-thrust direction and integrated circumfrentially to yield the total force. This geometry is illustrated in figure 2.5. The pseudo 1-D approach is considerably simpler than a full 2-D analysis, but assumes that the pressure gradient in the circumfrential direction is less significant than that in the axial direction. It is felt that this method will give a good compromise between the accuracy of the results and the computation time required.

The one dimensional form of the Reynolds equation is as follows,

$$\frac{\partial}{\partial x}\left(h^3 \frac{\partial p}{\partial x} \right) = 12\mu \frac{\partial h}{\partial t} + 6\mu U \frac{\partial h}{\partial x} \tag{2.32}$$

It is not possible to develop a full analytical solution to this equation for the oil film, and the usual approach is to apply some kind of numerical integration to arrive at a solution. However, the solution can be simplified greatly if the hydrodynamic pressure is considered to consist of two separate components – one due to squeezing in the oil film (related to the $\partial h / \partial t$ term), and the other due to the sliding velocity of the piston (related to the $\partial h / \partial x$ term), i.e.

$p = p_{sq} + p_{sl}$ where, p_{sq} = squeeze pressure and p_{sl} = slide pressure.

This allows equation 2.32 to split into two distinct parts ;

Squeezing Equation
$$\frac{1}{12\mu}\frac{\partial}{\partial x}\left(h^3 \frac{\partial p_{sq}}{\partial x} \right) = \frac{\partial h}{\partial t} \tag{2.33}$$

Sliding Equation
$$\frac{\partial}{\partial x}\left(h^3 \frac{\partial p_{sl}}{\partial x} \right) = 6\mu U \frac{\partial h}{\partial x} \tag{2.34}$$

The squeezing equation (2.33) can be integrated analytically to give a full solution for the squeeze pressure gradient $\partial p_{sq} / \partial x$ at discrete points along the axial grid. These discrete pressure gradients are then integrated axially to give the discrete pressure distribution and finally the total normal force. The discrete moments about the pin axis are also computed and then integrated to yield the total moment.

The sliding equation (2.34) cannot be integrated analytically due to the presence of the $\partial h / \partial x$ term. In order to arrive at a solution, a numerical correlation is applied to a

normalized form of the equation. This correlation essentially finds a solution which 'fits' both equation 2.34 and the Reynolds exit condition ($\partial p / \partial x = 0$ at the exit), assuming that the wetted region has a parabolic profile. The correlation is described in more detail in appendix B. After applying the numerical correlation to equation 2.34, the following power laws are obtained,

$$\bar{h}_o = 0.25\left[\frac{\mu U}{W}\left(\frac{2a}{B}\right)^2\right]^{0.528} \tag{2.35}$$

$$f = 2.05\left[\frac{\left(\frac{\mu U}{W}\right)^{0.68}}{\left(\frac{B}{2a}\right)^2}\right] \tag{2.36}$$

Equation 2.35 allows the normal load to be computed explicitly from the minimum film thickness, the sliding speed and the viscosity. This equation is applied to compute the normal force for each axial line. This sliding force is then added to the squeezing force to yield a total normal force for the axial location. Equation 2.36 allows the friction coefficient to be computed explicitly from the normal load, the sliding speed and the viscosity. This equation is applied, using the *total* normal load and the resulting friction coefficient is used to compute the axial friction force. The moment due to this friction force is computed by multiplying the force by the offset of the pin axis from the piston axis (this is usually a *very* small moment). The major drawback of this method is that the sliding pressure distribution is never actually computed. This distribution is necessary to accurately compute the sliding component of the hydrodynamic moment. However, it is known that the sliding pressure is usually concentrated at the point of minimum film thickness. Thus, for the purpose of computing the sliding moment, it is assumed that the *entire* sliding force acts through the point of minimum film thickness.

2.3.2 Ring Forces

The interaction of the piston (or crown) with the piston rings produces both *axial* and *lateral* forces (see figure 2.6).

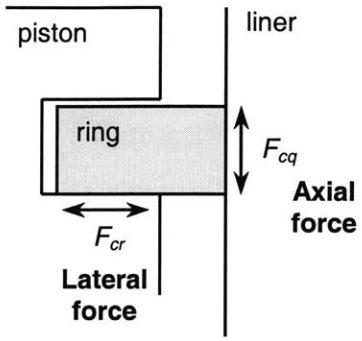

Figure 2.6 Components of the ring forces

Axial Ring Force

The axial force is a frictional force resulting from the rings sliding over the liner. There is a very thin oil film between each ring and the liner, and the axial friction force is a result of the shear stress in this oil film. A rigorous analysis would compute the pressure distribution under each ring by solving the Reynolds equation and use this to find the shear stress (as in [15]). In the present study, however, the axial ring friction is shown to have a very small effect on secondary motion, and hence a simpler approach is taken. Equation 2.36 is used to compute the friction coefficient, and the axial force is then computed by multiplying this coefficient by the normal load for each ring. The line of action of this force is along the bore center line, hence the moment is given by multiplying the force by the offset of the pin axis from the bore center line.

Lateral Ring Force

There is a lateral friction force generated due to the relative lateral motion of the ring and the groove in which it sits. Both asperity contact friction and hydrodynamic friction make up this total lateral friction force. However, the hydrodynamic friction force is negligible compared with the asperity contact friction, and hence only the latter component will be considered. The coefficient of friction for asperity contact can be considered to be exactly 0.1. In order to determine the frictional force generated it is necessary to compute the normal force due to asperity contact. It was initially intended to simply assume that 10% of the gas pressure force pushing the ring down was supported by asperity contact. It was

felt that this simplification would suffice, as the lateral ring friction had a small effect on the overall motion of the piston. However, while this assumption is true of a mono piston, the motion of the crown in an articulated piston is quite sensitive to the lateral ring friction (due to the absence of large side forces acting on the crown). Because of this sensitivity, a more detailed consideration of the lateral ring friction was deemed necessary.

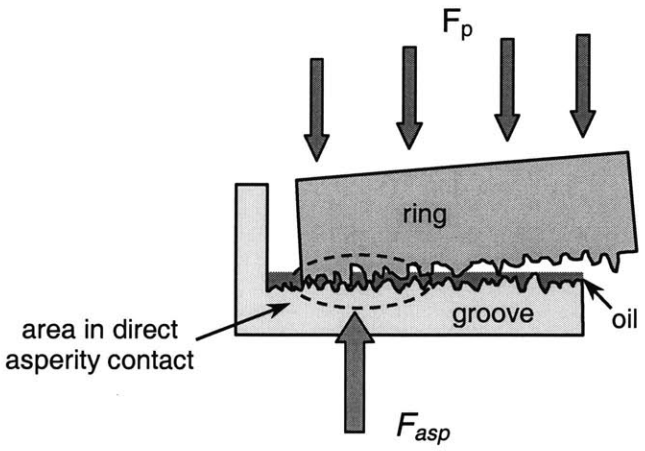

Figure 2.7 Asperity contact in lateral ring friction

In the model of ring dynamics previously developed at the Sloan Automotive Laboratory [1], Tian et. al. made an explicit calculation of the asperity contact force (F_{asp})as a fraction of gas pressure force (F_p) throughout the entire cycle. It has been decided to use this data as input to the present model, such that the lateral friction force can be determined more accurately. Results for a typical articulated piston assembly illustrate that the ratio of asperity contact force to gas pressure force varies widely through the cycle (see figure 2.8) . This illustrates the importance of including this data as input to the model. The input data is specified for the top ring (compression ring), but it is assumed that the same ration applies to the second ring as well. In order to compute the gas pressure force acting down on the second ring it is assumed that the second land pressure is 20% of the combustion chamber pressure. The oil control ring is assumed to produce no lateral friction.

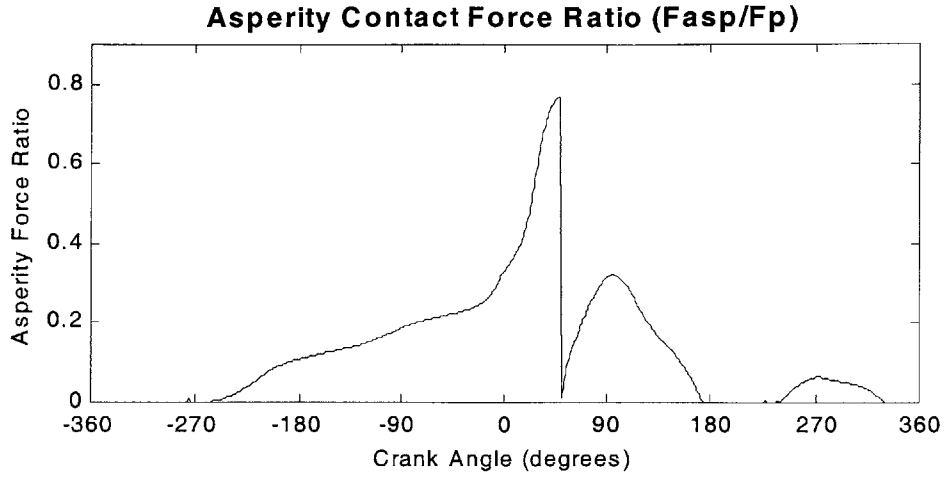

Figure 2.8 Asperity contact force ratio vs. crank angle

2.3.3 Wrist Pin Shear Torques

Due to the relative rotation of the wrist pin and the other components in the system, shear stresses are induced in the oil film in the wrist pin bearings. These shear stresses cause shear torques to be imparted to each of the components from the wrist pin. The most rigorous way to model these shear stresses would be to perform a full hydrodynamic analysis on each of the wrist pin bearings, solving the Reynolds equation and integrating to determine the total shear stress. However, this type of analysis is difficult to implement and computationally intensive. A more efficient method of determining the shear torques is adopted for the current model. This method is similar to the one used to compute the sliding component of the piston-liner hydrodynamics. In their paper detailing experimental measurements of connecting rod bearing friction [16] AUTHOR et. al. developed a semi-empirical Sommerfeld number correlation which gave good a fit to their engine measurements of friction.

$$f = 0.2\sqrt{\left(\frac{\mu U}{W}\right)\left(\frac{R_p}{C}\right)} \tag{2.36}$$

This correlation will be used to determine the friction coefficient in each of the bearings based on the bearing geometry, the viscosity, the sliding speed and the normal load. Once the friction coefficient has been determined, it is multiplied by the total normal load on the bearing to yield the local friction force, which is then converted to a torque about the

wrist pin center. However, as described earlier, the lateral components of the pin-crown and pin-skirt reaction forces are not explicitly determined in the model. Thus, some simplifying assumptions are needed in order to arrive at reasonable value for the normal forces in the crown-pin and skirt-pin bearings.

In the crown-pin bearing, it is intuitive that the axial reaction force (F_{cpy}) is considerably larger than the lateral reaction force (F_{cpx}) because the crown supports much higher axial forces (i.e. gas pressure and inertia) that side forces. Thus, it will be assumed that the normal reaction force in the crown-pin bearing is equal in magnitude to the axial reaction force (F_{cpy}). It is not reasonable to make the same assumption for the skirt-pin bearing as the skirt supports considerable side forces in addition to those in the axial direction. It will be assumed, however, that the lateral component of the skirt-pin reaction force (F_{spx}) is equal in magnitude to the lateral component of the rod-pin reaction force (F_{rpx}), which is explicitly determined. This side force (F_{rpx}) is transferred from the rod to the pin, and then from the pin to the skirt. The difference between the rod-pin force and the pin-skirt force is equal to the inertia force of the pin, which is considerably smaller than the side force (F_{rpx}). Thus, it is reasonable to assume that the entire side force from the rod is transferred to the skirt.

2.4 Computation Algorithm

The computation algorithm will be described in detail for the case of an articulated piston. Exactly the same method is used for the mono piston case. Consider the system of motion equations for the articulated piston (eqts. 2.5 – 2.8) as follows,

$$\ddot{\varepsilon} = f_1(\dot{\varepsilon}, \varepsilon, \dot{\phi}_s, \phi_s, \dot{\phi}_c, \phi_c, \dot{\phi}_p, \phi_p)$$

$$\ddot{\phi}_s = f_2(\dot{\varepsilon}, \varepsilon, \dot{\phi}_s, \phi_s, \dot{\phi}_c, \phi_c, \dot{\phi}_p, \phi_p)$$

$$\ddot{\phi}_c = f_3(\dot{\varepsilon}, \varepsilon, \dot{\phi}_s, \phi_s, \dot{\phi}_c, \phi_c, \dot{\phi}_p, \phi_p)$$

$$\ddot{\phi}_p = f_4(\dot{\varepsilon}, \varepsilon, \dot{\phi}_s, \phi_s, \dot{\phi}_c, \phi_c, \dot{\phi}_p, \phi_p)$$

These equations are first reduced to a system of eight first order differential equations as follows,

$$\frac{d\varepsilon}{dt} = \dot{\varepsilon} \qquad \frac{d\dot{\varepsilon}}{dt} = f_1$$

$$\frac{d\phi_s}{dt} = \dot{\phi}_s \qquad \frac{d\dot{\phi}_s}{dt} = f_2$$

$$\frac{d\phi_c}{dt} = \dot{\phi}_c \qquad \frac{d\dot{\phi}_c}{dt} = f_3$$

$$\frac{d\phi_p}{dt} = \dot{\phi}_p \qquad \frac{d\dot{\phi}_p}{dt} = f_4$$

These differential equations are then integrated implicitly to yield the following set of non-linear equations in the main system variables, $\dot{\varepsilon}, \varepsilon, \dot{\phi}_s, \phi_s, \dot{\phi}_c, \phi_c, \dot{\phi}_p$ and ϕ_p ;

$$\varepsilon_{t-\Delta t} - \varepsilon_t + (\delta t)\dot{\varepsilon}_t = 0 \tag{2.37}$$

$$\dot{\varepsilon}_{t-\Delta t} - \dot{\varepsilon}_t + (\delta t) f_{1t} = 0 \tag{2.38}$$

$$\phi_{st-\Delta t} - \phi_{st} + (\delta t)\dot{\phi}_{st} = 0 \tag{2.39}$$

$$\dot{\phi}_{st-\Delta t} - \dot{\phi}_{st} + (\delta t) f_{2t} = 0 \tag{2.40}$$

$$\phi_{ct-\Delta t} - \phi_{ct} + (\delta t)\dot{\phi}_{ct} = 0 \tag{2.41}$$

$$\dot{\phi}_{ct-\Delta t} - \dot{\phi}_{ct} + (\delta t) f_{3t} = 0 \tag{2.42}$$

$$\phi_{p_{t-\Delta t}} - \phi_{p_t} + (\delta t)\dot{\phi}_{p_t} = 0 \tag{2.43}$$

$$\dot{\phi}_{p_{t-\Delta t}} - \dot{\phi}_{p_t} + (\delta t) f_{4t} = 0 \tag{2.44}$$

where the subscript 't' refers to a variable's value at the current time step, and the subscript '$t - \Delta t$' refers to it's value at the previous time step. The values at the previous time step are, of course, known so the values at the current step are the system unknowns. This now constitutes a system of eight non linear equations in the eight system variables. These equations are solved simultaneously using the globally convergent Newton's method [17]. The standard Newton algorithm linearizes the system of equations and iterates towards a solution. The main advantage of the scheme is that it achieves rapid

local convergence. However, it is very sensitive to initial guess and has a tendency for the solution to wander off into the wide blue yonder when the guess is poor. In order to make convergence more robust, a globally convergent scheme was adapted. The essence of the globally convergent scheme is to check if the new values of the variables obtained from the Newton iteration satisfy the system equations better than the values from the previous iteration. If they do, these new values are accepted as the values for the current iteration. If they do not, the optimal values of the variables are found by backtracking along the tangent direction given by the Jacobians. Using the globally convergent scheme greatly improves the robustness and reliability of the program. The Jacobian calculations were performed numerically in the current model. Deriving and using the analytical Jacobians would improve the run-time of the model, but several of the forces are formulated in such a way that their dependence on the system variables cannot be expressed explicitly and hence they cannot be differentiated analytically. The use of a numerical Jacobian calculation also allows for more flexibility in the model – the formulation of any of the system forces can be changed without the need to alter the Jacobian calculations.

Normalization

In order to optimize the performance of the Newton algorithm, the system variables and equations must be normalized. Large difference in the order of the function evaluations will lead to an ill-conditioned Jacobian matrix, and poor convergence (if any). Each of the system variables is normalized by some representative reference value. Table 2.1 lists the reference values used to normalize each of the system variables. Equations 2.37, 2.39, 2.41 and 2.43 do not need further attention once they are written in terms of the normalized variables since they are trivial expressions of the system variables. However, equation 2.38, 2.40, 2.42 and 2.44 contain the more complex functions $f_1 - f_4$ and need to be normalized even after they are written in terms of the normalized variables. Each of these equations is simply divided across be some representative value of the functions $f_1 - f_4$. These normalization factors are evaluated during the program execution in the same fashion as the actual functions, but using a set of 'typical' conditions.

Reference variable	Value
Δt_{ref}	*Time for one crank revolution (= 2π/speed)*
ε_{ref}	*Radial skirt-liner clearance*
$\dot{\varepsilon}_{ref}$	$\varepsilon_{ref} / \Delta t_{ref}$
$\phi_{s\,ref}$	ε_{ref} */skirt height*
$\dot{\phi}_{s\,ref}$	$\phi_{s\,ref} / \phi_{s\,ref}$
$\phi_{c\,ref}$	*(radial crown-liner clearance)/(distance from crown to pin)*
$\dot{\phi}_{c\,ref}$	$\phi_{c\,ref} / \Delta t_{ref}$
$\phi_{p\,ref}$	*Maximum angular displacement of connecting rod* ($\phi_{r\,\max}$)
$\dot{\phi}_{p\,ref}$	$\phi_{p\,ref} / \Delta t_{ref}$

Table 2.1 Reference values for variable normalization

2.5 Sample Results for Mono Piston

The mono piston model was first applied to a standard 2.0 liter, four cylinder gasoline engine under test at the Sloan Automotive Laboratory. Table 2.2 lists the main engine parameters and operating conditions for the baseline case studied.

Parameter	Value
Engine Details	
Bore	86.0 mm
Stroke	86.0 mm
Pin Offset	0.5 mm
Operating Conditions	
Speed	3500 RPM
Load	Full Load
Oil Film Thickness on Liner	50 μm
Skirt-Liner Radial Clearance	25 μm

Table 2.2 Mono piston engine details and operating conditions

It is helpful at this point to re-iterate the sign convention used in the model. Positive forces and displacements refer to those in the direction of the *anti-thrust side* of the cylinder. Negative forces and displacements refer to those in the direction of the *thrust side*. Positive moments and angular displacements refer to those in the *anti-clockwise* direction. Negative moments and angular displacements refer to those in the *clockwise* direction.

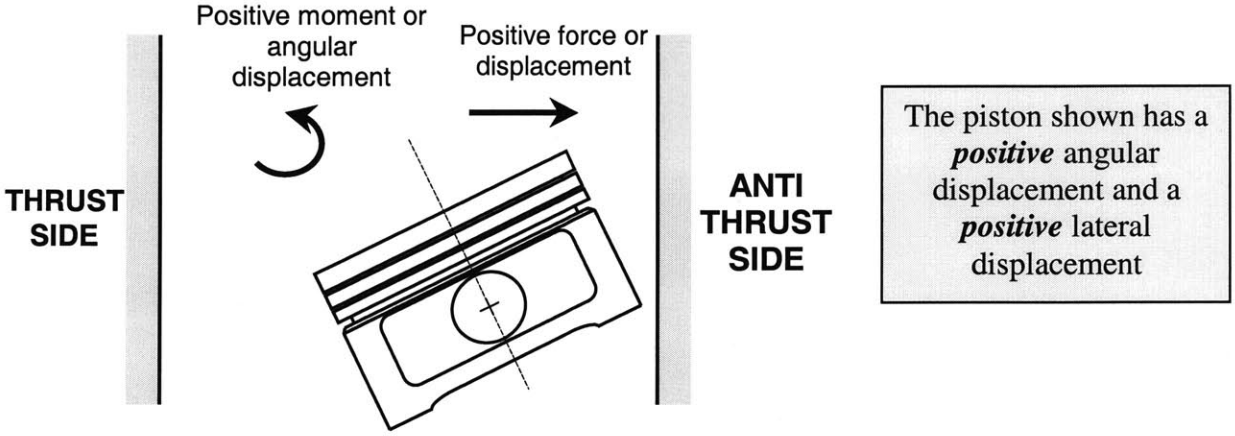

Figure 2.9 Sign conventions used in the model

As mentioned previously, the main driving force behind piston secondary motion is the side force imparted on the skirt by the connecting rod (through the pin). This force is plotted in figure 2.10.

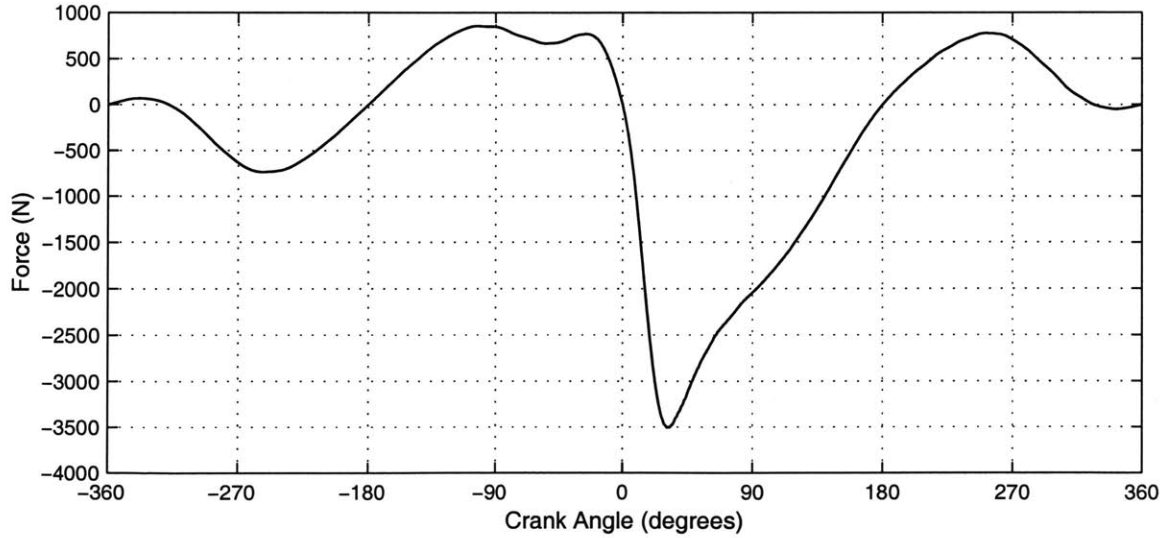

Figure 2.10 Side force from wrist pin to skirt

This piston side force is a combination of both the inertia of the connecting rod and it's reaction to the axial gas pressure force acting on it through the piston. In the absence of the gas pressure force the side force would be perfectly sinusoidal and periodic. However, when the gas pressure force is at it's greatest around top center, there is a large spike in the side force. This spike coincides with a change in direction of the force, due to the change in orientation of the connecting rod as the piston passes through top center. This change in direction and large increase in the side force is the cause of piston slap, i.e. it accelerates the piston towards the thrust side of the cylinder.

Figure 2.11 shows the lateral displacement of the wrist pin center (ε), along with the dimensionless piston side force. This plot illustrates clearly how the side force drives the motion of the piston. The displacement can be seen to follow the side force with a slight lag. This lag is due to the inertia of the piston and is largest when the driving force is smallest. Piston slap is evident immediately after top center as the piston moves quickly towards the thrust side of the cylinder.

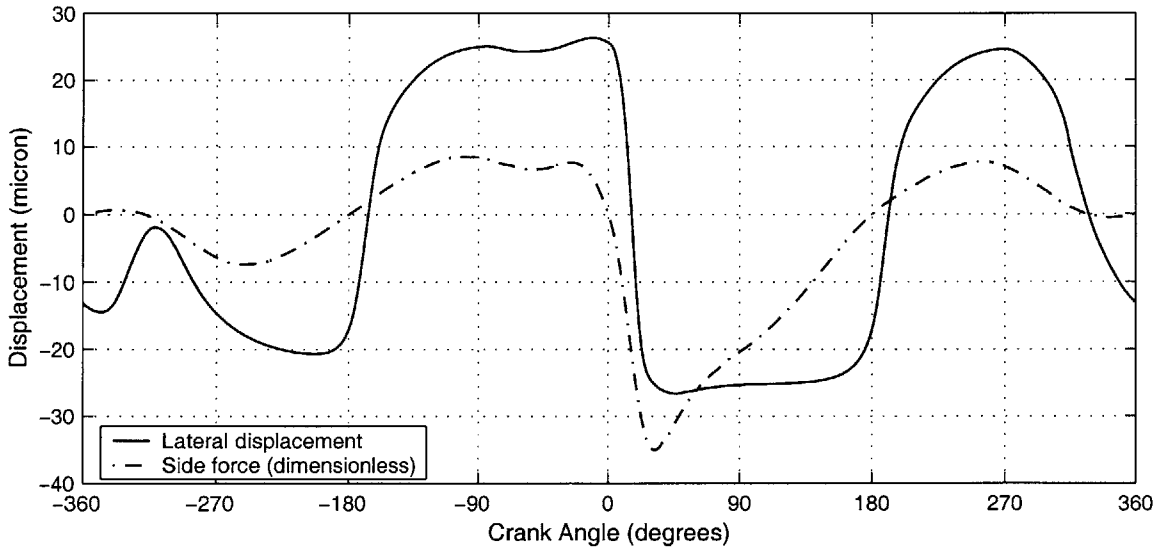

Figure 2.11 Piston lateral motion with dimensionless side force

The displacement at the end of this 'slap' is approximately 25 μm which is the same as the radial clearance between the skirt and the liner. This indicates that the piston comes very close to the liner wall during slap. Indeed, figure 2.12 shows the exact minimum oil film thickness' found on both sides of the piston during the cycle.

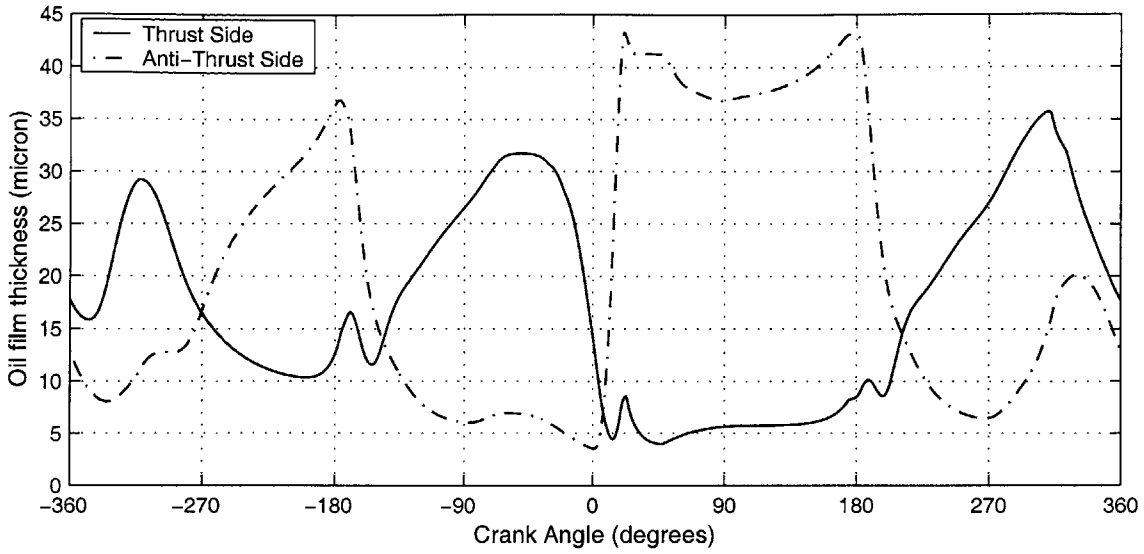

Figure 2.12 Minimum oil film thickness on both sides of the piston

The film thickness on the thrust side reduces to below 5 μm when slap occurs. This plot also illustrates how the piston "bounces" against the thrust side of the liner wall after the slap. It can be noted that the oil film thickness' on either side would be exact mirror images of one another were it not for the tilting motion of the piston.

In general, the hydrodynamic forces induced by the motion match the driving side force very closely. The small differences between these forces are what leads to acceleration of the assembly. Figure 2.13 shows the correspondence between the driving side force and the total hydrodynamic force that results.

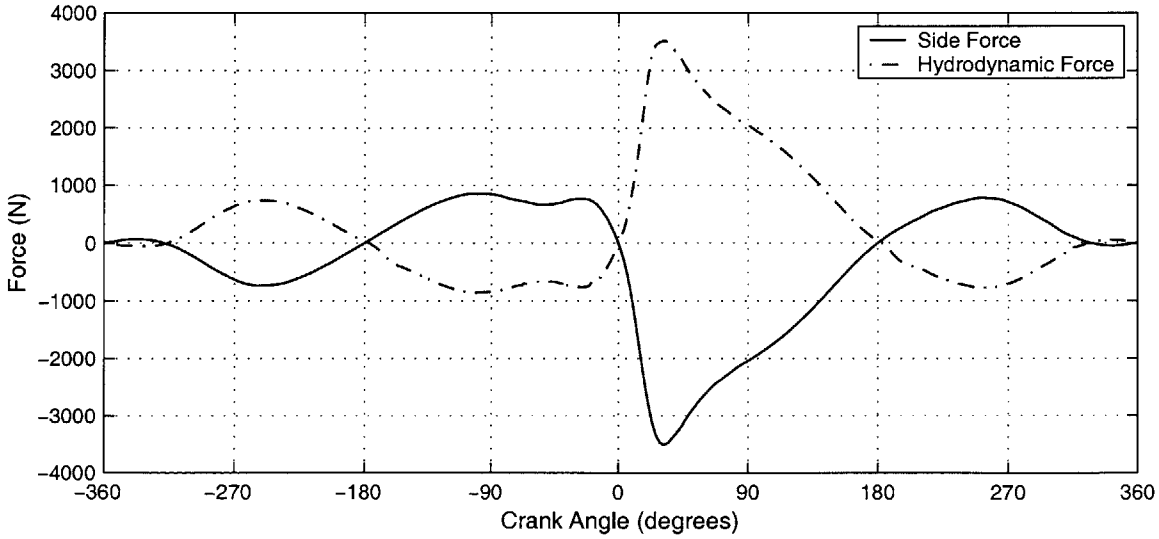

Figure 2.13 Piston side force and total hydrodynamic force

The composition of the total hydrodynamic force is crucial in determining how the piston motion will be retarded as it approaches and slides along the liner wall. The breakdown of the total hydrodynamic force into it's squeezing and sliding components for both sides are shown in figures 2.14 and 2.15.

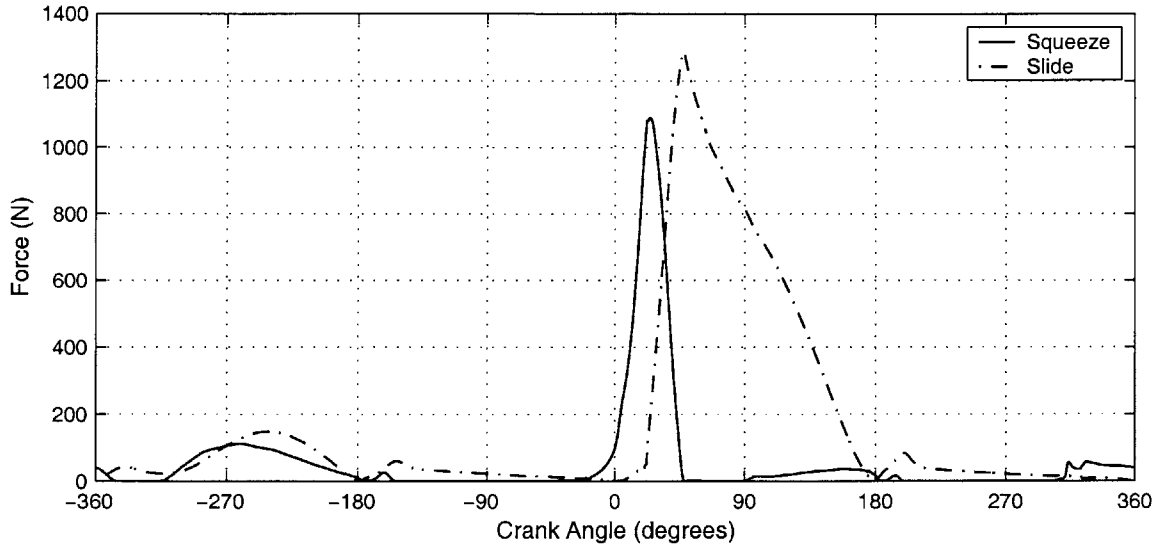

Figure 2.14 Thrust side hydrodynamic forces

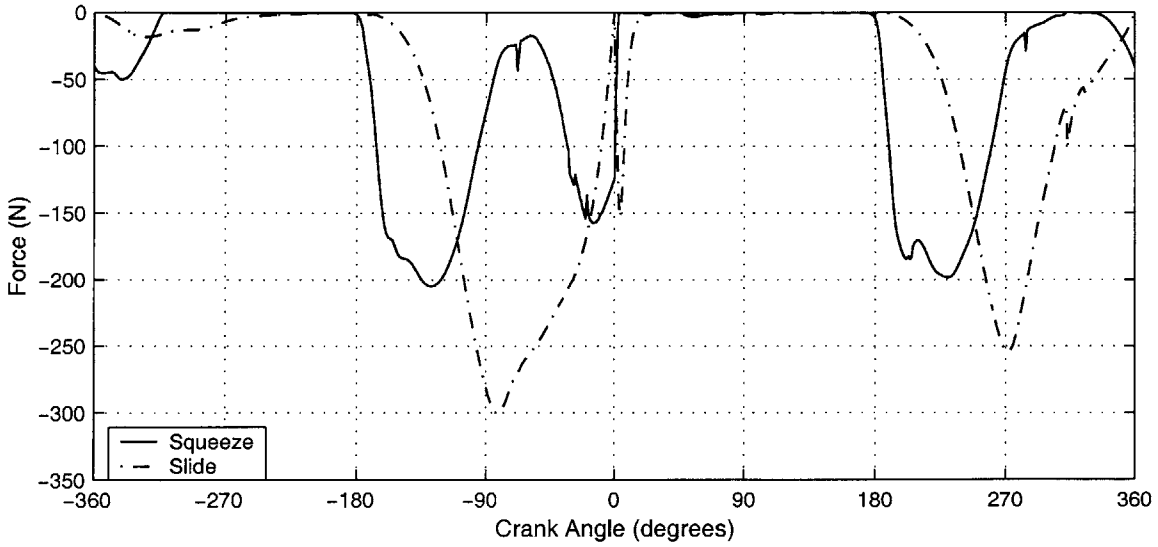

Figure 2.15 Anti-thrust side hydrodynamic forces

Generally, the piston moves across the bore each time it reaches either top or bottom center. When this happens, the sliding speed is very low and hence there is little or no

sliding force generated. Hence, the piston continues accelerating until it gets quite close to the liner wall. This generates a large squeezing force which decelerates the piston. As the piston slows down and eventually stops, the squeezing force goes to zero. At this point the piston is very close to the liner wall, and this coupled with the fact that the sliding speed begins to increase again after the top or bottom center position, causes the sliding force to rise quickly. This has the effect of pushing the piston away from the liner wall. This sequence of events can be seen quite clearly from figures 2.14 and 2.15 to occur on both side of the piston. It will be noted, however, that the magnitude of the forces induced on the thrust side after top center are far greater than during the rest of the cycle due to the severe forces and accelerations involved in the piston slap.

The tilt of the piston is shown in Figure 2.16. The tilting motion of the piston is driven in part by the shear torque from the wrist pin, but also by the hydrodynamic moments in the oil film between the skirt and the liner. The relative extent to which each of these factors influences the motion of the piston depends largely on the geometry of the piston skirt. The skirt generally has a barrel profile, and the location of the minimum point on the barrel is of great importance in determining the hydrodynamic moments that act on the piston during the cycle.

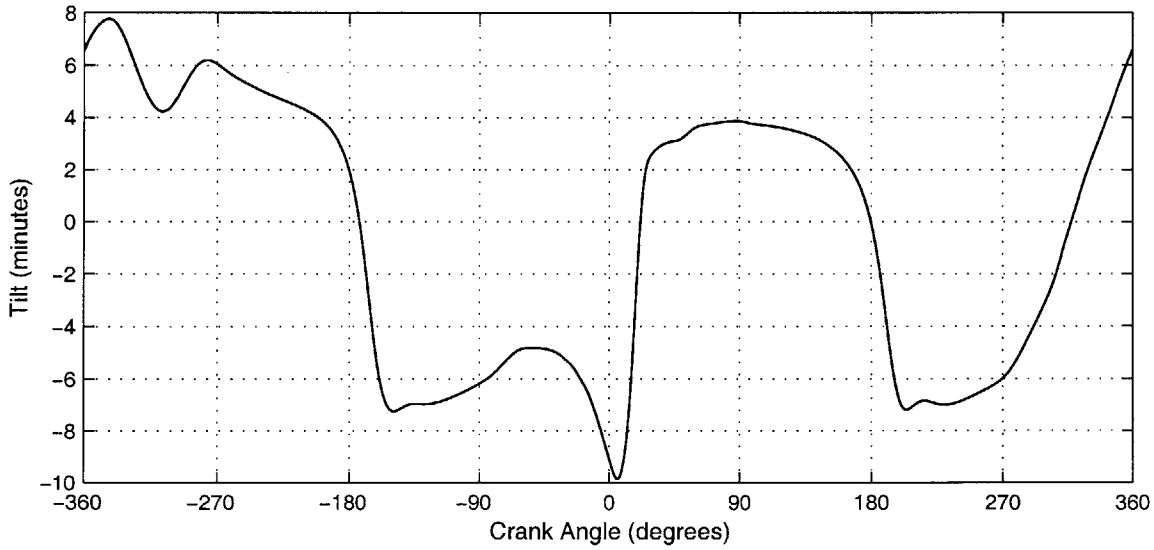

Figure 2.16 Piston tilt

Figure 2.17 shows a piston with such a barrel profile on the skirt (the barrel shape is greatly exaggerated in scale). It is generally the case that the minimum point on the skirt profile is located below the level of the wrist pin axis, as is shown in figure 2.17. When the piston comes close to the liner wall, a hydrodynamic force is generated in the oil film. This force is largely centered at the minimum point of the profile. When there is a separation between the minimum point and the level of the pin axis, the side force and resulting hydrodynamic force have different lines of action

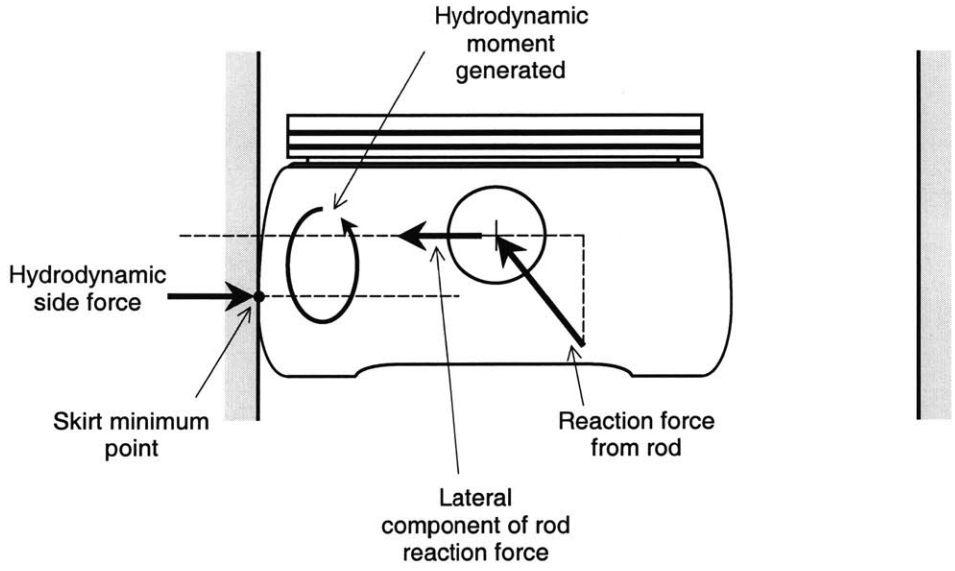

Figure 2.17 The effect of skirt profile on the hydrodynamic moments

and hence constitute a couple, which produces a moment. The magnitude of this moment is dependant on the distance between the two lines of action. For pistons with a sizeable distance between the wrist pin axis and the minimum point, this type of hydrodynamic moment tends to dominate the piston motion, and the pin shear torque has very little effect. This is the case for the piston in the engine under current consideration. In this engine the minimum point is located 10mm below the wrist pin axis.

From figure 2.16, it can be seen that the piston tilt changes sign at each of the top and bottom center positions. This is due to the fact that the side force changes direction at each of these points, and the piston moves across the bore. For example, just before bottom center of the intake stroke (i.e. $\theta = -180°$), the piston is towards the thrust side of

the bore (i.e. ε is negative), and the tilt is positive. Then, the side force changes direction and acts towards the anti-thrust side. This moves the piston across the bore to the anti-thrust side, generating a hydrodynamic force on the anti-thrust side of the piston. This force acts below the wrist pin axis and hence produces a negative moment on the piston, causing the tilt to become negative. This effect is most notable immediately after top center of the combustion stroke, i.e. during slap. At this point the piston is accelerated across the bore very rapidly and the resulting hydrodynamic moment is quite large. The hydrodynamic moments for each side of the piston can be seen in figures 2.18 and 2.19.

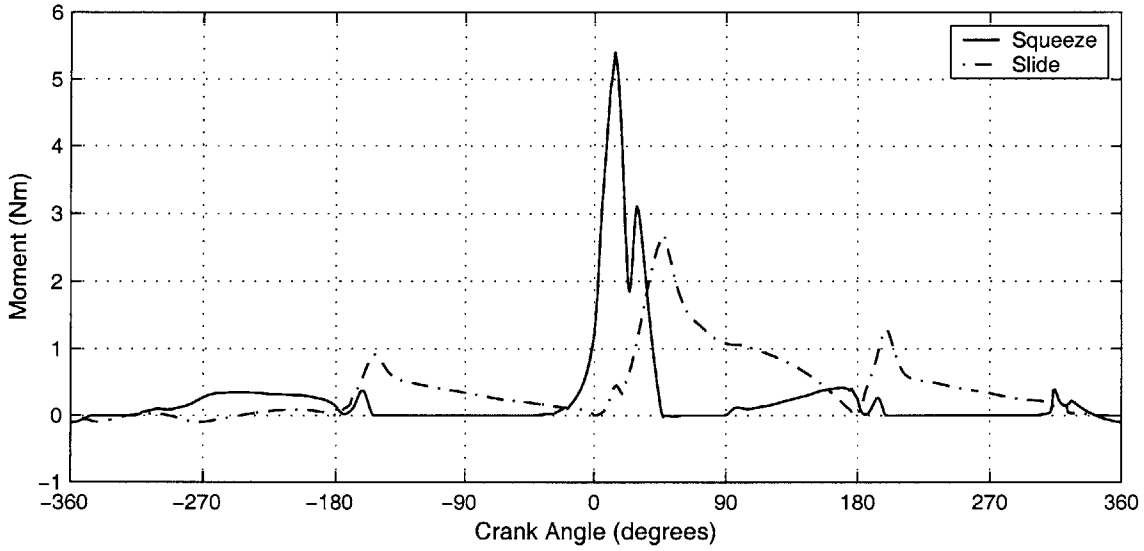

Figure 2.18 Thrust side hydrodynamic moments

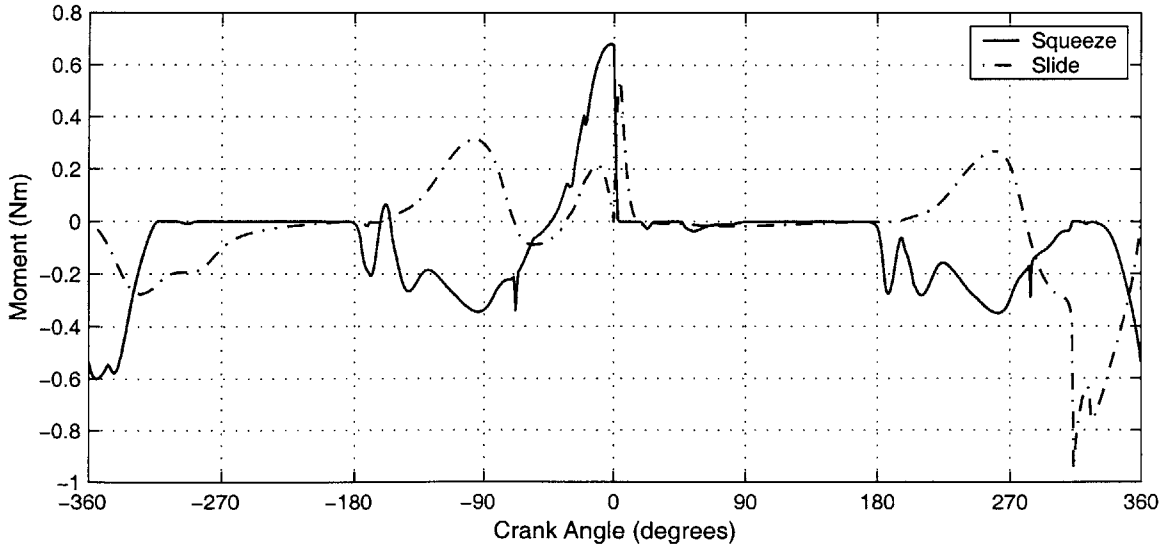

Figure 2.19 Anti-thrust side hydrodynamic moments

The sliding component of the hydrodynamic moments is a direct product of the hydrodynamic side force and the location of the minimum film thickness. The location of this point is dependant on the tilt of the piston, and is illustrated in figure 2.20 (Note that the horizontal grid lines represent the bottom edge, the pin axis level and the top edge of the skirt respectively).

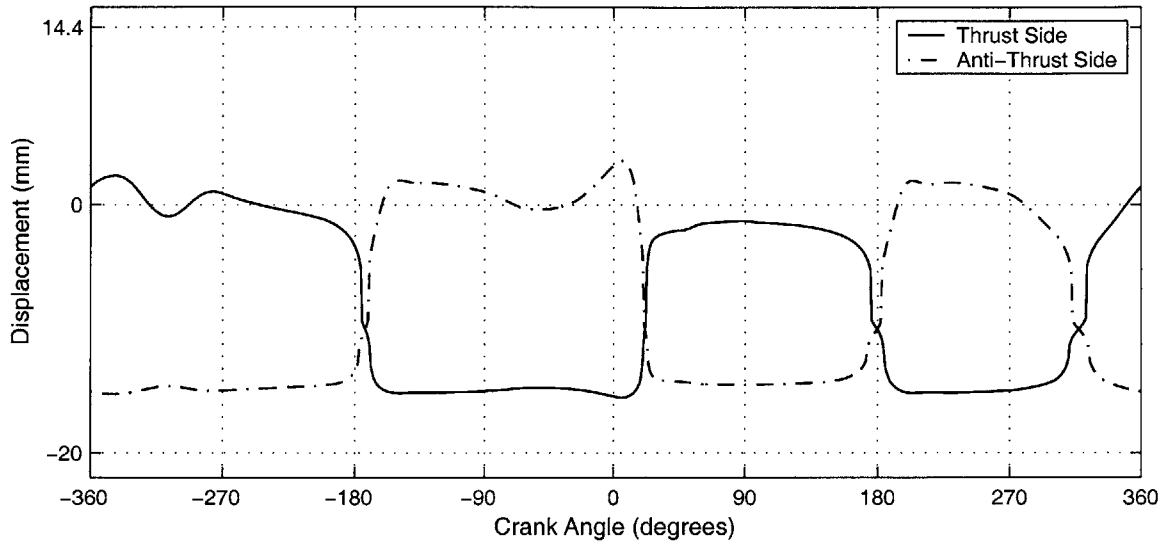

Figure 2.20 Location of the minimum point on both sides of the piston

The effect on the tilting motion of the wrist pin offset can also be seen in figure 2.16. Offsetting the wrist pin towards the thrust side of the piston causes a moment to be induced about the wrist pin axis by the gas pressure force. The gas pressure force acts down the central axis of the piston, and with the wrist pin axis offset towards the thrust side, this leads to a negative moment about the pin. The purpose of this measure is to reduce the magnitude of the piston slap (this will be discussed in more detail later). The magnitude of the gas pressure moment produced by the offset reaches it's peak around top dead center where the gas pressure is at it's highest. The negative downturn in piston tilt just before top center can clearly be seen in figure 2.16, and is a direct result of this gas pressure moment.

2.6 Sample Results for Articulated Piston

The articulated piston model was applied to a 12 liter Volvo Truck diesel engine. The details of this engine and the operating conditions used in the baseline case studied are listed in table 2.3.

Parameter	Value
Engine Details	
Bore	131.0 mm
Stroke	150.0 mm
Pin Offset	0.0 mm
Operating Conditions	
Speed	1800 RPM
Load	Full Load
Oil Film Thickness on Liner (skirt calculation)	50 μm
Skirt-Liner Radial Clearance	35 μm
Oil Film Thickness on Liner (crown calculation)	10 μm
Crown-Liner Radial Clearance	65 μm

Table 2.3 Articulated piston engine details and operating conditions

The motion of the skirt in an articulated piston assembly is controlled by similar forces to those that influence the motion of a mono piston. The driving side force is almost identical in nature, and is the dominant influence on the lateral motion of the skirt. The lateral motion of the wrist pin axis of the and the driving pin to skirt side force are shown in figure 2.21.

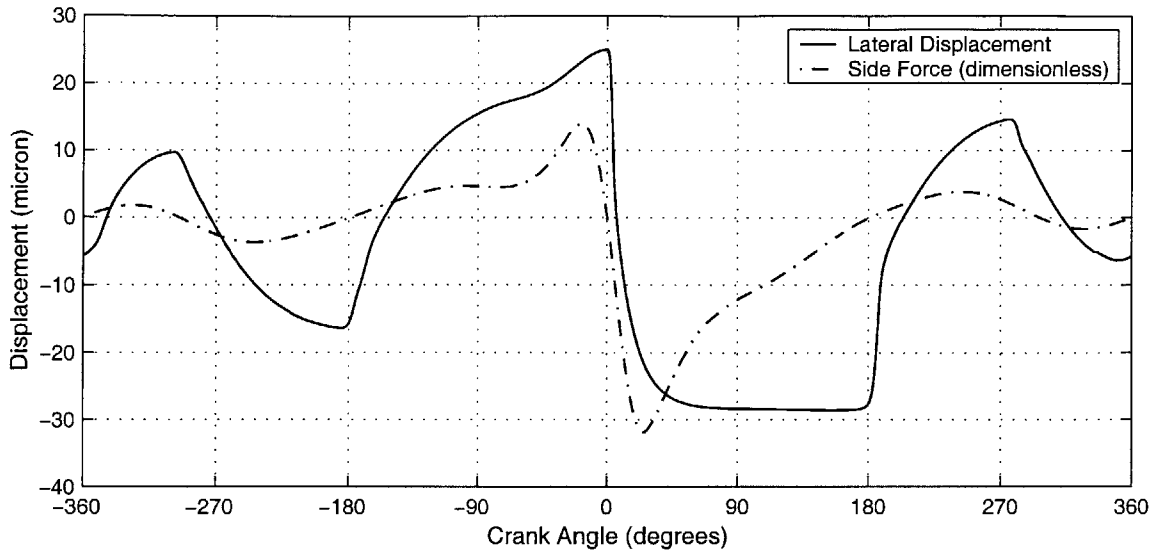

Figure 2.21 Skirt lateral motion with dimensionless side force

Once again, it can be seen that the lateral motion of the skirt follows the side force, but lags due to the inertia of the assembly. Very severe piston slap can be seen just after top center as the piston is accelerated towards the thrust side of the bore. The slap is more severe in this heavy duty diesel engine due to the much higher combustion pressures (this engine has a peak cylinder pressure of approximately 170 bar). The breakdown of the hydrodynamic forces induced on both sides of the skirt are shown in figures 2.22 and 2.23.

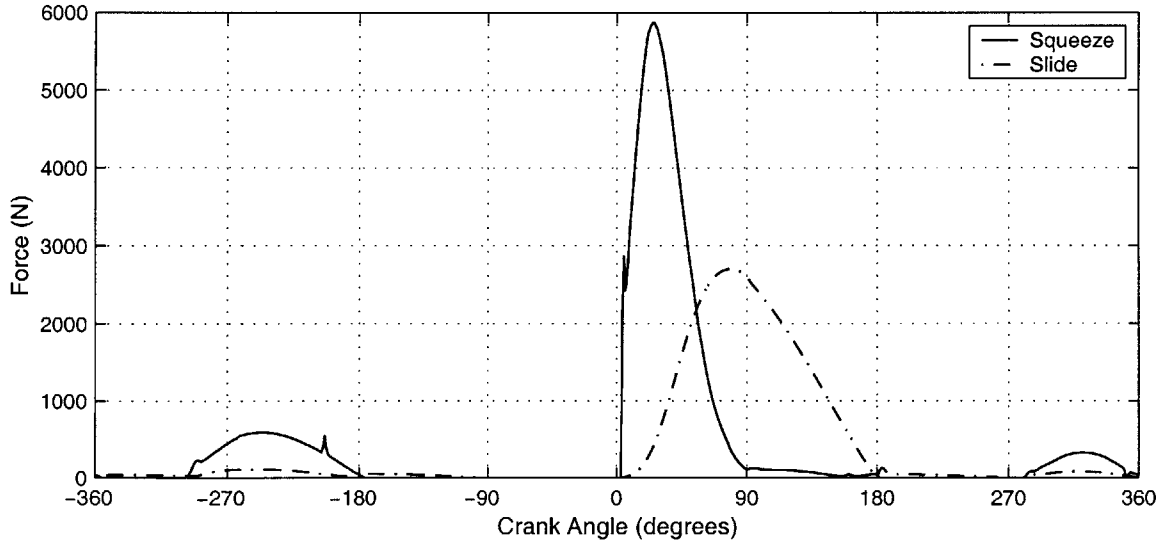

Figure 2.22 Skirt thrust side hydrodynamic forces

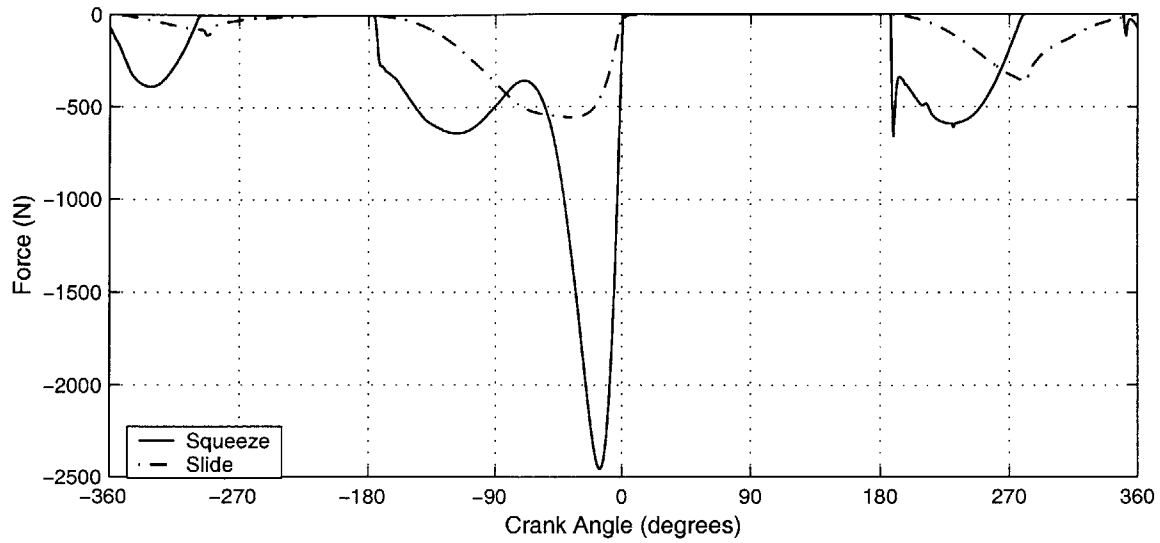

Figure 2.23 Skirt anti-thrust side hydrodynamic forces

Similar to the mono piston, it is the squeezing force that is first to react as the skirt approaches the liner. Once the squeeze force has stopped the approach of the piston, the slide force increases and pushes it away from the liner.

While the lateral motion of the articulated piston is controlled in a similar way to that of a mono piston, the tilting motion of the skirt and crown are entirely different. These are both predominantly driven by the shear torques from the wrist pin. These shear torque terms are plotted in figure 2.24.

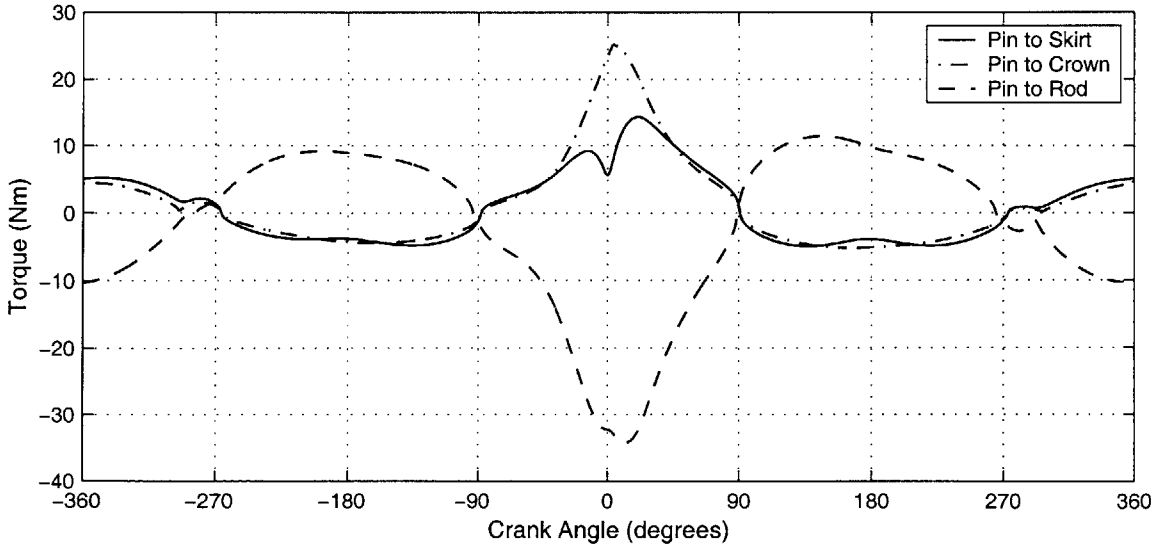

Figure 2.24 Wrist pin shear torques

The origin of the shear torque in the pin bearings is the angular motion of the connecting rod. As the connecting rod turns, it imparts a shear torque to the pin which is in turn imparted to the crown and skirt. Hence the sign of the rod shear torque is opposite to that for the crown and skirt. The difference between the torques acting on the skirt and crown are due mainly to the differences in the normal forces acting on these bearings. The normal force acting on the pin-crown bearing is essentially equal to the sum of the axial crown inertia and gas pressure forces. The normal force acting on the pin-skirt bearing is the resultant of the total axial force on the skirt *and* the total side force. It is this dependence on the side force that leads to the peaks in the pin–skirt shear torque either side of top center.

The skirt tilt can be seen in figure 2.25 along with the pin to skirt shear torque term.

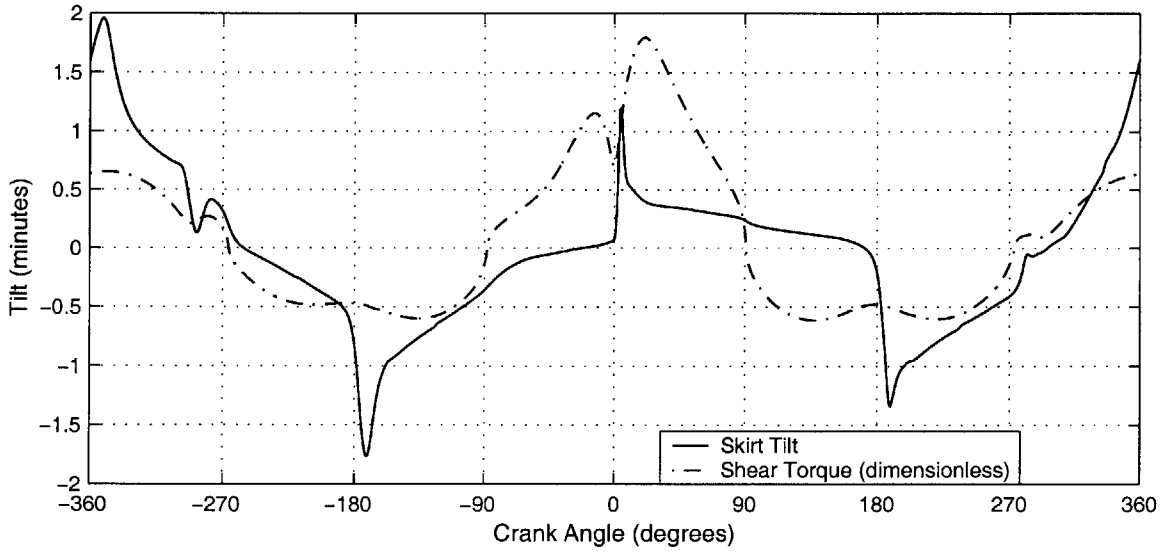

Figure 2.25 Skirt tilt with dimensionless skirt shear torque

It is immediately evident that the tilting motion of the skirt is markedly different to that in the mono piston case. The reason for this is that the tilt for this articulated piston is not controlled by the hydrodynamic side forces, but by the shear torque. The minimum point on the skirt profile for the piston under consideration is very close to the wrist pin axis (2mm below). Because of this, there is no significant moment produced by the hydrodynamic forces until the skirt tilt gets quite large (moving the minimum point away from the wrist pin axis). Hence, the skirt motion tends to be predominantly driven by the

shear torque acting on it. When the shear torque begins to move the skirt away from the vertical, there is little hydrodynamic resistance to the motion as the tilt is small. The skirt is thus accelerated by the shear torque until the tilt becomes quite large. When this happens, a large squeezing moment is induced which tends to slow the angular motion. Subsequently, the sliding moment increases in size due to the small clearance between the skirt and liner and the distance between the minimum point and the wrist pin axis which has increased with the tilt. This large sliding moment tends to push the skirt back towards the vertical. The squeezing and sliding moments for each side of the skirt can be seen in figures 2.26 and 2.27.

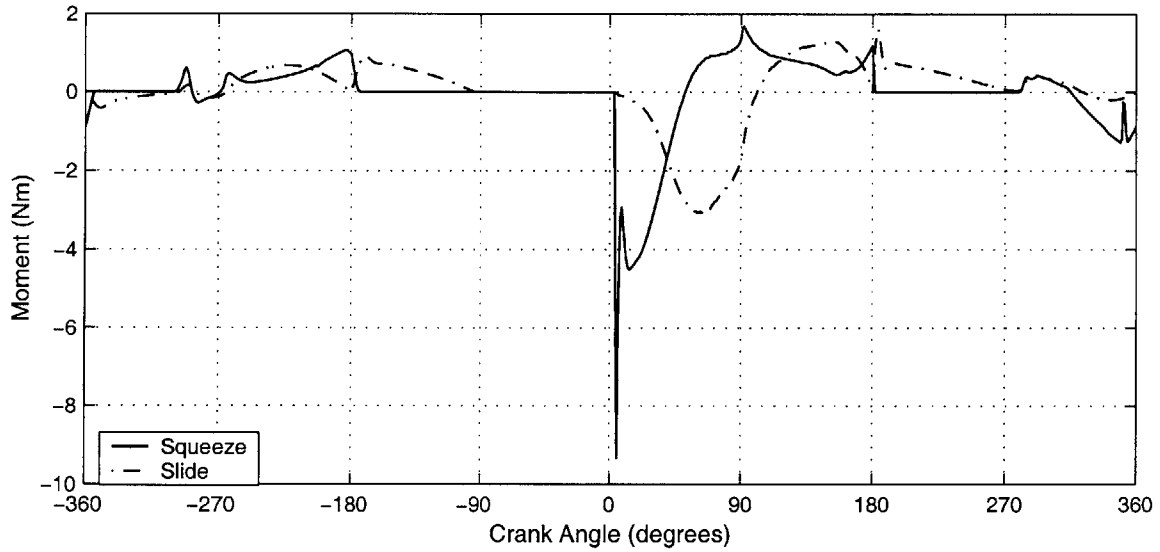

Figure 2.26 Skirt thrust side hydrodynamic moments

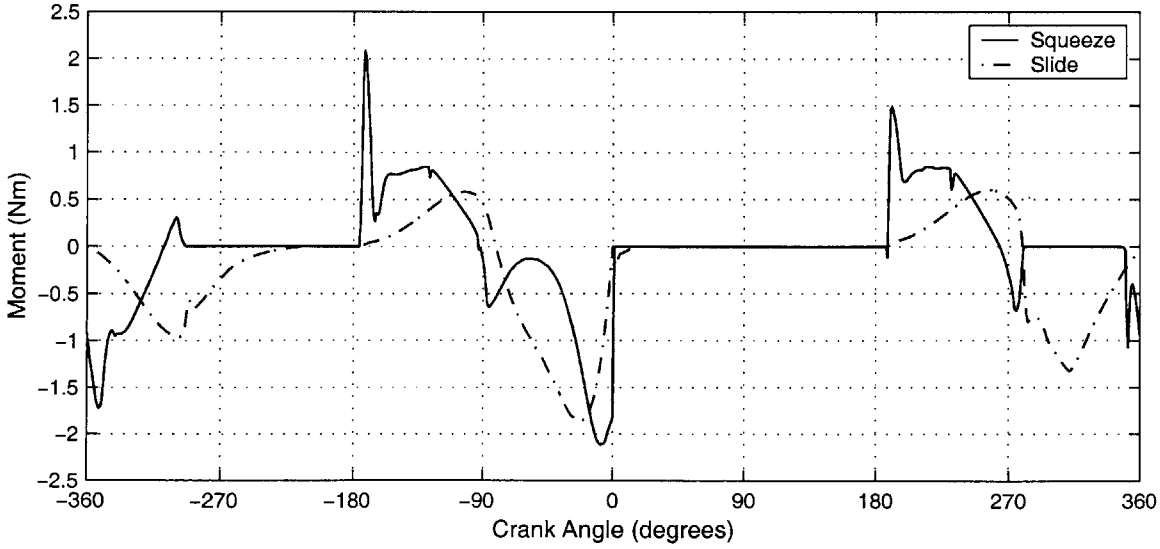

Figure 2.27 Skirt anti-thrust side hydrodynamic moments

In the absence of any large side forces, the motion of the crown is almost completely driven by the shear torque from the wrist pin. The angular motion is retarded by both the crown hydrodynamic moments and the moment due to the lateral ring friction. The latter moment becomes particularly important during the end of the compression stroke and the early part of the power stroke, when the asperity contact ratio becomes large (see figure 2.8). The crown tilt and pin shear torque are shown in figure 2.28.

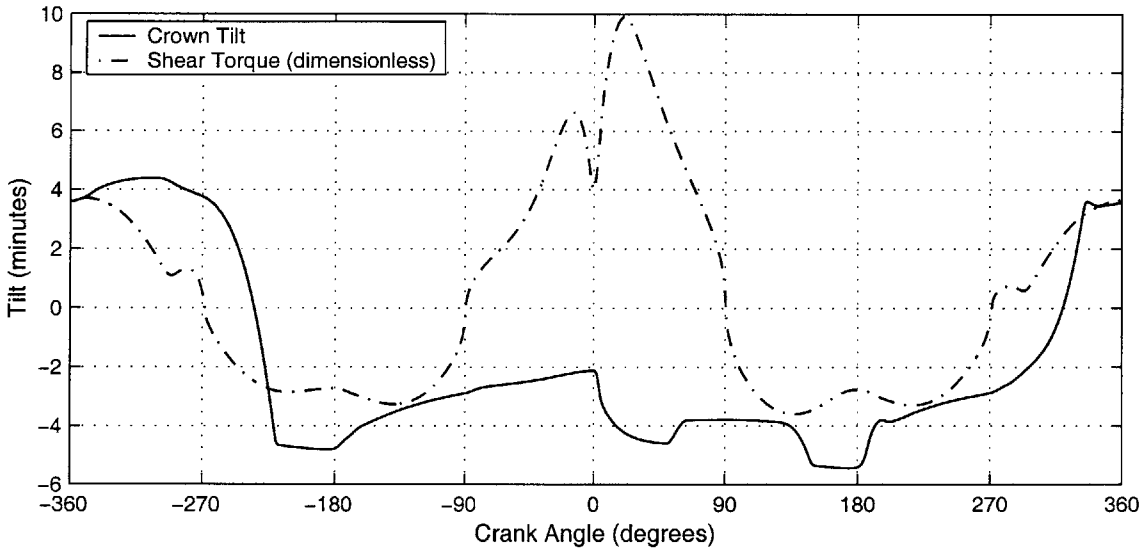

Figure 2.28 Crown tilt with dimensionless crown shear torque

During the intake and exhaust strokes, the crown motion is controlled almost exclusively by the shear torque. Once the shear torque changes direction to become positive in the middle of the exhaust stroke (at $\theta = 270°$), the crown is tilted in the positive direction until the contacting land comes up against the liner wall on the thrust side (the motion of the crown contacting land can be seen in figure 2.28). Since the oil film is very thin on the liner in this area ($\approx 10\mu m$), the contacting land comes very close to the liner before it is stopped by the hydrodynamic force (minimum oil film thickness' for both sides of the crown are shown in figure 2.29). While the shear torque remains positive, the crown is held against the liner wall. Once the shear torque changes back to a negative value at the middle of the intake stroke (at $\theta = -270°$), the crown is tilted back until the contacting land comes up against the anti-thrust side liner wall. This type of angular motion would continue throughout the entire cycle in the absence of any other retarding moments.

However, during the compression and power strokes, the ring friction moment becomes large and essentially holds the crown in a negative tilting mode, not allowing it to tilt towards the thrust side. The moment produced by the lateral ring friction can be seen in figure 2.30.

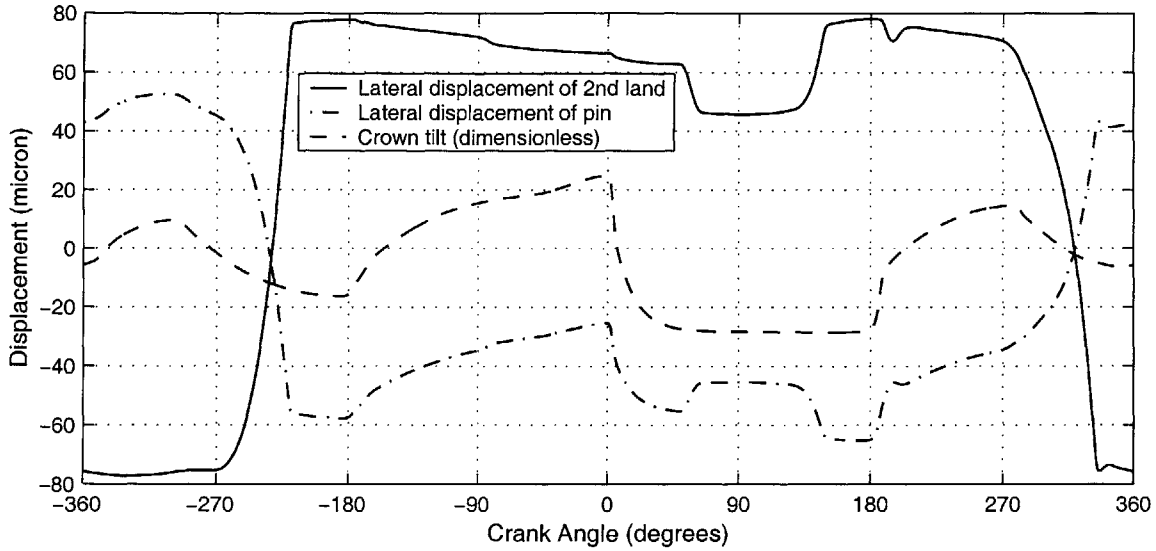

Figure 2.29 Motion of the crown contacting land (2nd land) with lateral and angular motion of the crown

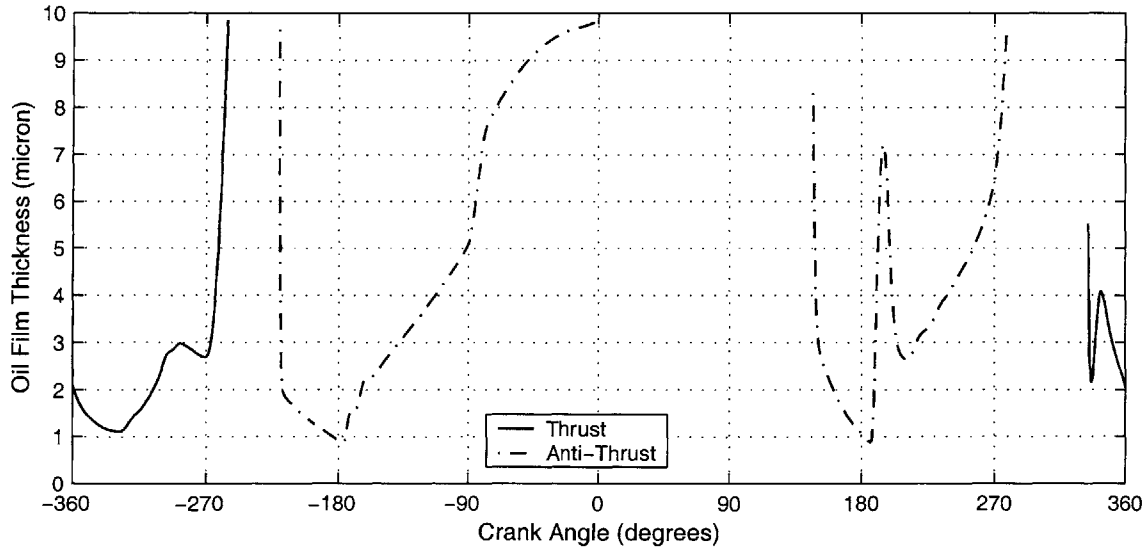

Figure 2.30 Minimum oil film thickness for both sides of the crown

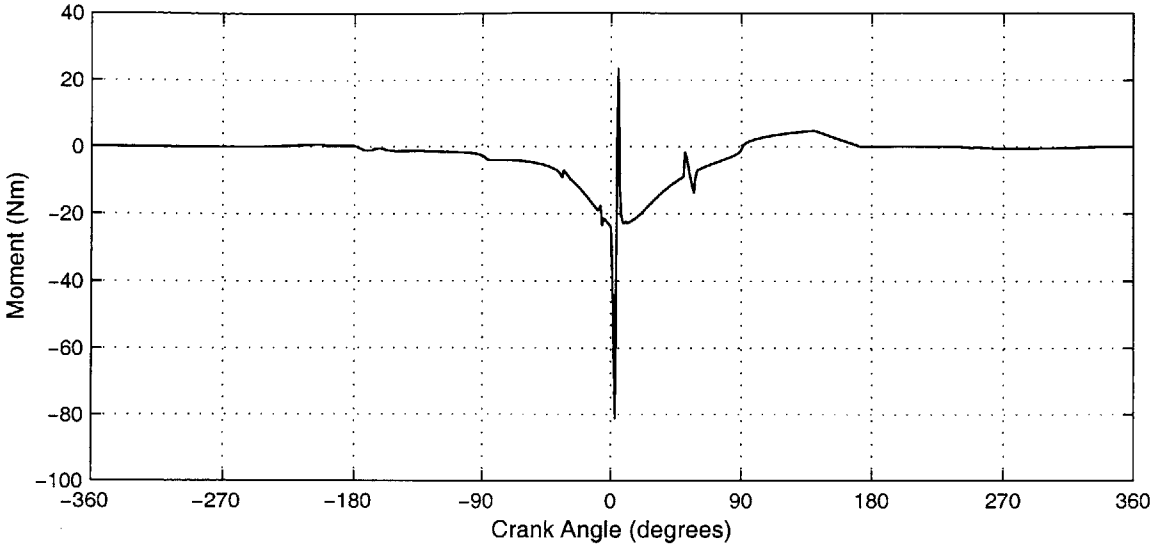

Figure 2.31 Moment due to lateral ring friction

Figure 2.28 also illustrates the effect that the lateral motion of the wrist pin bearing has on the crown angular motion. Even though there is a large positive shear torque acting on the crown through top center, it can be seen to tilt markedly in the negative direction immediately after the top center position. This motion is due solely to the acceleration of the wrist pin center towards the thrust side during piston slap, which produces a negative moment on the crown.

In general, the motion of the crown is controlled by the balance between the driving shear torque and the retarding ring friction. When the ring friction is low, the crown is rotated from one side of the bore to the other when the shear torque changes direction. When the ring friction is high, the crown is essentially held at a particular orientation.

2.7 Summary of First Generation Models

The models that have been described in this chapter can be considered as the first generation in the overall development of a complete secondary motion simulation. In developing these first generation models, the primary goal was to incorporate the general dynamics model with a fast and efficient code. Several simplifying assumptions were made along the way to avoid excessive computation effort. The results presented thus far indicate that the models are physically consistent and stable. However, the primary value of these first generation models was to gain an understanding of the physics involved in the system, and they are not expected to yield numerically accurate results. As described in the previous sections, the first generation models give an excellent insight into the driving forces behind the secondary motion of the piston system. Armed with this knowledge, the models can be improved and advanced by focusing attention on those factors which have the greatest influence on the overall motion of the system.

For the mono piston model, the dynamics and the driving forces behind the motion are well understood and modeled in first generation code. The area that requires further development is the modeling of the hydrodynamic forces and moments. In particular, the most important step required to yield more accurate results from the model is the inclusion of skirt elastic deformation. It is known that the piston skirt deforms elastically during the cycle due to both pressure and temperature effects. The magnitude of these deformations is similar to the currently predicted oil film thickness. The first generation code has illustrated that the running profile of the skirt is a crucial element in determining the hydrodynamic forces and can have a great influence over the overall motion. Hence, inclusion of the skirt deformation is vital if the hydrodynamic forces are to be determined accurately.

For the articulated piston model, it is also extremely important to include the effects of skirt deformation for the same reasons just mentioned. However, of primary importance

in the study of engine oil consumption is the tilting motion of the crown. It has been illustrated in the first generation model that the crown motion is not greatly influenced by the skirt-liner hydrodynamics. As mentioned earlier, the crown motion is determined by the balance between the driving shear torque from the wrist pin and the retarding lateral ring friction. In order to develop the model further, both of these mechanisms must be looked at more closely. In the case of the wrist pin shear torque, a relatively simple correlation has been used in the first generation model, and this must be replaced with a more rigorous hydrodynamic model.

Chapter 3

Improvements to the Hydrodynamic Model

3.1 Introduction

As mentioned in the previous chapter, it is essential to include the effects of skirt deformation into the model in order to improve the accuracy of the results. The skirt deforms during the cycle due to both temperature and pressure effects. The thermal deformation can easily be computed at the start of the simulation based on an operating temperature and a thermal deformation matrix, and is then considered as steady-state throughout the rest of the cycle. However, the pressure deformation is dependant on the local pressures on the piston, and must be computed at each time-step throughout the cycle. While pressure deformation is caused by the local pressures both on the top of the piston and on the skirt faces, it is only the pressures acting on the skirt faces that will be considered. Inclusion of skirt pressure deformation effects complicates the hydrodynamic calculation considerably.

In the absence of any deformation considerations, the hydrodynamic model seeks to solve only the Reynolds equation for the oil film, which can be expressed in the following manner,

$$hydrodynamic\ pressure = f(separation)$$

Inclusion deformation effects requires solution of the deformation equation which can be expressed as follows,

$$separation = g(hydrodynamic\ pressure)$$

It is clear from this that the Reynolds equation and deformation equation are coupled and so must be solved in parallel. This requires the use of an iterative solution scheme. The deformation equation can be expressed in more detail as follows

$$h(x,y) = \iint K_r(x,y,x',y')[p(x',y')]dx'dy'$$

where $h(x,y)$ refers to the deformation at a point on the skirt defined by the co-ordinates x

and y, K_r is the deformation matrix and p is the total pressure on the skirt at the point in question. This total pressure is actually the sum of both the contact pressure and the hydrodynamic pressure, but for the current model only the hydrodynamic pressure will be considered. In order to solve this equation, the hydrodynamic pressure must be explicitly known at each discrete point on the skirt surface. In the context of the current model, this means that the pressure distribution must be determined for a series of circumfrentially distributed axial lines. The hydrodynamic model presented in the last section determines the full axial distribution of the *squeezing* component of the pressure, but does not determine the sliding pressure distribution. This simplified approach to treating the sliding pressure term will not allow for the inclusion of deformation effects, and hence a new hydrodynamic model must be developed that can yield a *full* pressure distribution for the skirt.

It has been decided to incorporate an adapted version of the scheme used by Tian [18] in his model of piston ring motion. This scheme solves the hydrodynamics for the oil film between a piston ring and the liner. The essence of the solution scheme is supplement the Reynolds equation with further equations describing the system, and then solve each equation in parallel. This allows for a full solution of the Reynolds equation, including the complete pressure distribution.

3.2 Development of the New Hydrodynamic Model

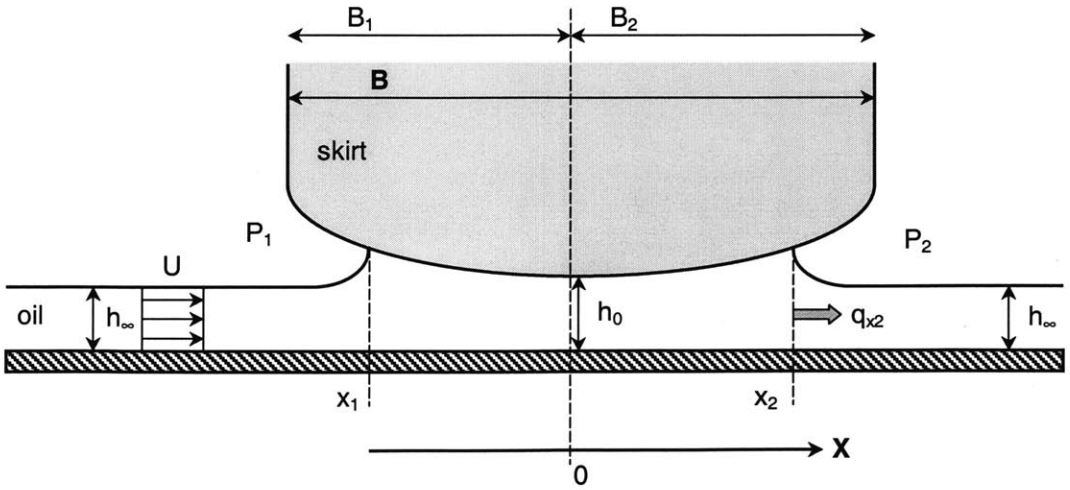

Figure 3.1 Schematic of skirt-liner hydrodynamic system

Consider the sketch of the skirt-liner hydrodynamic system in figure 3.1. Note that for convenience, the skirt has been chosen as the frame of reference, and hence the oil is considered to move along the liner with the same velocity as the piston sliding speed (U). The pressure distribution in the oil film is defined by the Reynolds equation,

$$\frac{\partial}{\partial x}\left(h^3\frac{\partial p}{\partial x}\right)=12\mu\frac{\partial h}{\partial t}+6\mu U\frac{\partial h}{\partial x} \tag{3.1}$$

Now, consider a control volume enclosing the oil trapped between the skirt and the liner (i.e. between x_1 and x_2). The oil inflow to this control volume consists of two parts – one due to the flow along the liner and the other one due to the variation of the inlet position x_1. The inflow from the liner can be expressed as,

$$R_{liner}=Uh_{\infty} \tag{3.2}$$

The effect of the variation in inlet position is quite complex in reality, but can be treated in a simplified manner. As depicted in figure 3.1, when the skirt is starved there is a transition region where the oil goes from the free stream height h_∞ to become fully attached at x_1. If viscous diffusion is the only mechanism driving this oil attachment, the length (l_E) of the transition region can be approximated as,

$$l_E\approx\frac{{h_0}^2}{\nu}U \tag{3.3}$$

where ν is the kinematic viscosity of the oil and h_0 is the minimum oil film thickness. Equation 3.3 is obtained by using (${h_0}^2/\nu$) as the estimate for the viscous penetration time in the vertical direction. For the case of skirt lubrication, $h_0\approx 1\mu m$, $U\approx 10m/s$, $\nu\approx 10^{-5}m^2/s$ and $B\approx 30mm$. Thus, it can be concluded that l_E is considerably smaller than the ring width B

$$\frac{l_E}{B}=\frac{{h_0}^2}{\nu}\frac{U}{B}<<1 \tag{3.4}$$

and hence it can be assumed that the free stream oil immediately attaches to the ring at the inlet position x_1. Thus the inflow rate due to the variation of the inlet position (R_{inlet}) can be expressed as

$$R_{inlet}=\frac{dx_1}{dt}\left(h(x_1)-h_{\infty}\right) \tag{3.5}$$

There are two components of outflow from the control volume. The first of these is the outflow along the liner at the exit point q_{x2}. The other is due to the motion of the skirt normal to the liner ('squeeze' motion). This component of the outflow can be expressed as follows

$$flow = \int_{x_1}^{x_2} \frac{dh}{dt} dx$$

The separation h between the skirt and liner at each discrete point can be expressed as follows,

$$h(x) = h_{ref} + \varepsilon + \phi x + h_{pr}$$

where h_{ref} is some reference separation determined by the skirt-liner clearance, ε is the lateral displacement of the piston, ϕ is the piston tilt and h_{pr} is the additional separation due to the machined skirt profile.

Overall, summing the inflows and outflows for the control volume, the continuity equation can be expressed as follows,

$$q_{x2} + \int_{x_1}^{x_2} \frac{dh}{dt} dx - \frac{dx_1}{dt}\left[h(x_1) - h_\infty\right] - Uh_\infty = 0 \tag{3.6}$$

The Reynolds equation (3.1) can be used to derive the following expression for the average flow rate at any point under the skirt,

$$q_x = -\frac{h^3}{12\mu}\frac{dp}{dx} + \frac{U}{2}h \tag{3.7}$$

By applying mass conservation to a control volume between the point x and x_2 the following expression is obtained for the average flow rate,

$$q_x = q_{x2} + \int_{x}^{x_2} \frac{dh}{dt} dx' \tag{3.8}$$

Combining equations 3.7 and 3.8 yields the pressure gradient

$$\frac{dp}{dx} = \frac{12\mu}{h^3}\left[\frac{U}{2}h - \int_{x}^{x_2} \frac{dh}{dt} dx' - q_{x2}\right] \tag{3.9}$$

Integrating this term from x_1 to x_2 and including the pressure boundary conditions yields this final equation,

$$\int_{x_1}^{x_2} \frac{12\mu}{h^3}\left[\frac{U}{2}h - \int_{x}^{x_2}\frac{dh}{dt}dx' - q_{x2}\right]dx - (p_2 - p_1) = 0 \tag{3.10}$$

where p_1 and p_2 are the pressures at either end of the skirt.

A further equation is derived by applying the Reynolds exit condition to the trailing edge of the skirt.

$$\left.\frac{dp}{dx}\right|_{x=x_2} = 0 \tag{3.11}$$

This condition is an empirically derived result for steady state lubrication with a sufficiently high load. Details can be found in [REF]. Combining equation 3.11 with 3.9 yields the following expression,

$$\frac{U}{2}h(x_2) - q_{x2} = 0 \tag{3.12}$$

Now, equations 3.6, 3.10 and 3.12 constitute a system of three equations in the unknown variables x_1, x_2 and q_{x2} which completely describe the hydrodynamics between the skirt and the liner.

Hydrodynamic System Equations

$$F_1 = q_{x2} + \int_{x_1}^{x_2}\frac{dh}{dt}dx - \frac{dx_1}{dt}\left[h(x_1) - h_\infty\right] - Uh_\infty = 0 \tag{3.13}$$

$$F_2 = \int_{x_1}^{x_2}\frac{12\mu}{h^3}\left[\frac{U}{2}h - \int_{x}^{x_2}\frac{dh}{dt}dx' - q_{x2}\right]dx - (p_2 - p_1) = 0 \tag{3.14}$$

$$F_3 = \frac{U}{2}h(x_2) - q_{x2} = 0 \tag{3.15}$$

Solving these three equations concurrently will yield a solution for the wetting condition (i.e. x_1 and x_2) and also for the pressure distribution under the skirt.

3.2 Implementation of the New Hydrodynamic Model

The system of equations 3.13 – 3.15 describes the most general case of skirt wetting, i.e. where both x_1 and x_2 are inside the edges of the skirt. During the course of the cycle either or both of the edges of the skirt may become fully flooded. When this occurs, the number of system variables is reduced and the system of equations must be modified. In all there are four distinct lubrication regimes to be considered in this model, and table 3.1 details each of these and the modifications required for the system equations.

Regime	Description	Changes to system equations
1	Leading edge : starved Trailing edge : Reynolds exit condition $\rightarrow$ x_1 and x_2 must be solved	No changes required
2	Leading edge : starved Trailing edge : fully flooded $\rightarrow x_2 = B_2$, x_1 must be solved	Equation 3.15 becomes $F_3 = x_2 - B_2 = 0$
3	Leading edge : fully flooded Trailing edge : Reynolds exit condition $\rightarrow$ $x_1 = -B_1$, x_2 must be solved	Equation 3.14 becomes $F_2 = x_1 + B_1 = 0$
4	Leading edge : fully flooded Trailing edge : fully flooded $\rightarrow$ $x_1 = -B_1$, $x_2 = B_2$	Equation 3.15 becomes $F_3 = x_2 - B_2 = 0$ Equation 3.14 becomes $F_2 = x_1 + B_1 = 0$

Table 3.1 Description of hydrodynamic regimes

A set of criteria must be developed which govern when the model should transition from one regime to another. For either edge to transition to a fully flooded condition, the criteria is quite obvious, i.e. x_1 or x_2 becomes greater than B_1 or B_2 respectively. Transitioning from fully flooded back to a starved condition requires more detailed

consideration. For the leading edge, transition to a starved condition is set to occur when the oil inflow rate at the leading edge is greater that the free stream oil flow rate, i.e. when $q_{x1} > Uh_{\infty}$. For the trailing edge, the transition to a starved condition is set to happen when the Reynolds exit condition is no longer satisfied, i.e. $dp/dx(x_2) > 0$. A summary of the transition criteria between the various regimes is shown in figure 3.2.

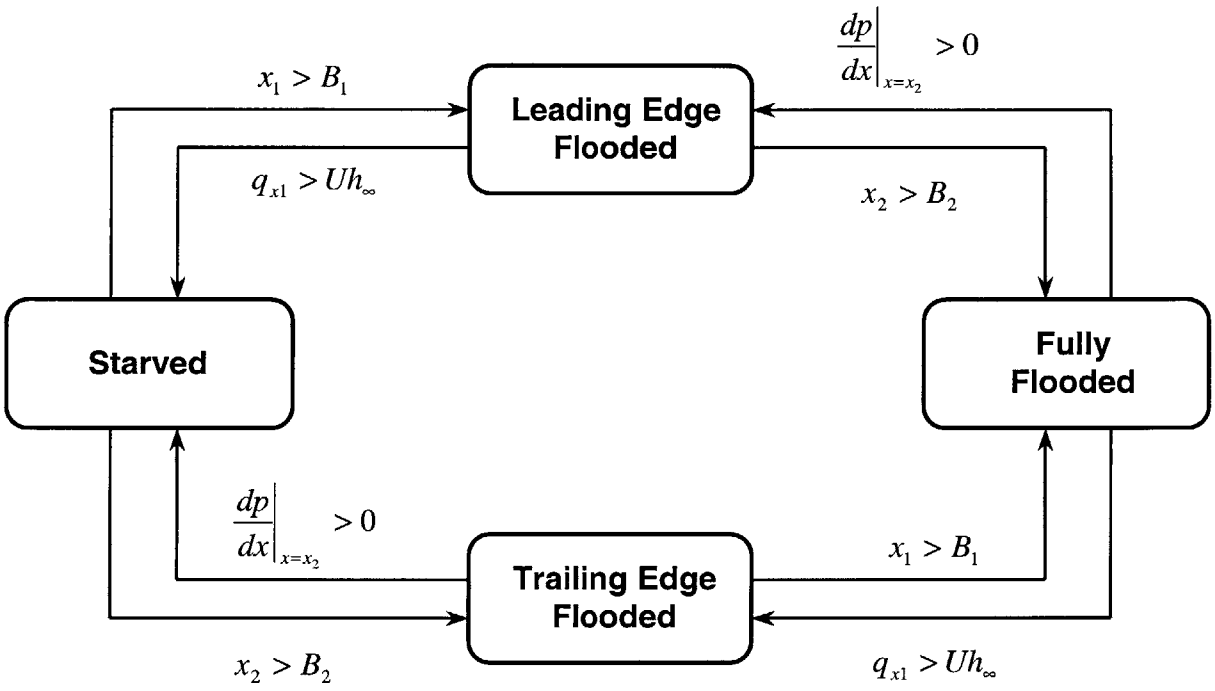

Figure 3.2 Transition criteria for the various hydrodynamic regimes

At each time-step the relevant system equations are solved using a globally convergent Newton method. Each of the equations are normalized, and the Jacobian matrix of partial derivatives is evaluated using analytical partial derivatives. Integration in the axial direction is performed numerically using a grid of 31 node points. In addition to solving the equations for the system unknowns, the pressure gradient is evaluated explicitly using equation 3.9. This pressure gradient is then integrated to yield the full axial skirt pressure distribution.

The new hydrodynamic model was incorporated into the existing mono piston code, replacing the original hydrodynamic calculation while leaving the rest of the code

unchanged. However, it was found that the new hydrodynamic model was unstable and often produced spurious results. After extensive testing and analysis it was determined that the system equations in this new model are finely balanced, and extremely sensitive to both the initial guess and to any perturbations in the external forces. Given a good initial guess the equations could be well solved, and stable behaviour was often exhibited for portions of the cycle. However, once the system was perturbed in some way, the code would struggle to find a solution for the equations, and would often crash.

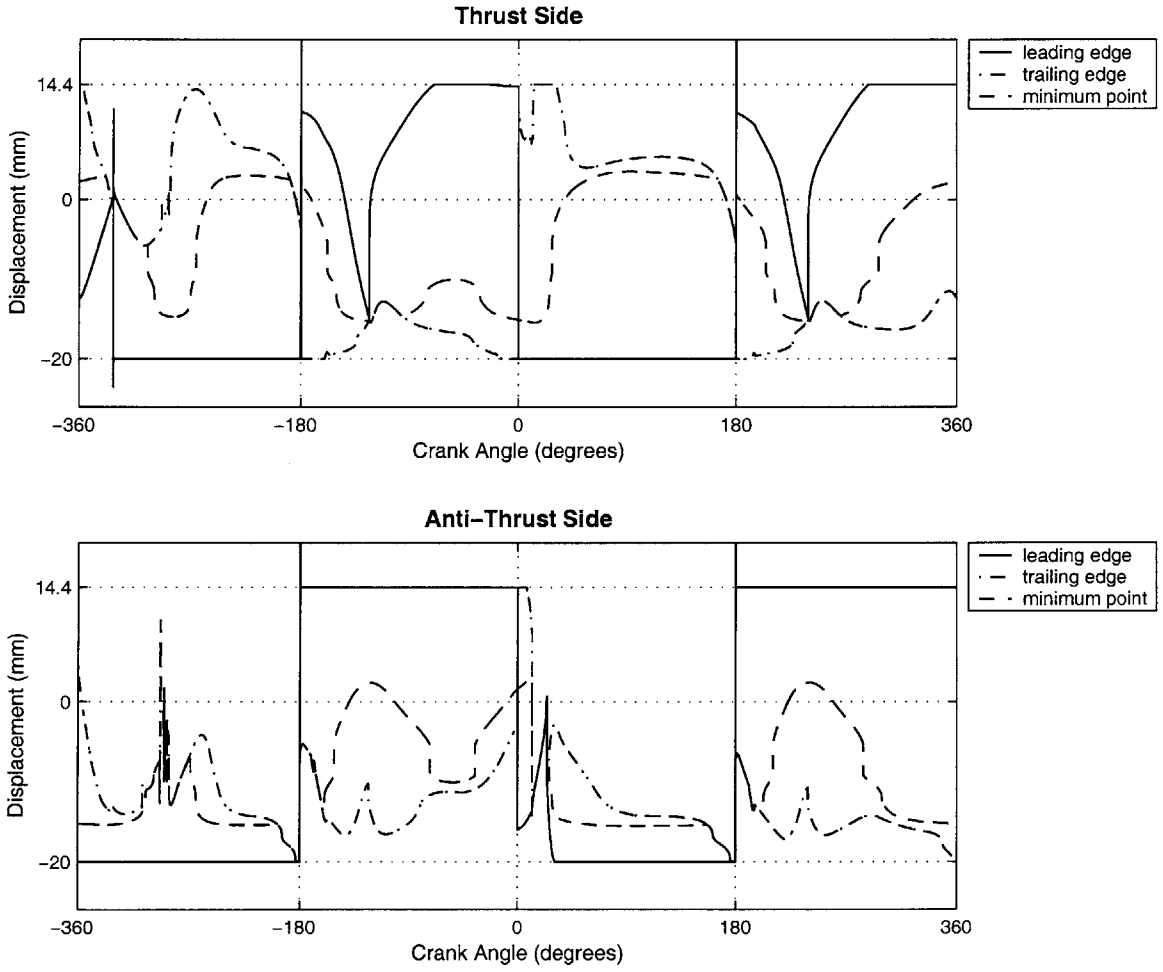

Figure 3.3 Wetting condition for thrust and anti-thrust sides with new hydrodynamic model

The major cause of this instability was found to be the re-attatchment of the oil film to the skirt. At certain places in the cylce, the skirt would move away from the liner to an extent where it would no longer be wetted by the oil film. At some subsequent point the skirt would begin to approach the liner again and the oil film would have to re-attatch. Unless an accurate initial guess for the wetting locations was used at this re-attatchment point, the equations could not be solved and the code would crash. Several algorithms were tested to determine an appropriate initial guess, but none produced consistent results. Fine tuning of the code for a specific test case allowed for a complete cycle to be run with this new model. Figure 3.3 shows the results for the wetting locations for this test case.

It can be seen from figure 3.3 that there is an instability on the thrust side just before the middle of the intake stroke. Leading up to this point the wetting locations converge together, i.e. the model predicts that there is no wetting, and the skirt leaves the oil film. Shortly afterwards, the skirt moves back and re-attatches to the oil film. At this point the model struggles to find a solution, and the results fluctuate for several degrees before a stable solution is found. In this particular case the model was able to regain control after the instability, but generally this is not the case and the code crashes.

It is felt that the fundamental reason for the sensitivity of the system equations is the relative magnitude of the squeeze and slide components of the hydrodynamic pressure in the case of skirt lubrication. In ring lubrication, for which this scheme was developed and works well, the squeeze component of the hydrodynamic pressure is considerably smaller than the slide component for the majority of the stroke, due to the small ring width. However, in skirt lubrication the squeeze component of the pressure is of the same magnitude as the slide component for the entire cycle, i.e.

$$\frac{\frac{dh}{dt}}{U\frac{dh}{dx}} \approx \frac{B}{stroke} \approx \frac{1}{2}$$

where B is the width of the skirt.

Balancing the system equations is a far more difficult task when dealing with large squeeze forces, and thus it was decided not to pursue this hydrodynamic scheme any further until greater stability could be achieved in the results.

Instead, an alternate approach was developed which combines aspects of both the original hydrodynamic model and this new scheme. The original model was able to compute the squeeze component of the hydrodynamic pressure accurately by solving the squeeze part of the Reynolds equation. The deficiency of the original model was in it's cmputation of the slide force, in which no explicit calculation was made of the pressure distribution. Thus, a hybrid scheme has been developed in which the new hydrodynamic model is adapted to compute only the *sliding* component of the hydrodynamic pressure and this calculation is coupled with the squeeze calculation from the original model. This scheme yields a full pressure distribution due to both squeeze and slide effects, and is thus suitable for coupling with a deformation calculation.

The new hydrodynamic model is easily adapted to compute the slide pressure by eliminating all the unsteady terms from the system equations (3.13 – 3.15). This slide calculation is performed first in the hybrid scheme, and the wetted region computed is then passed on to the squeeze calculation. The hybrid scheme is found to be extremely stable and robust and produces accurate results not only of the pressure distribution, but also for the wetted region on the skirt.

3.4 Sample Results from the New Hydrodynamic Model

The mono piston code with the revised hydrodynamic model was run for exactly the same engine and baseline condition as that described in table 2.2. The results are now compared to those generated by the original model.

Figures 3.4 and 3.5 illustrate the wetting conditions for both the new and old models.

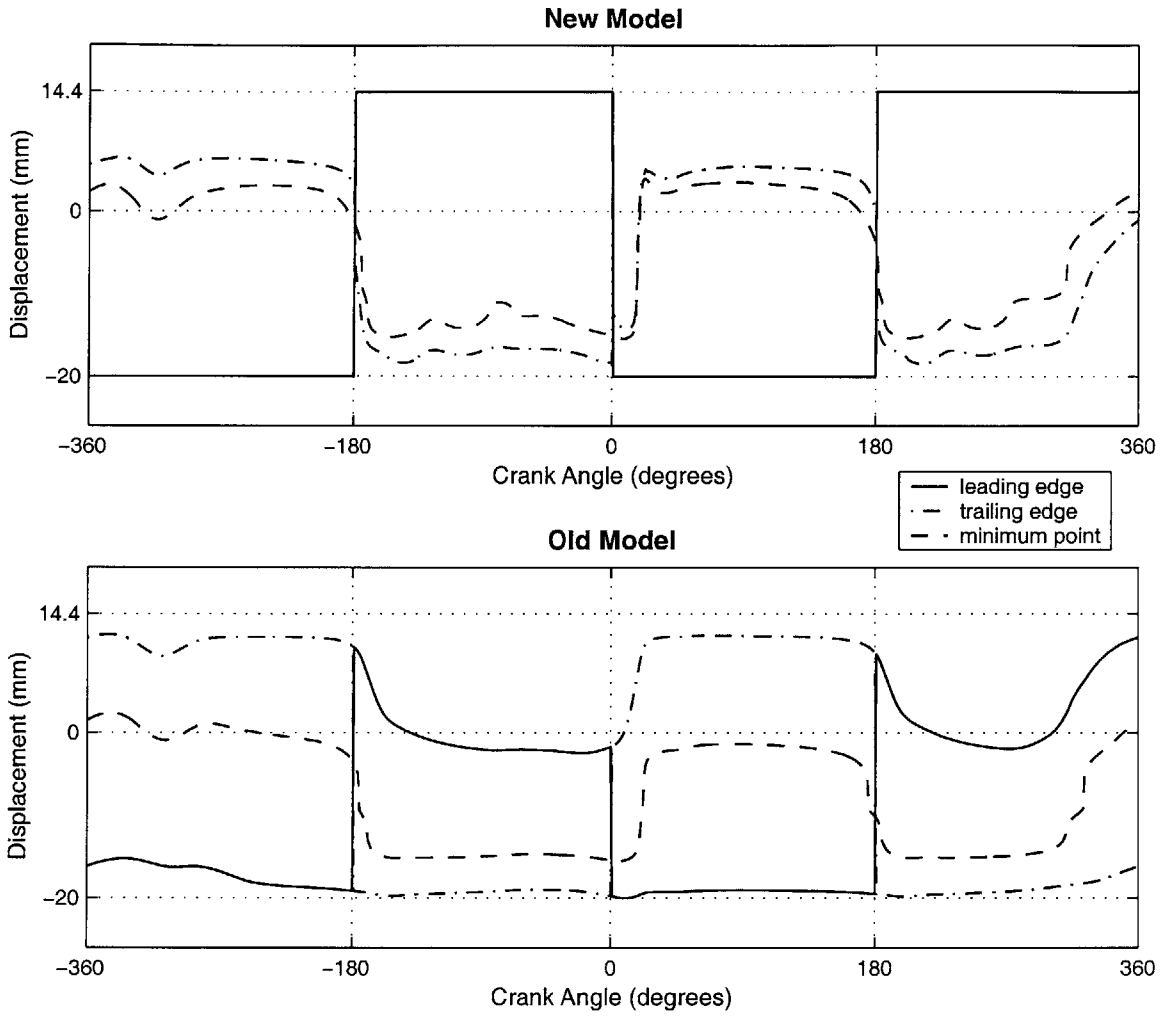

Figure 3.4 Thrust side wetting condition for new and old model

It is immediately apparent that the results for the revised model differ considerably from those for the old model. The old model simply assumed that a certain oil film thickness remained undisturbed on the liner, and computed the wetted region by finding the geometrical intersection of the skirt profile and this imaginary oil line. With the revised hydrodynamic model, a supply of oil is specified for the skirt and the actual wetting locations are computed concurrently with the hydrodynamic pressure. Hence the wetting locations become an integral part of the system solution. This is one of the major benefits of this type of analysis, and leads to far more realistic results. Even the more complex two dimensional hydrodynamic solution schemes, such as the finite difference and finite element methods, do not yield solutions for the wetting conditions in this way.

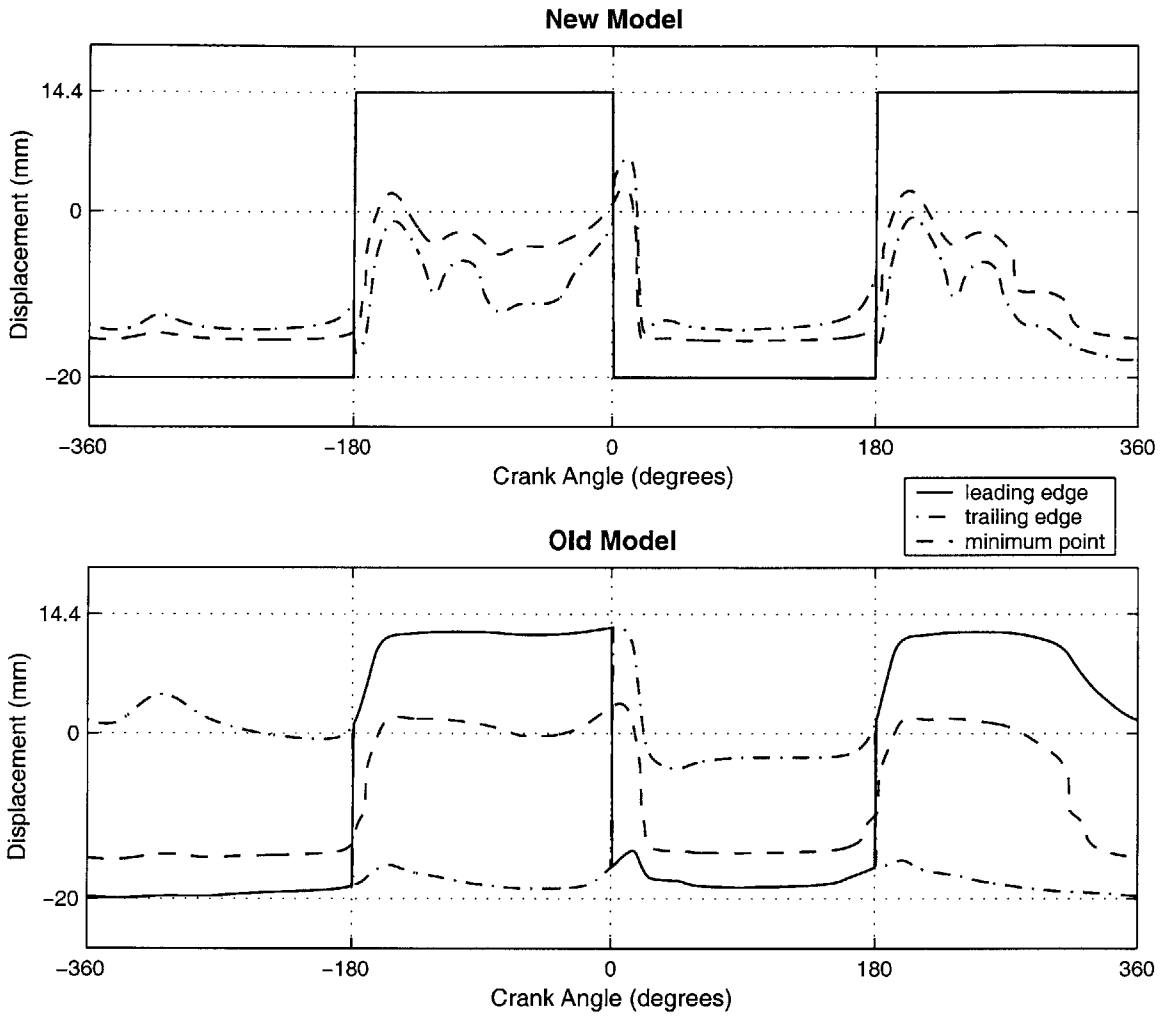

Figure 3.5 Anti-thrust side wetting condition for new and old model

The first major difference that can be seen with the revised hydrodynamic model is that the leading edge remains fully flooded throughout the cycle. This is far more realistic than the solution for the old model, and is due to the fact that oil builds up at the leading edge of the skirt as it slides along the liner. Another major difference with the new model is that the location of the trailing edge is far more sensitive to the lateral position and tilt of the piston. This is due to the fact that the wetting solution is so dependant on the hydrodynamic pressure, which is very sensitive to the piston motion (the trailing edge location is actually determined by enforcing the Reynolds exit condition). It can also be seen that the wetted region is much narrower on the down stroke for the new model. This is especially apparent for the anti-thrust side (see figure 3.5). The reason for this is that the minimum point on the skirt profile is *below* the wrist pin axis and hence there is a

large diverging section leading up the trailing edge on the down stroke. This diverging section tends to reduce the pressure in the oil film and the solution for the trailing edge moves forward in order to preserve the Reynolds exit condition.

Figures 3.6 and 3.7 compare both the lateral and angular motion of the piston for the two models.

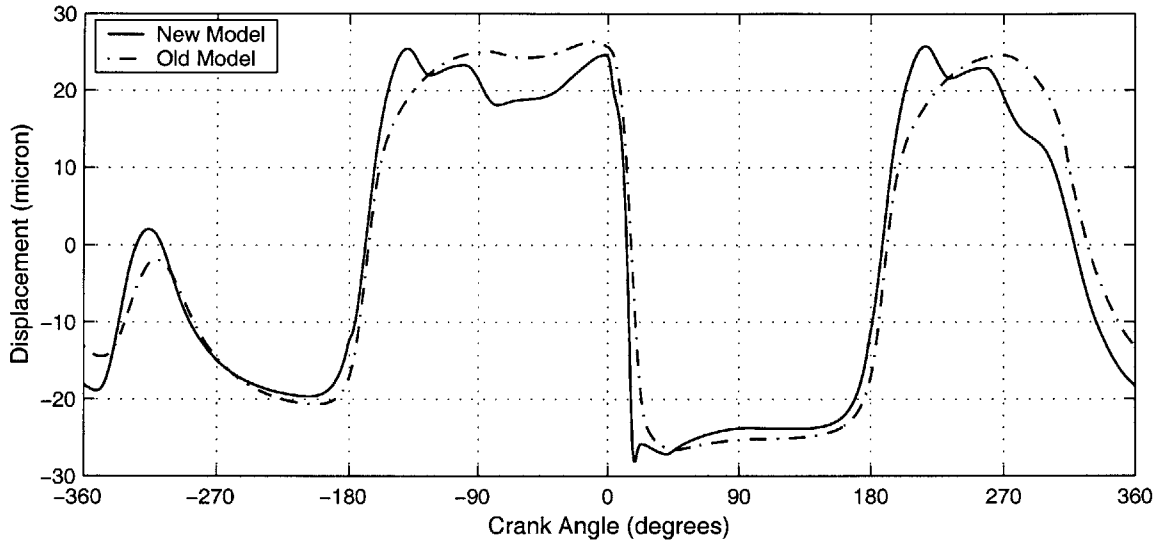

Figure 3.6 Lateral motion for both new and old models

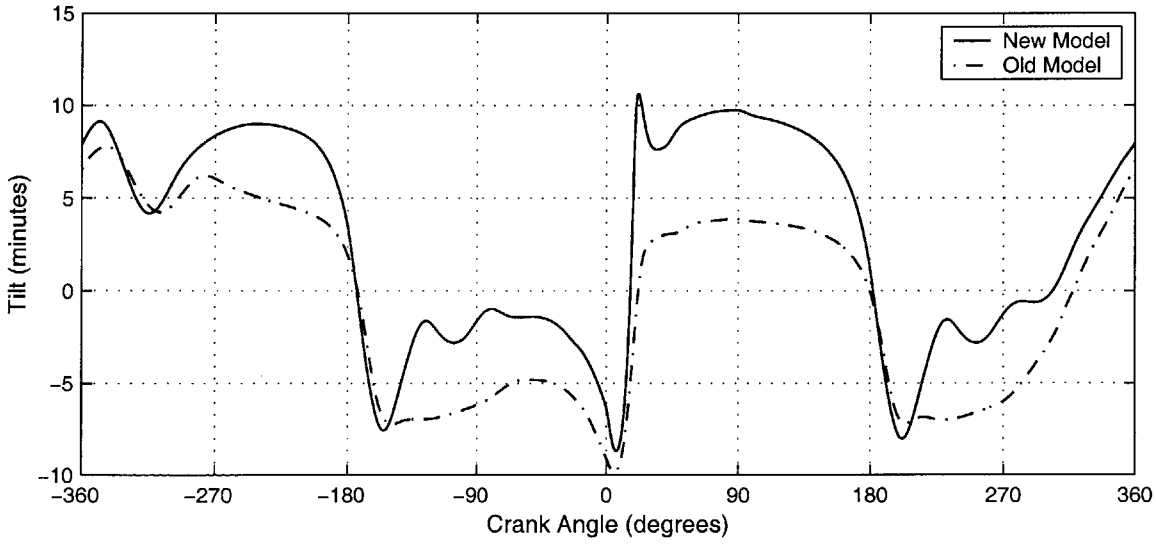

Figure 3.7 Angular motion for both new and old models

It can clearly be seen that the new model predicts a more violent piston slapping motion than the old model. The main reason for this is the fact that the wetted region on the thrust side is very narrow immediately after top center with the new model (see figure 3.4). In fact the wetted region predicted by the new model is approximately three times narrower than that given by the old version. A narrower wetted region means less oil to slow and absorb the motion of the piston, and in order to produce the force required to retard the piston, the oil film thickness must get much smaller. This is illustrated in figures 3.8 and 3.9, where the minimum oil film thickness for both models are compared.

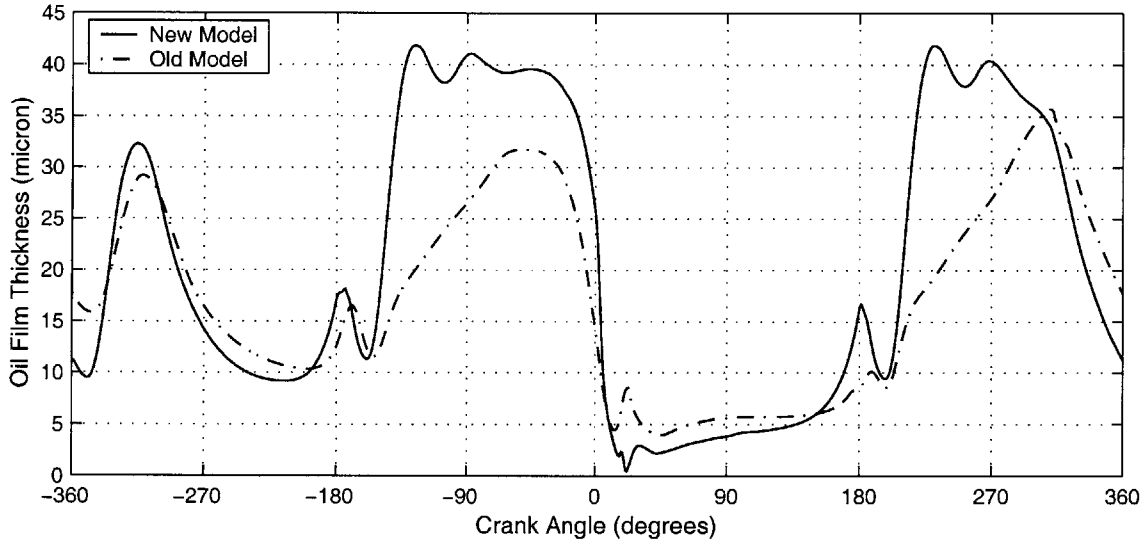

Figure 3.8 Thrust side minimum oil film thickness for both models

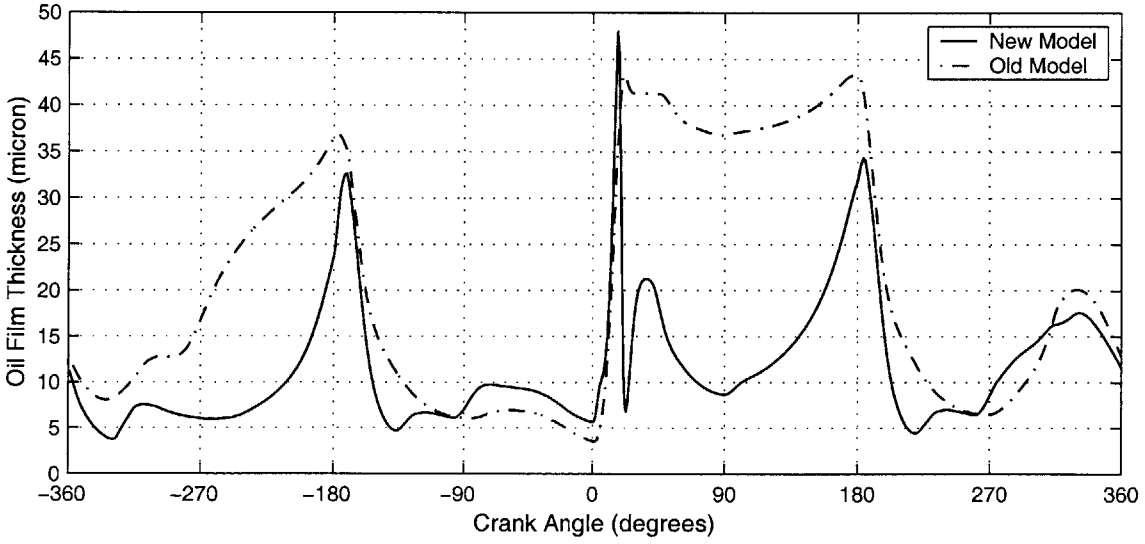

Figure 3.9 Anti-thrust side minimum oil film thickness for both models

The piston can clearly be seen to 'bounce' against the liner wall during slap, a situation that has been shown by experiment to occur in real engines.

The positive piston tilt associated with the slapping motion is also seen to be much more pronounced with the new model, and indeed the new model predicts much higher piston tilt throughout the rest of the power stroke (and also throughout the latter part of the intake stroke). This higher tilting during the down strokes is largely due to the narrower wetted regions that occur on both sides of the skirt. During the down stroke, the connecting rod imparts a side force towards the thrust side of the liner. This side force combines with the hydrodynamic force produced on the thrust side to form a couple, giving a positive moment to the piston (as described in figure 2.10). In the new model, the wetted region on the thrust side is concentrated more towards the lower part of the piston than in the old version. This, coupled with the fact that the sliding force is now distributed over the *entire* wetted region, means that the resultant hydrodynamic force acts lower down on the skirt, producing a bigger positive moment. This larger moment tends to tilt the piston to a greater extent, letting the lower part of the anti-thrust side get much closer to the liner wall than in the original model (see figure 3.8).

Figure 3.7 indicates that during the up stroke, the piston has a more positive tilt with the new model than with the old, and that this tilt fluctuates somewhat. During the up strokes the side force directed is towards the anti-thrust side. The wetted region on the anti-thrust side with the new model is again concentrated more towards the leading edge of the skirt (the top edge in this case). This means that the resultant hydrodynamic force from the thrust side acts higher up the skirt than with the old model, and so produces a greater positive moment. This can clearly be seen in figure 3.10 which shows the hydrodynamic moments for the anti-thrust side of the skirt. This bigger moment from the anti-thrust side causes the piston to tilt less in the negative direction during the up stroke. Having an essentially neutral tilt during these periods of the cycle is what leads to the angular fluctuations seen in figure 3.7. The fluctuations are caused by the piston "rolling" about the flat section that exists on the profile around the minimum point. As the piston tilts through the vertical plane, the minimum point moves quickly across this flat section and

the wetted region changes in size rapidly. This causes a rapid change in the hydrodynamic moment, which attempts to tilt the piston back in the opposite direction. The piston is thus in an unstable position when it has a neutral tilt during the cycle, and this instability can cause the fluctuations in angular motion seen in figure 3.7. These variations in tilt also lead to the fluctuations seen in the lateral motion of the piston around the same positions (figure 3.6).

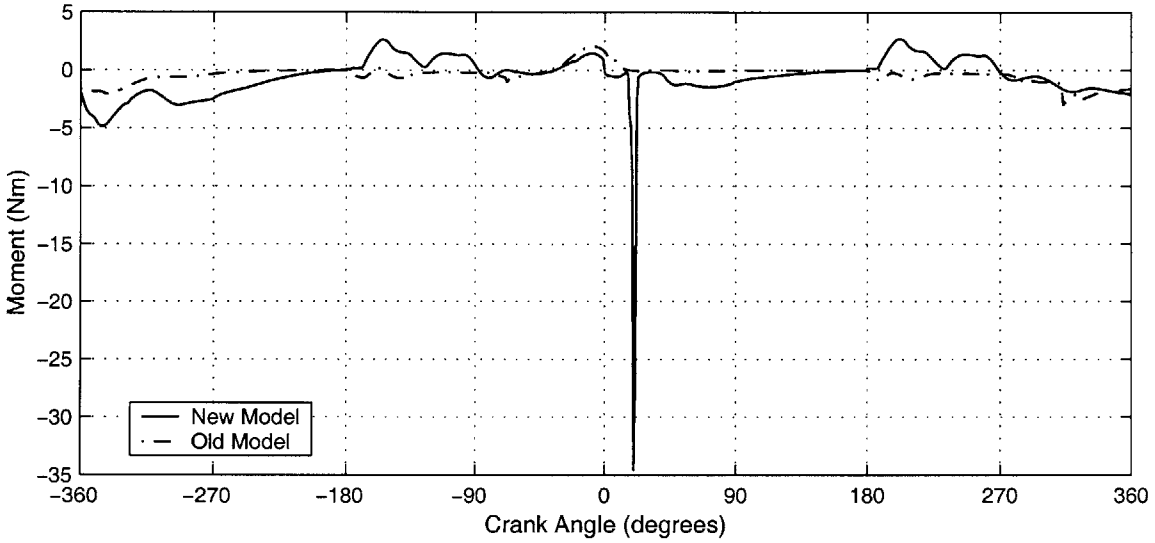

Figure 3.10 Anti-thrust side hydrodynamic moments for both models

3.5 Comparison with Experimental Data

Without the inclusion of skirt deformation in the model, comparisons of the results to experimental data have only a limited relevance. It is expected that deformation will alter the skirt profile, and hence the hydrodynamics, to such an extent that the magnitude of the results will change considerably. However, it is useful at this point to make some general comparisons with experimental data to ensure that the major trends and patterns in the secondary motion are being predicted correctly by the model. To this end, the experimental measurements taken by Ryan et al. [12] were used as a benchmark, and the current model was run using the input data for the experimental engine. Unfortunately,

not all the input data relevant to the engine in [12] was available, and so there are expected to be some slight differences in the results. However, since the purpose of the exercise is only to look for general similarities between model prediction and experimental results, this discrepancy in input data is not seen as a problem.

Figure 3.11 below shows a comparison between the model results for lateral and angular displacement and the experimental measurements of these parameters. Note that the sign convention used in [12] for piston tilt is opposite to the one used in the current model, and so the plot of tilt has been transposed.

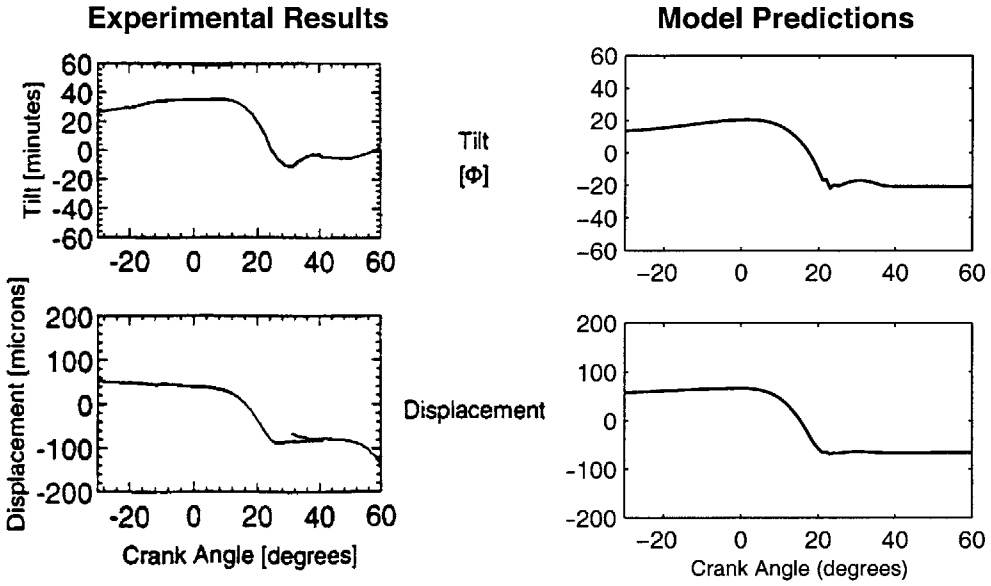

Figure 3.11 Comparison of results with experimental data

Chapter 4

Parametric Studies

In order to provide some preliminary validation for the model and to illustrate it's usefulness in engine analysis, a series of parametric studies were performed on various aspects of engine performance for a standard gasoline engine. The engine analyzed was identical to that described in table 2.2 and the parametric analyses performed are described in the following sections.

4.1 Engine Speed Analysis

An analysis of the effect of engine speed was performed by using the same baseline condition as that described in table 2.2 and varying the speed from 2500 rpm to 5000 rpm. Figures 4.1 and 4.2 show the variation in both lateral and angular displacement of the piston with engine speed.

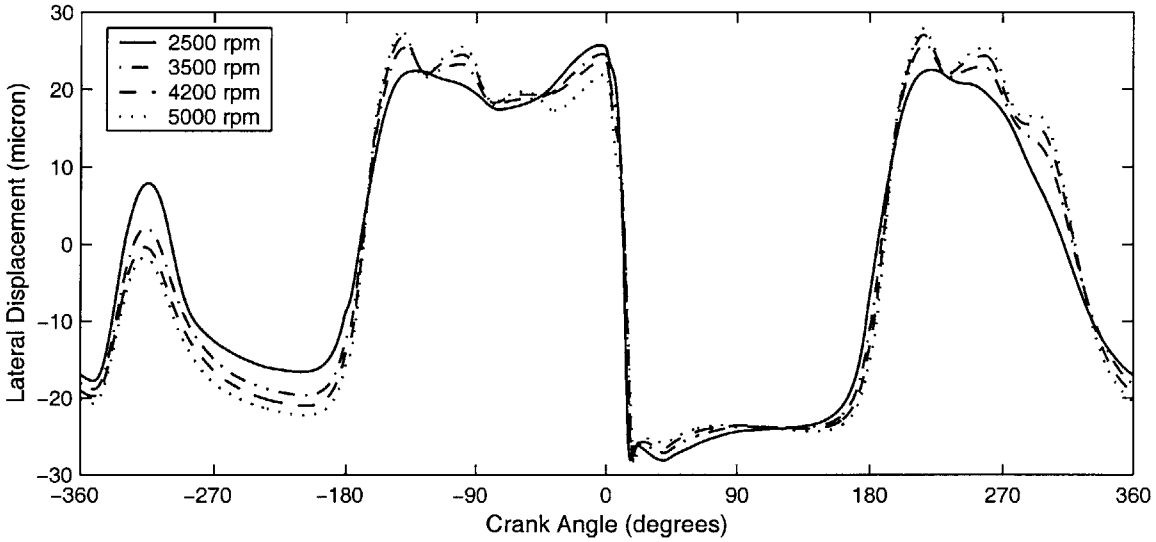

Figure 4.1 Variation in piston lateral motion with engine speed

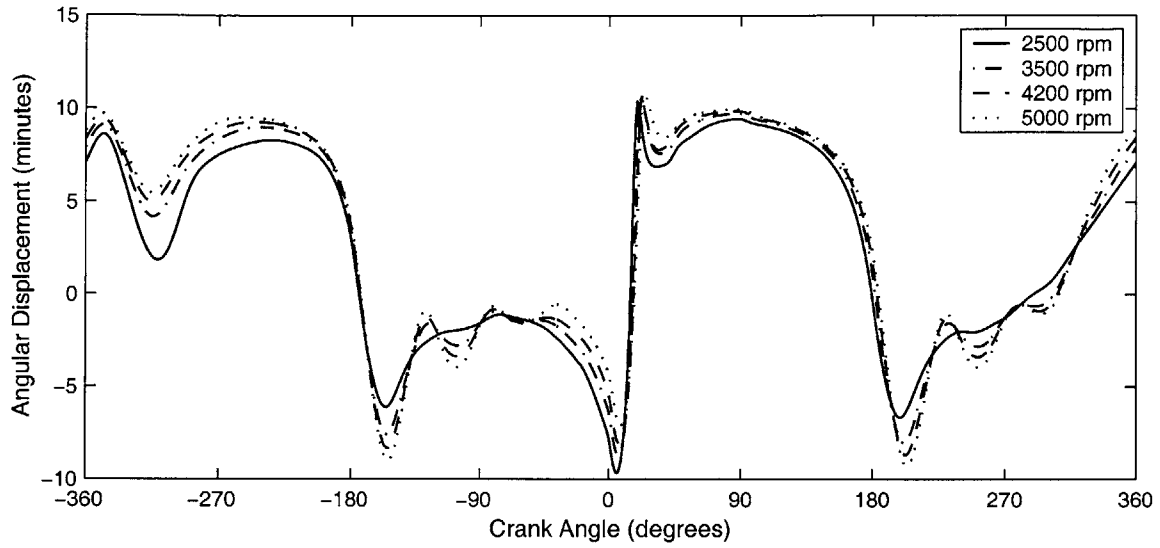

Figure 4.2 Variation in piston tilt with engine speed

In general, the effect of increasing the engine speed is to increase the axial inertia force acting on the piston. This has the general effect that the piston motion is more controlled by the inertia force and less so by gas pressure. It is apparent from figure 4.2 that the major effect of engine speed on the motion occurs where gas pressure is lowest and mainly during the mid stroke regions where piston sliding speed is the highest. In these regions there is generally a greater magnitude of both lateral and angular motion with higher engine speed as well as larger fluctuations in each of these parameter. The greater magnitude of motion is due the additional force acting on the system, and can be seen clearly in figure 4.3 which depicts the hydrodynamic forces acting on both sides of the piston. The hydrodynamic force is a direct response to the driving side force acting on the piston, and when the inertia force is increased, the side force increases accordingly, causing higher hydrodynamic forces to be induced. The biggest increases in hydrodynamic forces can be seen to occur during mid stroke due to the higher piston sliding speed, and this is what leads to the greater magnitude of piston motion in these regions.

As described in chapter 3, the cause of the fluctuations in both lateral and angular motion is the "rolling' of the piston about the vertical position when the tilt is close to neutral. This "rolling" is due to the flat region that exists on the skirt profile about the minimum

point. With higher engine speed, the angular velocity induced in the piston during this "rolling" is higher and hence the piston has a greater angular momentum. This extra angular momentum causes the piston to tilt further before it is retarded by the hydrodynamic moments from the oil film. Hence, the fluctuations in both angular and lateral motion are greater with higher engine speed as illustrated in figure 4.2.

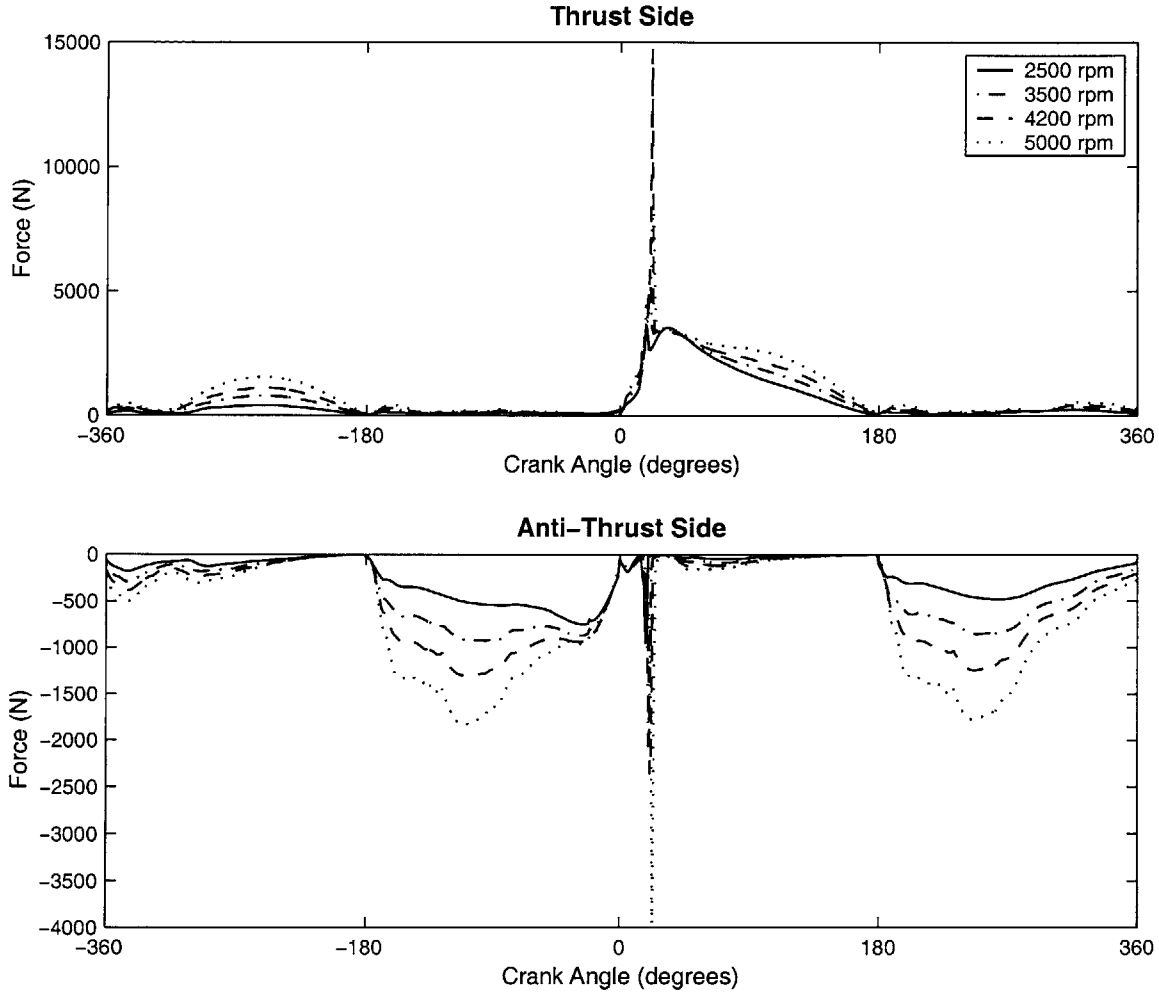

Figure 4.3 Variation of hydrodynamic forces with engine speed

Higher engine speed also causes the piston slap motion to be more violent. The increased velocity of the piston throughout the cycle leads to a more rapid movement across the bore during slap. This means that at higher engine speed the piston carries a lot more momentum into the collision with the liner wall during slap. This increased momentum drives the piston closer to the wall before it is retarded by the hydrodynamic force, and also causes more "bounce" to occur. The hydrodynamic force induced in the oil film

increases accordingly with engine speed, due to the higher piston momentum carried into the impact. Figure 4.4 highlights the hydrodynamic forces for both sides of the piston during the period of slap.

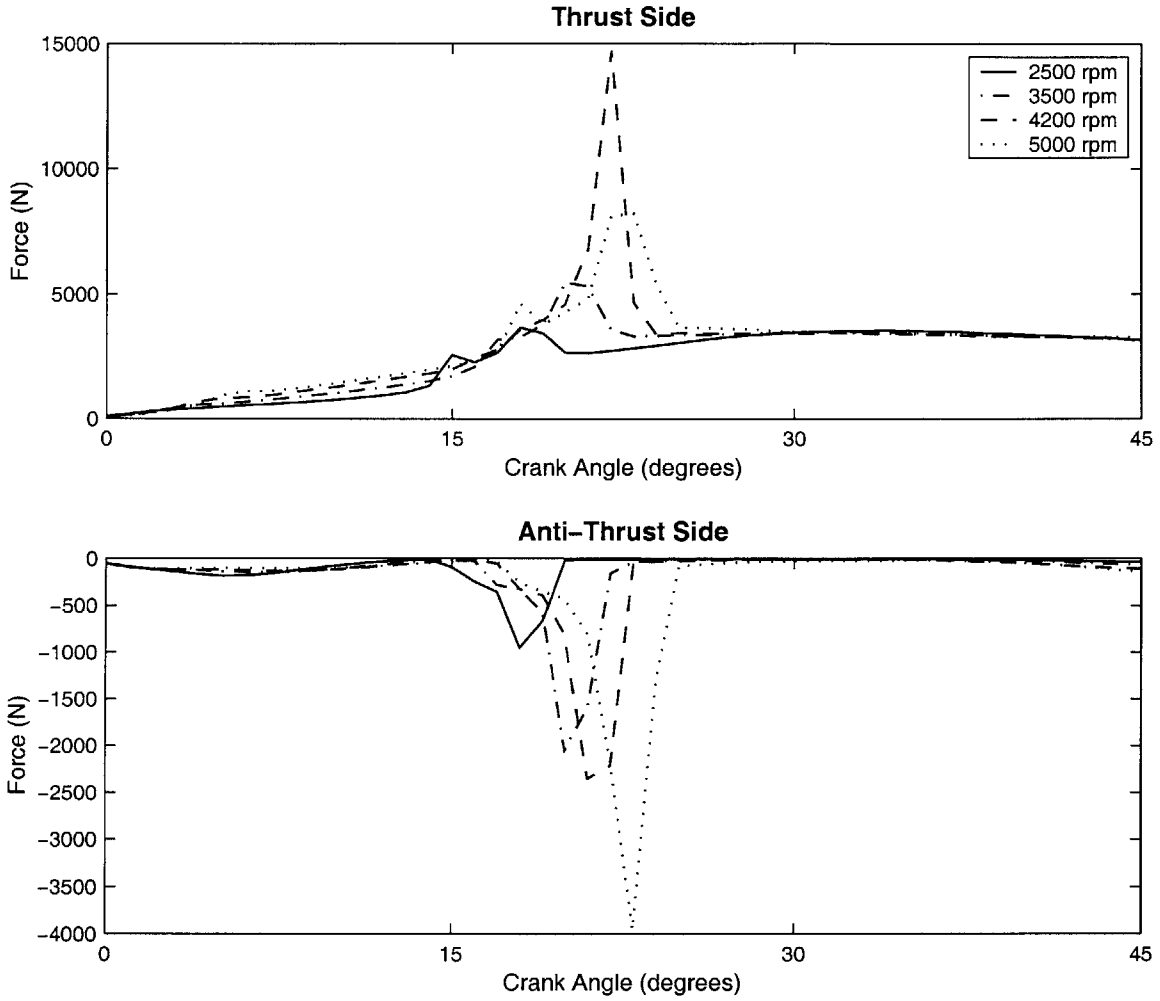

Figure 4.4 Variation of hydrodynamic forces with engine speed during period of piston slap

It can clearly be seen that the peak hydrodynamic force on both sides increases with increasing engine speed. The fact that there is such a peak in hydrodynamic force on *both* sides of the skirt illustrates very clearly that piston slap is a combination of both lateral *and* angular motion. As the piston is accelerated across the bore towards the thrust side, it is also given an angular acceleration in the positive direction. Hence when impact occurs, it is the upper part of the thrust side and the lower part of the anti-thrust side that collide

with the oil film on the liner wall. It can also be seen from figure 4.4 that the peaks in hydrodynamic force occur later in the stroke with increasing engine speed. The reason for this is that the initial side force that causes piston slap is due to the hydrodynamic interaction of the skirt and the liner, and thus is not completely dependant on engine speed. Hence, as the engine speed is increased the slap force does not increase proportionately and so acceleration of the piston across the bore takes longer (in crank angle degrees).

4.2 Engine Load Analysis

In order to study the effects of engine load, the same baseline condition as that described in table 2.2 was once again used. This time the load on the engine was varied from 0% (no load) up to 100% (full load).

Increasing the load on the engine causes an increase in the cylinder pressure throughout the cycle. Figure 4.5 below illustrates the cylinder pressure trace for each load condition analyzed.

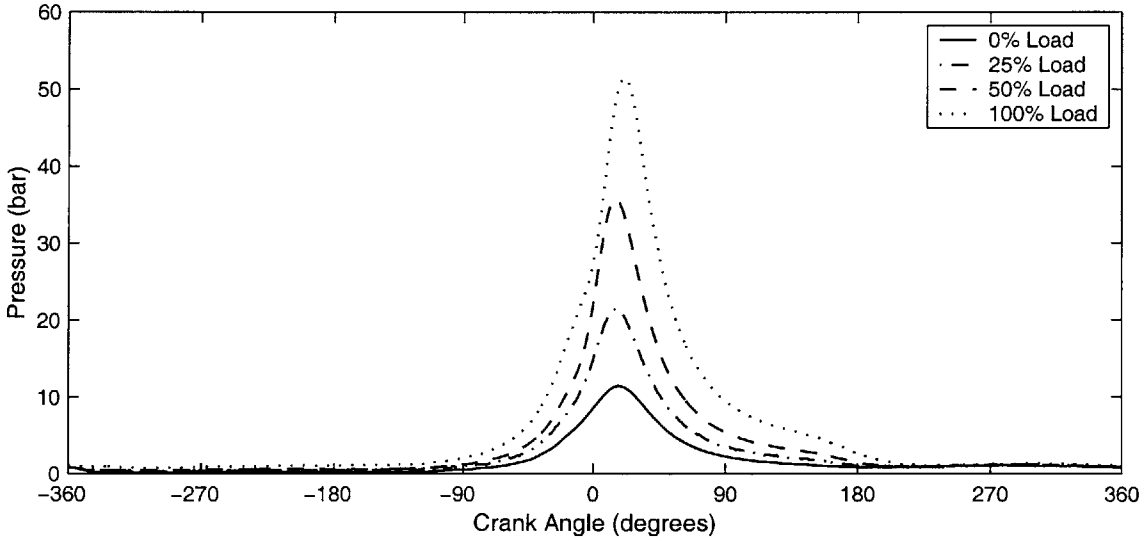

Figure 4.5 Variation of cylinder pressure with engine load

As figure 4.5 shows, the main increases in gas pressure due to higher engine load occur during the compression and combustion strokes of the cycle. Hence, it is only during these cycles that increasing engine load has an effect on the motion of the piston. In general, a higher axial gas pressure force leads to a higher side force imparted on the piston, and this is what affects the secondary motion. The higher side force leads to a greater magnitude of both lateral and angular motion during the compression and combustion cycles. This effect can be seen in figures 4.6 and 4.7, which show the lateral and angular displacements for the region of the cycle around combustion top center.

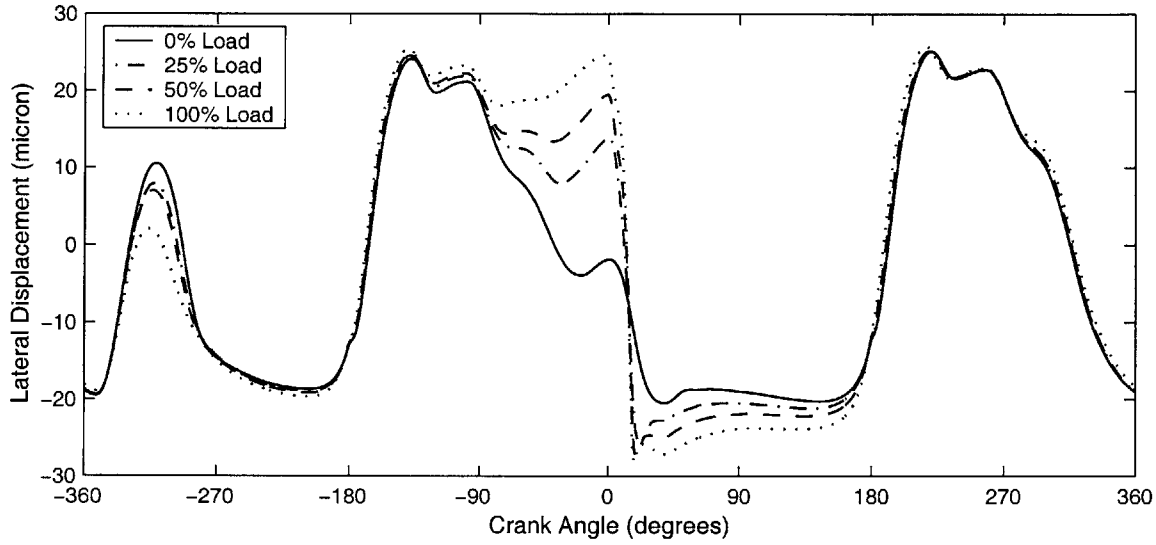

Figure 4.6 Variation of lateral motion with engine load

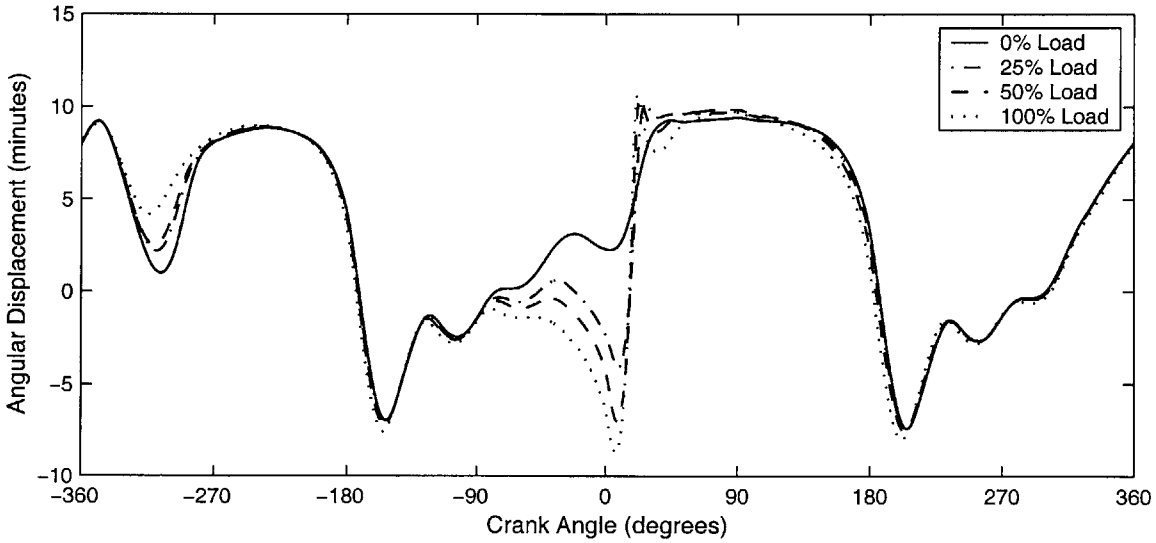

Figure 4.7 Variation of angular motion with engine load

One of the major effects of an increased side force due to higher engine load is a more violent slap motion. With higher load, the magnitude of the side force is much greater at the top center position. When the side force changes direction at this point, the piston is accelerated across the bore and thus the accelerating force will be much higher with an increased engine load. It can be seen from figure 4.6 that with increased engine load the piston is driven closer to the liner wall and also tens to "bounce" more, both laterally and angularly. Figure 4.8 shows the hydrodynamic side forces for both sides of the piston for the period about combustion top center.

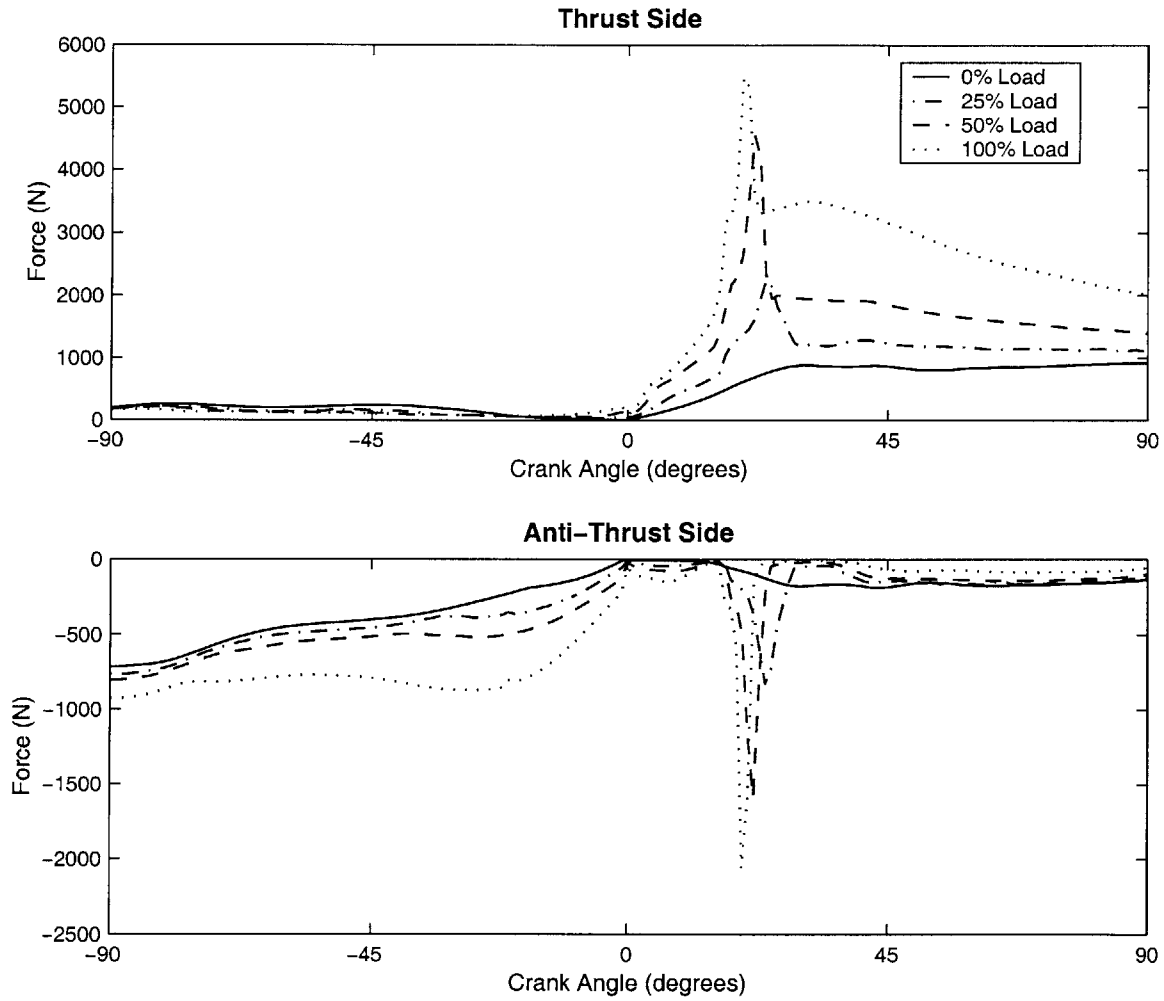

Figure 4.8 Variation of Hydrodynamic side forces with engine load

Figure 4.8 illustrates clearly that increasing the engine load leads to generally higher side forces throughout the top center region, as well as bigger peaks in the force during piston

slap. It can also be seen that the peaks in side force caused by the slapping motion occur earlier with increasing load. This is due to the fact that accelerating side force is greater with increased engine load, and the piston is pushed across the cylinder at a faster rate. Looking at figure 4.7, it can be seen that the piston tilts increasingly more in the negative direction just before top center as the engine load is increased. This is a result of the gas pressure moment acting on the piston due to the pin offset. This moment is directly proportional to the cylinder pressure, and thus is increased greatly as the load goes up. The increased negative tilt also tends to hold the piston further towards the anti-thrust side of the cylinder during this period, as is illustrated in figure 4.6.

4.3 Skirt Clearance Analysis

The radial clearance between the skirt and the liner is a parameter that affects the piston motion greatly. A study of the effects on piston motion of varying the skirt clearance will give valuable insights to the possible effects of skirt deformation, as this deformation also changes the effective skirt clearances during the cycle. To this end the model was run using the same baseline condition as that described in table 2.2, while varying the radial skirt-liner clearance from 5 μm to 50 μm.

Figures 4.9 and 4.10 show the variation in both lateral motion and tilt with the radial clearance. Generally, since increasing the clearance serves to increase the size of the volume in which the piston moves, the motion tends to follow the same patterns but with greater magnitude. Indeed, the driving forces and moments in the system remain unaffected by the clearance, and it is only the geometry that has an effect on the motion. It can be seen in figure 4.9 that with a clearance of 50 μm the piston tends to oscillate markedly during the up strokes. This is a result of the fluctuations in tilt that occur during this period, as seen in figure 4.10. These fluctuations are far more severe for the case with a high clearance, since the piston is free to tilt further. Once the fluctuations reach such a high magnitude, they tend to have a greater effect on the lateral motion.

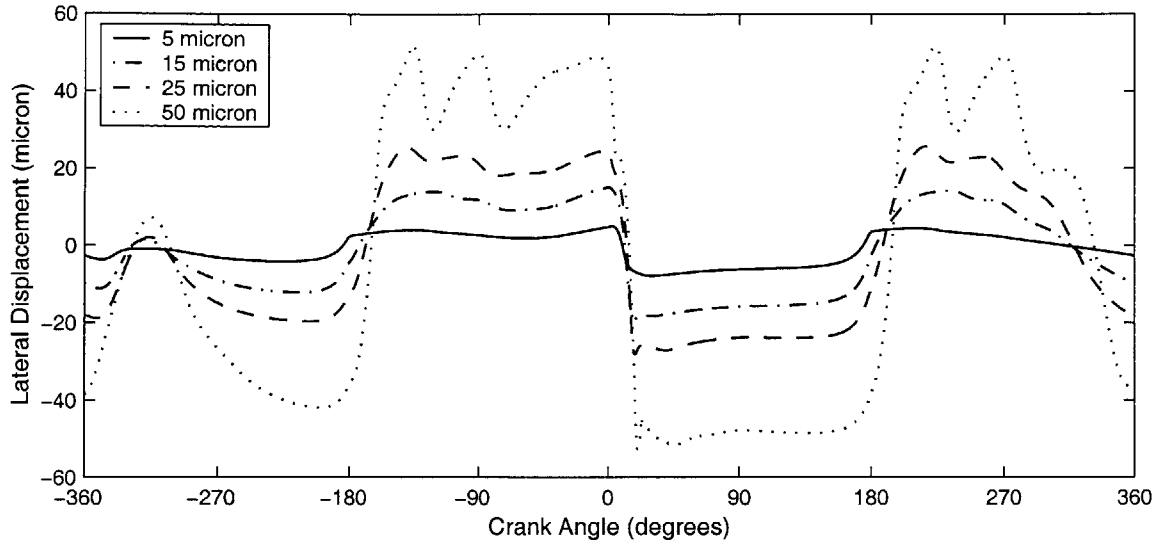

Figure 4.9 Variation of lateral motion with skirt clearance

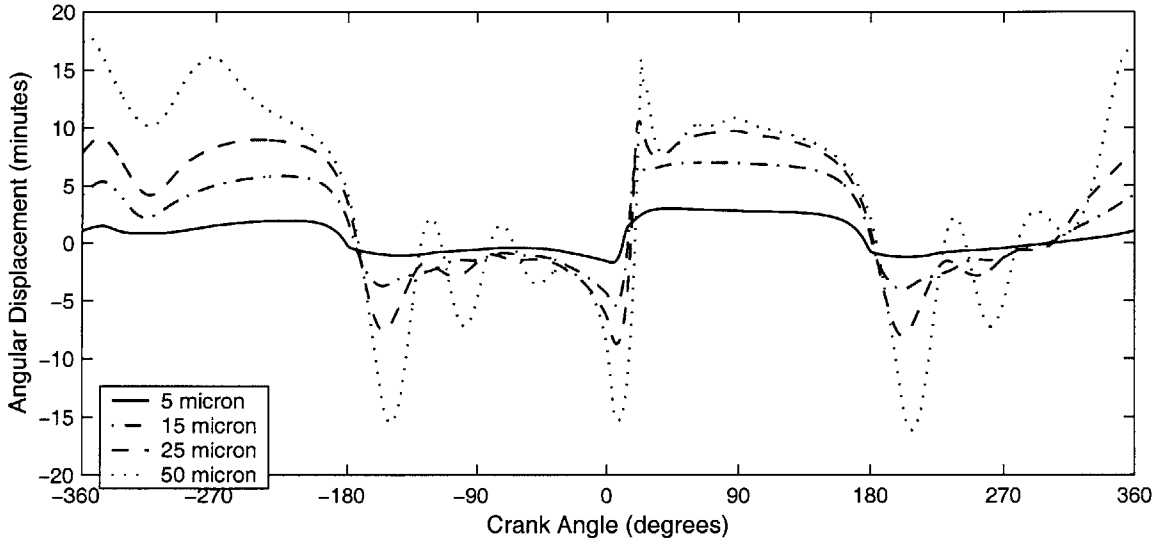

Figure 4.10 Variation of angular motion with skirt clearance

Reducing the skirt-liner clearance also leads to significantly higher pressures in the oil film. This increase in hydrodynamic pressure is mainly attributable to the sliding effect, as defined by the Reynolds equation (3.1). The sliding pressure increases greatly in inverse proportion to the separation. This can clearly be seen in figure 4.11 which shows the variation in hydrodynamic forces for both sides of the piston with skirt-liner clearance.

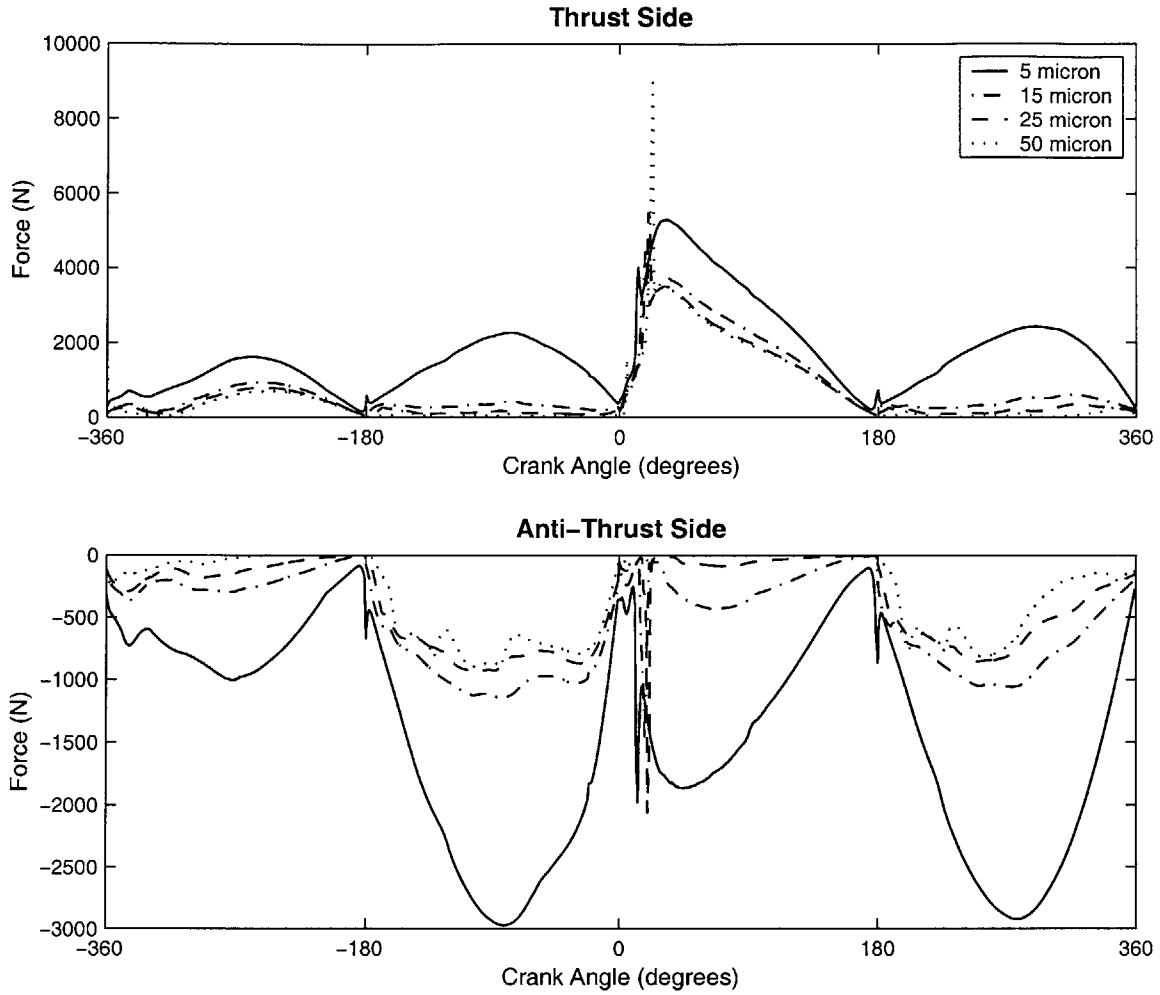

Figure 4.11 Variation of hydrodynamic forces with skirt-liner clearance

It is this increased hydrodynamic force, coupled with the more constrained geometry, that tends to restrict the piston motion when the clearances are small. Figure 4.10 also illustrates the fact that the slap motion is considerably more violent with a larger clearance. The peaks in hydrodynamic force are greater during the slap region for the cases with higher clearances.

4.4 Skirt Profile Analysis

As mentioned in previous chapters, the profile of the skirt surface has a very great influence over the motion of the piston. Indeed, it is through careful control of the effective running profile of the skirt that both piston secondary motion and friction are minimized. In general the piston skirt is machined with a barrel shape, where the point of minimum skirt-liner clearance is located *below* the level of the wrist pin axis, and in the center of a 'flat' region on the profile. A typical profile shape can be seen in figure 4.12 below (note that the scale of the skirt profile has been greatly exaggerated)

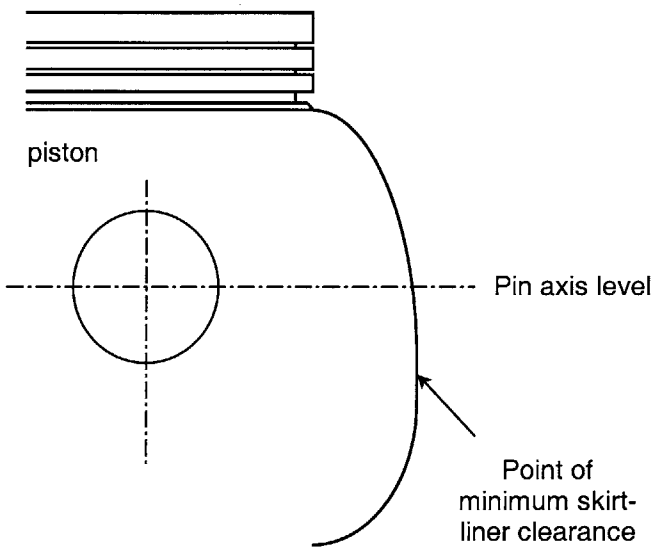

Figure 4.12 A typical skirt profile shape

Giving the profile a flat section about the minimum point tends to render the piston more 'stiff' for angular motion. In other words this flat region makes the piston more resistant to angular displacement and keeps it more vertical in the bore. This helps to limit the amount of secondary motion that the piston experiences during the cycle, both lateral *and* angular. Locating the minimum point at a level below the pin axis leads to a hydrodynamic moment being induced on the pisotn due to the side force, as described earlier in figure 2.17. This hydrodynaic moment has the effect of holding the piston in a particular orientation for periods of the stroke and hence limits the amount of secondary motion. In order to attain a better understanding of the specific effects of the skirt profile

on piston motion, a couple of alternative profiles were generated and used as input for the current model. The same baseline conditions as those detailed in table 2.2 were once again used. The new skirt profiles used can be described as follows ;

(i) ***Parabolic*** A profile with the minimum point located in exactly the same position as the original profile, but with no flat region. Instead the profile is perfectly parabolic on either side of the minimum point.

(ii) ***Shifted*** Another parabolic profile, but this one has the minimum point shifted up to the level of the wrist pin axis.

Both of these profiles can be seen, along with the original, in figure 4.13 below.

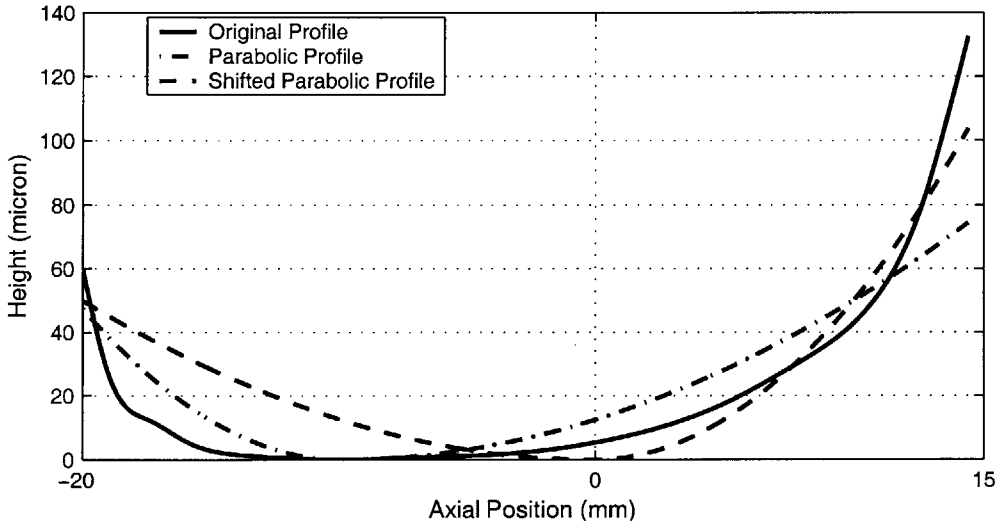

Figure 4.13 Skirt profiles used for parametric analysis

The main effect of using the parabolic profile is that the skirt, with it's more rounded shape, is less 'stiff' for angular motion. This allows for much freer motion of the piston, both laterally angularly. Figures 4.14 and 4.15 show the lateral and angular motion of the piston for each of the skirt profiles analyzed. It can clearly be seen that the parabolic profile leads to a greater magnitude of both lateral and angular motion. It should be noted that the driving forces are exactly the same for each case analyzed, so the differences in motion are due solely to the specific profiles used. The larger amplitude of angular motion for the parabolic profile seen in figure 4.15 is due to the lower resistance to tilt caused by removing the flat region around the minimum point. This increase in

magnitude of the angular motion leads to a corresponding increase in magnitude of the lateral motion, illustrated in figure 4.14.

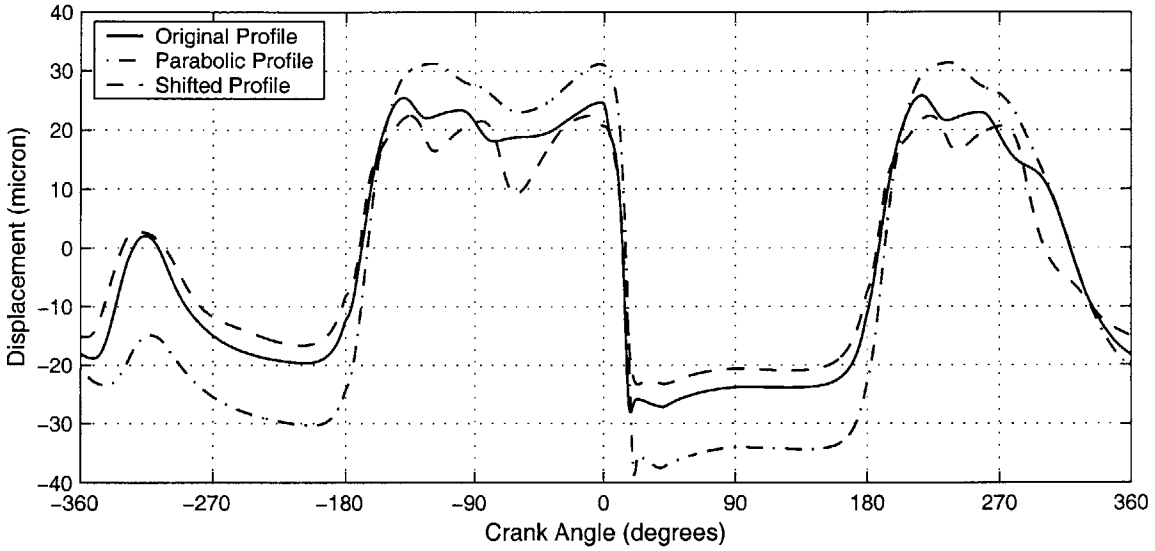

Figure 4.14 Lateral displacement of the piston for various skirt profiles

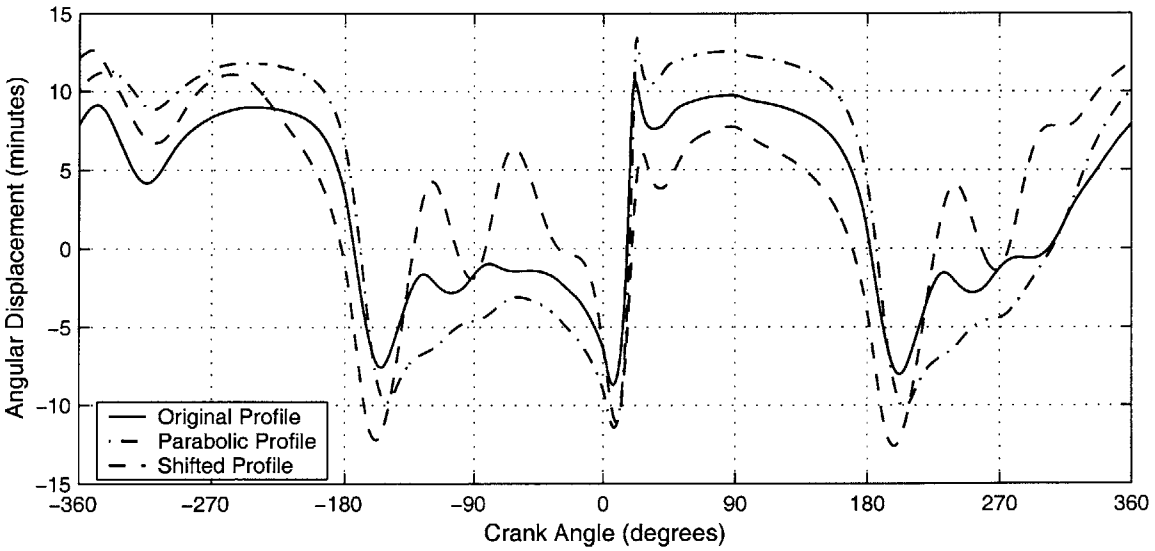

Figure 4.15 Angular displacement of the piston for various skirt profiles

It should also be noted from figure 4.15 that there are less fluctuations in the tilt during the up stroke for the parabolic profile that the original profile. This is again due to the removal of the flat region around the minimum point. Withoun the flat region, the piston tends to be more stable when it has a neutral tilt, and does not oscillate in the same way

as the original profile. This stability can also be seen in figure 4.16, which depicts the location of the minimum point in the oil film between the skirt and liner.

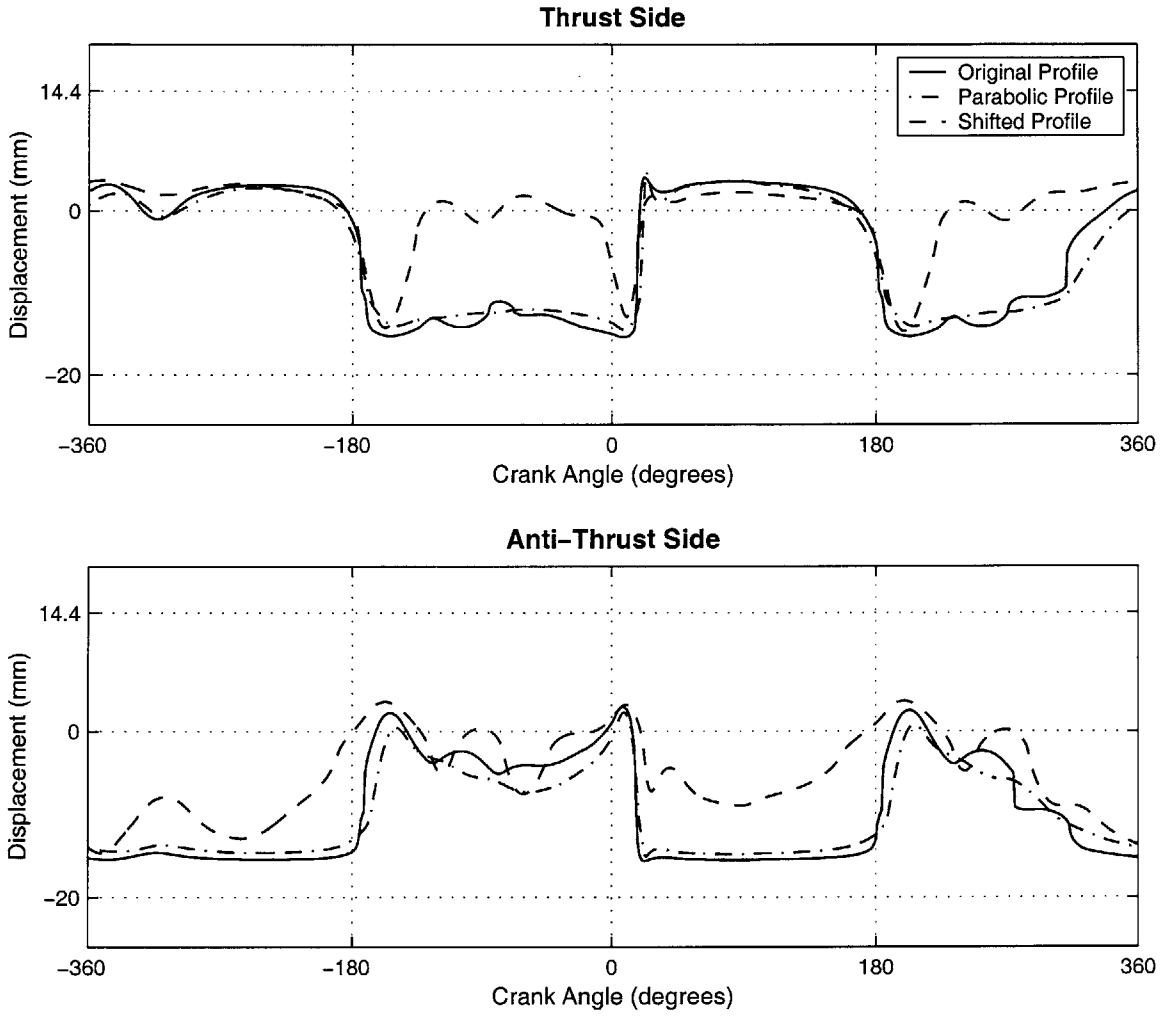

Figure 4.16 Location of the minimum point for various skirt profiles

The minimum point for the original profile tends to fluctuate greatly about the flat region on the profile. This is due to the piston 'rolling' about the section, which causes the minimum point to move quickly across the flat region. This phenomenon is clearly absent in the case of the parabolic profile, as the profile is much smoother about the minimum point.

When the minimum point is shifted up to the level of the wrist pin axis, there is no longer a significant hydrodynamic moment generated by the side force, and hence the angular

motion of the piston tends to fluctuate much more widely about the vertical. This can clearly be seen in figure 4.15. While the fluctuations in tilt are more severe in this case, the overall magnitude of the motion is lower that the other two cases due to the absence of the significant driving moments. Both the lateral and angular motion induced by piston slap are less severe for the shifted profile, once again due to the fact that there is a smaller hydrodynamic moment acting on the piston through top center. It can be seen from figure 4.16 that the minimum point for the shifted profile stays much closer to the pin axis level throughout the cycle, and also tends to fluctuate to a greater amplitude about this point.

4.5 Crankshaft Offset Analysis

Offsetting the center of the crankshaft towards the thrust side of the cylinder has been shown to both improve thermodynamic efficiency and reduce the piston side force and hence piston friction. Several studies have been conducted investigating the effects of crankshaft offset on various engine operating parameters. It was decided to perform an analysis using the current secondary motion model to investigate the specific effects of crankshaft offset on piston motion.

Figure 4.17 below shows the geometry of an engine with an offset crankshaft.

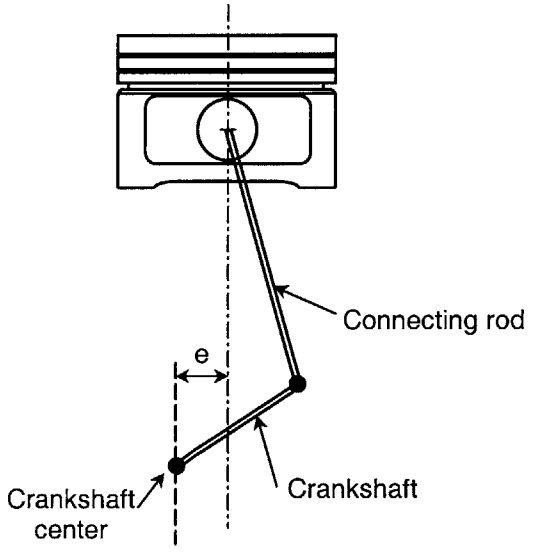

Figure 4.17 Engine geometry for crankshaft offset

The crankshaft offset is offset from the center line of the cylinder bore towards the thrust side by the distance 'e' (see figure 4.17). Such an offset of the crankshaft has two main effects on the performance of the system. Firstly, the duration of the expansion stroke is increased. This is what leads to an increase in the thermodynamic efficiency, as the amount of power extracted from the combustion gases is increased. Secondly, the peak side force on the piston is reduced, which lessens the severity of the piston slap and also reduces the peak sliding friction.

When the crankshaft is offset towards the thrust side of the cylinder, the tilt angle of the connecting rod is shifted to become more negative throughout the cycle. Figure 4.18 below illustrates the variation in connecting rod tilt angle with crankshaft offset.

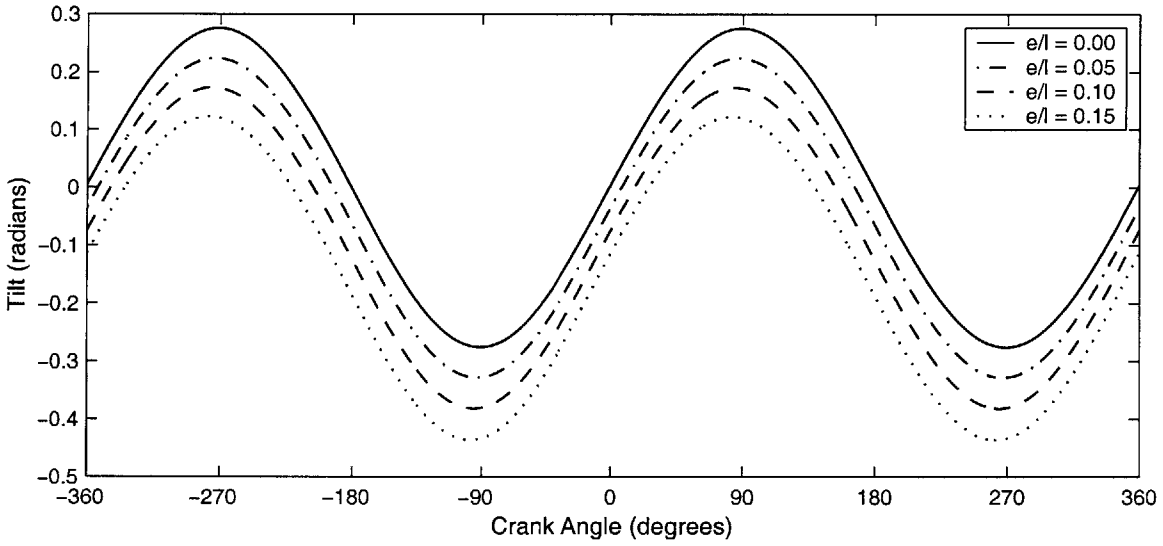

Figure 4.18 Variation in connecting rod angle with crankshaft offset

It can also be noticed that the transition in sign of the con rod angle occurs at differing times witht eh introduction of crankshaft offset. The transition occurs *later* after top center and *earlier* before bottom center. The change in the connecting rod tilt angle with crankshaft offset has a marked effect on the side force profile imparted on the piston. The variation in side force with crankshaft offset can be seen in figure 4.19.

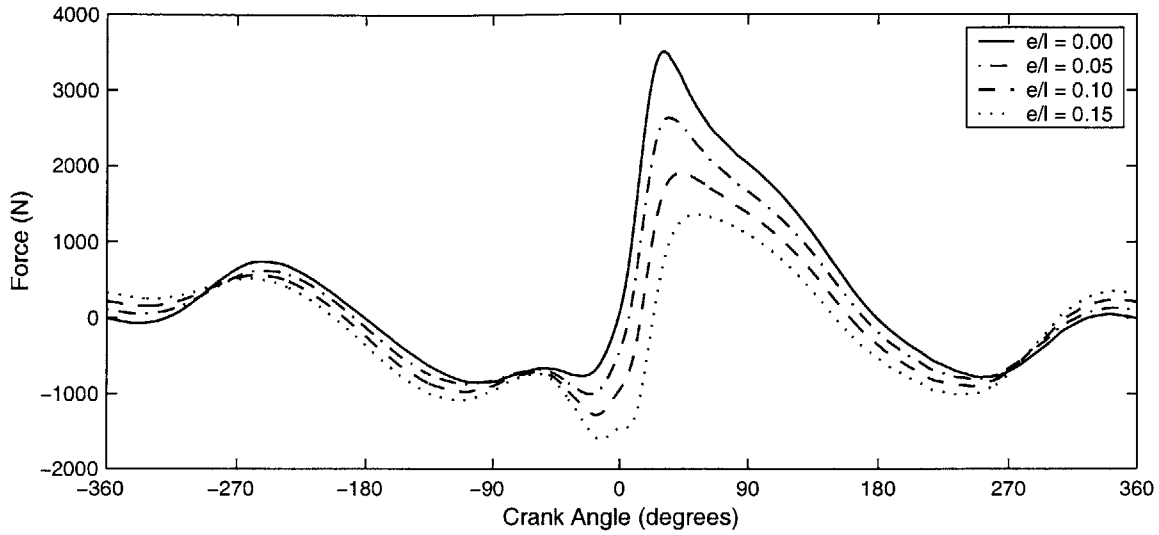

Figure 4.19 Variation in side force with crankshaft offset

The magnitude of the side force is slightly increased at the beginning of each up stroke, due to the fact that the connecting rod has a larger tilt during these periods. However, the side force is greatly reduced in the region after top center because of the smaller tilt angle of the rod. This reduction in peak side force is the greatest benefit of offsetting the crankshaft. It can also be noticed that the peak side force occurs later with increasing crankshaft offset. The impact of varing the side force on the piston motion can be seen in figures 4.20 and 4.21, which show the variation in both lateral and angular motion of the piston with crankshaft offset.

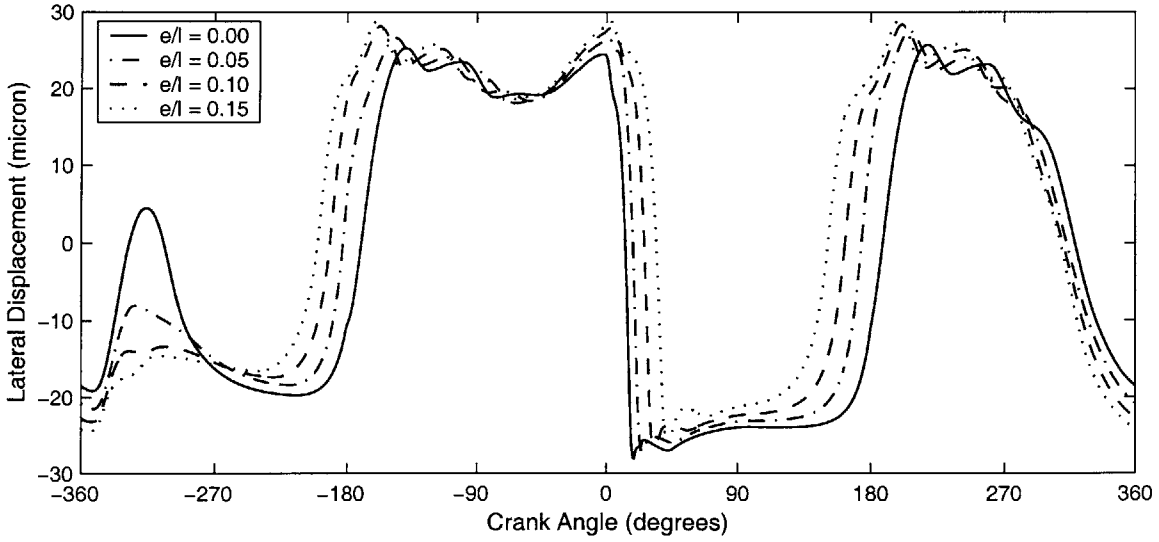

Figure 4.20 Variation in lateral motion of the piston with crankshaft offset

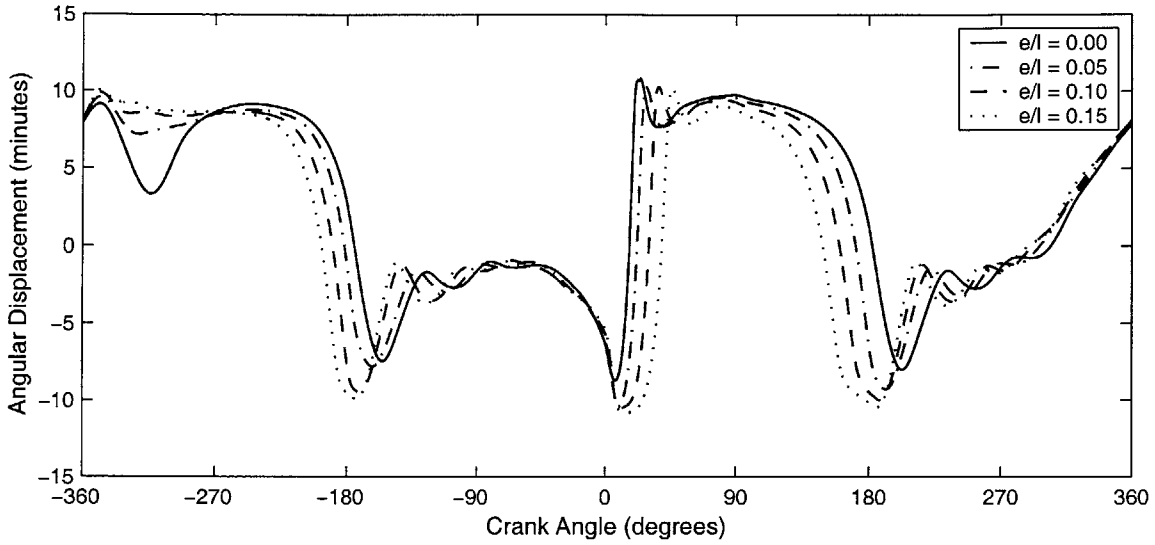

Figure 4.21 Variation in angular motion of the piston with crankshaft offset

Increasing the crankshaft offset doesn't affect the magnitude of the piston motion greatly for most of the cycle. The major effect is in delaying or retarding the times at which the piston transitions from one side of the cylinder to the other and from one tilt orientation to the other. These time shifts are clearly as a result of the change of the instant at which the connecting rod angle changes sign. The most important effect of the crankshaft offset, however, occurs during the period of slap. Since the peak force is both reduced in magnitude and delayed with increasing offset, the severity of the slap motion is greatly reduced.

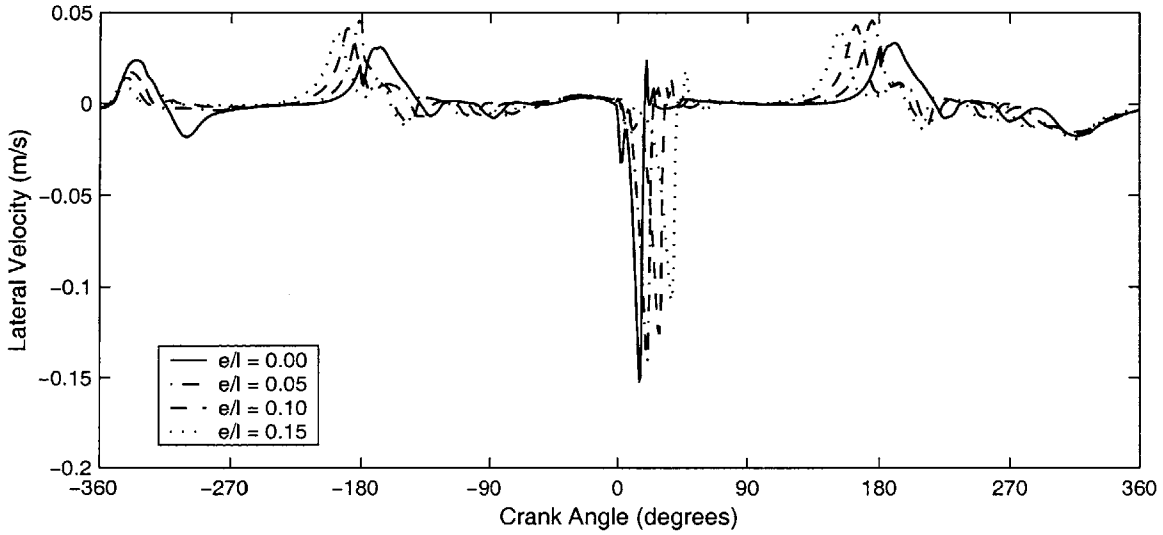

Figure 4.22 Variation in lateral piston velocity with crankshaft offset

This reduction in severity of slap is perhaps best illustrated in figure 4.22 which shows the variation in piston velocity with crankshaft offset. The energy transferred from the piston to the liner wall during piston slap is proportional to it's kinetic energy, which is obviously dependant on the velocity on impact. Figure 4.22 clearly illustrates that increasing the amount of crankshaft offset serves to reduce the peak piston velocity during slap as well as delaying the instant of the slap.

Chapter 5

Summary and Conclusions

5.1 Summary

First generation models were formulated and coded for both mono and articulated piston assemblies. These first generation models sought to include the effects of all the major physical phenomena in the piston system. The equations of motion were formulated and solved independently for each component in the system, using some relevant simplifying assumptions. The hydrodynamic forces were modeled using a pseudo-two dimensional technique where the Reynolds equation was solved along several axial lines on the piston. The first generation models are able to predict the complete motion of the piston along with the axial hydrodynamic friction. Each model was tested for a specific engine configuration and the results were presented and discussed in detail.

The results from the first generation models were used to gain valuable insights into the nature of secondary motion, and the main driving forces responsible for this motion. Crucial areas of each model were identified for further development. Elastic deformation of the skirt was deemed to be the most important improvement needed in each model in order to produce more meaningful results. To this end, a more detailed hydrodynamic model was developed, initially for the mono piston model, which was capable of solving the wetting condition on the skirt and producing a full pressure distribution for the entire skirt. This new hydrodynamic code was incorporated into the existing mono piston model and results were generated and compared to those attained with the original hydrodynamic calculation. Furthermore, the new version of the mono piston model was used to perform a series of parametric studies for a baseline engine condition.

5.2 Conclusions

The results from the first generation mono piston model illustrate that the major driving factors for secondary motion are the side force from the connecting rod and skirt profile. The side force is modeled quite accurately, and is shown to be influenced by both piston pin offset and crankshaft offset. The hydrodynamic forces that balance the driving side force are shown to be very sensitive to the skirt profile, and can alter the piston motion greatly. The specific skirt profile dictates how the hydrodynamic forces and moments generated in the oil film will react to the driving forces, and how these forces and moments will be distributed on the skirt surface. The importance of the skirt profile in affecting the results indicates that elastic deformation of the skirt will have a major impact on the motion of the system, and that a model of this deformation must be included if more accurate results are required.

The results for the first generation articulated model show that the skirt motion in this system is influenced in a similar way to the piston in the mono piston configuration. The motion of the crown is shown to be mainly driven by the shear torque from the wrist pin and retarded by the lateral friction from the piston rings (especially during periods of high cylinder pressure). Since these forces are so critical to the motion of the crown, a more detailed analysis and more in depth models of each are required in order to have more faith in the results.

In developing the improved hydrodynamic model, the importance of the squeezing component of the hydrodynamic pressure was illustrated. This squeezing component of the pressure has a far greater magnitude in skirt lubrication than in ring lubrication, and leads to great difficulties in applying the standard Reynolds exit condition. While it is extremely valuable to have a hydrodynamic model that computes the specific wetting locations on the skirt, it was shown that such a model is extremely difficult to implement in practice. Using a hybrid form of the new and old hydrodynamic models in the code illustrated the advantages of direct computation of the wetting locations. The size of the wetted region was shown to have a major impact on the motion of the piston.

References

[1] Wong, V.W., Tian, T., Lang, H., Ryan, J.P., Sekia, Y., Kobayashi and Y., Aoyama, S., 1994, "A Numerical Model of Piston Secondary Motion and Piston Slap in Partially Flooded Elastohydrodynamic Skirt Lubrication," SAE Paper 940696.

[2] Nakashima, K., Yajima, Y. and Suzuki, K., 1999, "Approach to Minimization of Piston Slap Force for Noise Reduction – Investigation of Piston Slap Force by Numerical Simulation," JSAE Paper 9930720.

[3] Nakayama, K., Yasutake, Y., Takiguchi M and, Furahama, S., 1997, "Effects of Piston Motion on Piston Skirt Friction of a Gasoline Engine," SAE Paper 970839.

[4] Ungar, E.E. and Ross, D., "Vibration and Noise Due to Piston-Slap in Reciprocating Machinery," Journal of Sound Vibration 2(2), 132, pp. 132-146 (1965).

[5] Griffiths, W.J. and Skorecki, J.,"Some Aspects of Vibration on a Single Cylinder Diesel Engine," Journal of Sound Vibration, Vol. 1, No. 4, pp 345-364 (1964).

[6] Li, D.F., Rohde, S.M. and Ezzat, H.A., "An Automotive Piston Lubrication Model," ASLE Transactions, Volume 26, 2, 151-160 (1982).

[7] Knoll, G. D. and Peeken, H.J., "Hydrodynamic Lubrication of Piston Skirts," ASME Journal of Lubrication Technology, Vol. 104 October 1982.

[8] Oh, K.P., Li, C. H. and Goenka, P.K., "Elastohydrodynamic Lubrication of Piston Skirts," ASME Journal of Tribology, Vol. 109 April 1987.

[9] Zhu, D., Cheng, H, Arai, T. and Hamai, K, "A Numerical Analysis for Piston Skirts in Mixed Lubrication – Part I : Basic Modeling," ASME Journal of Tribology (1991).

[10] Zhu, D., Hu, Y-Z., Cheng, H, Arai, T. and Hamai, K, "A Numerical Analysis for Piston Skirts in Mixed Lubrication – Part II : Deformation Considerations," ASME Journal of Tribology (1991).

[11] Wong, V.W., Tian, T., Lang, H., Ryan, J.P., Sekiya, Y., Kobayashi, Y. and Aoyama, S., "A Numerical Model of Piston Secondary Motion and Piston Slap in Partially Flooded Elastohydrodynamic Skirt Lubrication," SAE paper 940696 (1994).

[12] Ryan, J.P., Wong, V.W., Tian, T., Lyon, R.H., Hoult, D.P., Sekiya, Y., Kobayashi, Y. and Aoyama, S., " Engine Experiments on the Effects of Design and Operational Parameters on Piston Secondary Motion and Piston Slap," SAE paper 940695 (1994).

[13] Dursunkaya, Z, and Keribar, R., "Simulation of Secondary Dynamics of Articulated and Conventional Piston Assemblies," SAE paper 920484 (1992).

[14] Dursunkaya, Z, and Keribar, R., "A Comprehensive Model of Piston Skirt Lubrication," SAE paper 920483 (1992).

[15] Tian, T., Noordzij, L., Wong, V. and Heywood, J., "Modeling Piston-Ring Dynamics, Blowby and Ring-Twist Effects," ICE-Vol. 27-2, 1996 Fall Technical Conference, Volume 2. ASME.

[16] Tadahiro, S., Shinji, A., Masaaki, T, Shoichi, T., "Reduction of Friction for Piston Pin Boss Bearing of Automotive Gasoline Engine by Utilizing Oil Around the Boss", ASME ICE-Vol.30-2, No. 98-ICE-101 (1998).

[17] Press, W., Teukolsky, S., Vetterling, W. and Flannery, B., *Numerical Recipes in C* , Cambridge University Press, second edition (1997).

[18] Tian, T., "Modeling the Performance of the Piston Ring-Pack in Internal Combustion Engines," Doctoral Thesis submitted to the Mechanical Engineering Department, Massachusetts Institute of Technology, (1997).

[19] Dowson, D., and Taylor, C.M., "Cavitation in Bearings," *Ann. Rev. Fluid Mechanics 1979*, pp. 35-66.

Appendix A

Nomenclature

1. Kinetic Variables

The motion of the components in the model is generally described by the following variables ;

ε	-	lateral displacement of the component or point from the bore centerline.
ϕ	-	angular displacement of the component's central axis from vertical.
γ	-	axial displacement of the component or point from the *nominal wrist pin position* (i.e. the position that the wrist pin would be in if there were no secondary motion).

Subscripts

c	-	refers to motion of the crown
s	-	refers to motion of the skirt (articulated) or piston (mono)
p	-	refers to motion of the wrist pin
r	-	refers to motion of the connecting rod
cm	-	refers to motion of the mass center of the component in question
b	-	refers to motion of the big end center of the connecting rod

The first time derivative of each kinetic variable is denoted by a single dot above the variable, e.g. $\dot{\varepsilon}$ refers to the 1st time derivative of ε. Similarly, the second time derivative is denoted by two dots above the variable, e.g. $\ddot{\varepsilon}$ refers to the second time derivative of ε.

The primary acceleration of the assembly in the axial direction is denoted by a_p.

2. Forces and Moments

In general, the forces and moments are represented as follows ;

F - refers to a *force*

M - refers to a *moment*

τ - refers to a *shear torque*

All moments and shear torques are *about the wrist pin axis.*

The following is a list of the *external* forces and moments acting on the system ;

F_p - gas pressure force in the axial direction

F_{CL} - crown-liner hydrodynamic force

F_{SL} - skirt-liner hydrodynamic force

F_{cq} - axial ring friction force acting on piston or crown

F_{cr} - lateral ring friction force acting on piston or crown

F_f - axial friction force due to skirt-liner hydrodynamics

M_p - moment due to gas pressure force

M_{CL} - crown-liner hydrodynamic moment

M_{SL} - skirt-liner hydrodynamic moment

M_{cq} - moment due to axial ring friction force

M_{cr} - moment due to lateral ring friction force

M_f - moment due to skirt-liner hydrodynamic friction force

The inter component reaction forces and shear torques all follow the same naming convention. The first subscript refers to the component on which the force/torque is acting. The second subscript refers to the component from which the force/torque originates. The third component (for reaction forces only) refers to the plane in which the force acts. For example ;

F_{rpx} - refers to the component of the reaction force exerted by the wrist pin on the connecting rod in the *x-direction.*

τ_{cp} - refers to the shear torque exerted by the pin on the crown.

3. System Properties

The following variables represent the geometric, mass and moment of inertia properties of the system ;

l_c - distance between the center of mass and the pin bearing center for the crown.

ϕ_{co} - offset angle of the center of mass from the central axis of the crown.

l_s - distance between the center of mass and the pin bearing center for the skirt (articulated) or piston (mono).

ϕ_{so} - offset angle of the center of mass from the central axis of the skirt (articulated) or piston (mono).

l_r - distance between the center of mass and the pin bearing center for the connecting rod.

ϕ_{ro} - offset angle of the line joining the big end bearing center of the rod to the center of mass and the rod's central axis.

ϕ_{rc} - offset angle of the line joining the small end bearing center of the rod to the center of mass and the rod's central axis.

l_r - distance between the pin axis center and the big end bearing center of the connecting rod.

l_{pc} - distance between the pin axis center and the center of mass of the connecting rod.

l_{cb} - distance between the center of mass and the big end bearing center of the connecting rod.

m_c - mass of the crown

m_s - mass of the skirt (articulated) or piston (mono)

m_p - mass of the wrist pin

m_r - mass of the connecting rod

I_c - moment of inertia of the crown about the pin axis center

I_s - moment of inertia of the skirt/piston about the pin axis center

I_p - moment of inertia of the wrist pin about it's center

I_r - moment of inertia of the connecting rod about the pin axis center

Appendix B

Analysis of "Sliding" Hydrodynamics

The sliding component of the Reynolds equation can be written as follows,

$$\frac{\partial}{\partial x}\left(h^3 \frac{\partial p_{sl}}{\partial x} \right) = 6\mu U \frac{\partial h}{\partial x} \tag{B.1}$$

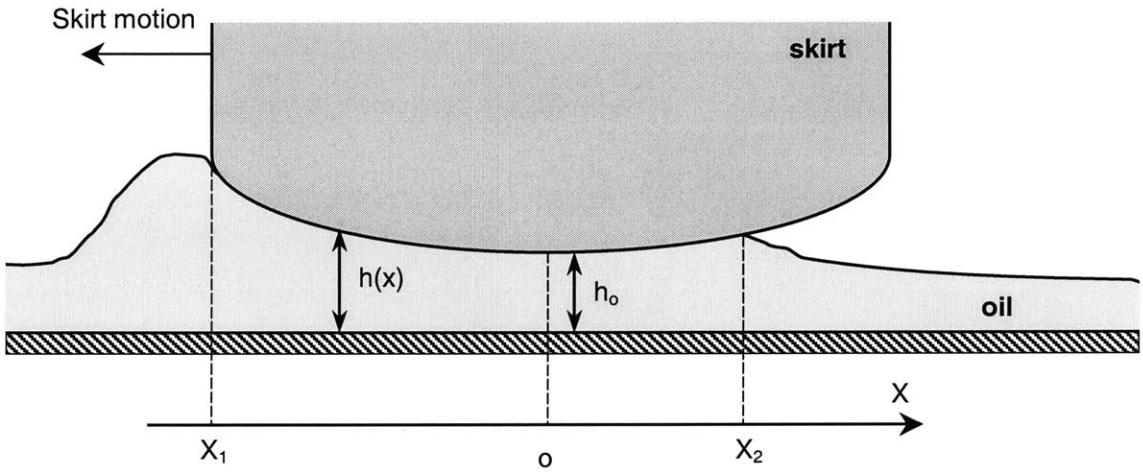

Figure B.1 Sketch of skirt lubrication during "sliding"

In order to derive the necessary correlations it will be assumed that the leading edge of the skirt is fully flooded. The pressure boundary conditions for the oil film are

$$p(x_1) = p_1 \tag{B.2}$$

$$p(x_2) = p_2 \tag{B.3}$$

The Reynolds exit condition is assumed to apply at the trailing edge, i.e.

$$\frac{dp}{dx}(x_2) = 0 \tag{B.4}$$

The skirt is assumed to have a parabolic profile defined by

$$h(x) = h_o + x^2 / 2a \tag{B.5}$$

In order to obtain the minimum oil film thickness (h_o) and the exit wetting condition (x_2), the sliding part of the Reynolds equation (B.1) is integrated, applying both the boundary conditions and a load condition. After some manipulation, the following results are obtained

$$\int_{x1}^{x2} \frac{h(x)-h(x_2)}{h^3(x)}dx = 0 \tag{B.6}$$

$$6\mu U \int_{x1}^{x2} \frac{(x-x_1)[h(x)-h(x_2)]}{h^3(x)}dx + W = 0 \tag{B.7}$$

Now, let

$$x = \bar{x}B$$

and

$$h_o = \overline{h_o}(B^2/2a)$$

Therefore,

$$h(x) = \frac{B^2}{2a}\bar{h}(x) \tag{B.8}$$

where,

$$\bar{h}(x) = \overline{h_o} + \bar{x}^2 \tag{B.9}$$

For the non-dimensionalized quantities $\overline{h_o}$ and $\overline{x_2}$, we have

$$\int_{\bar{x}1}^{\bar{x}2} \frac{[\bar{h}(\bar{x})-\bar{h}(\bar{x}_2)]}{\bar{h}^3(\bar{x})}d\bar{x} = 0 \tag{B.10}$$

$$\int_{\bar{x}1}^{\bar{x}2} \frac{(\bar{x}-\bar{x}_1)[\bar{h}(\bar{x})-\bar{h}(\bar{x}_2)]}{\bar{h}^3(\bar{x})}d\bar{x} + \frac{W}{6\mu U}\left(\frac{B}{2a}\right)^2 = 0 \tag{B.11}$$

From equations B.10 and B.11, we can derive the following generalized expressions for the non-dimensional values of the minimum film thickness and the exit location,

$$\overline{h_o} = H\left[\frac{\mu U}{W}\left(\frac{2a}{B}\right)^2\right]$$

$$\overline{x_2} = X\left[\frac{\mu U}{W}\left(\frac{2a}{B}\right)^2\right]$$

The shear stress on the piston skirt can be derived as follows,

$$\mu \left.\frac{\partial u}{\partial y}\right|_{y=h(x)} = -\frac{\mu U}{h} + \frac{dp}{dx}\frac{h}{2} = \frac{\mu U[2h(x) - 3h(x_2)]}{h^2(x)} \tag{B.12}$$

Integrating this expression for the shear stress yields the following expression for the friction coefficient, f

$$f = \frac{\int_{x1}^{x2} \mu \left.\frac{\partial u}{\partial y}\right|_{y=h(x)} dx}{W} = \frac{\mu U}{W}\frac{2a}{B}\int_{\bar{x}1}^{\bar{x}2} \frac{[2\bar{h}(\bar{x}) - 3\bar{h}(\bar{x}_2)]}{\bar{h}^2(\bar{x})} d\bar{x} \tag{B.13}$$

From this the following generalized expression for the friction coefficient can be derived,

$$f = \frac{\mu U / W}{B / 2a} F\left[\frac{\mu U}{W}\left(\frac{2a}{B}\right)^2\right] \tag{B.14}$$

Equations B.10, B.11 and B14 are difficult to solve analytically. Hence, a numerical method was used to find solutions that would satisfy these equations, and a correlation was then used to derive the following power laws

$$\bar{h}_o = 0.25\left[\frac{\mu U}{W}\left(\frac{2a}{B}\right)^2\right]^{0.528} \tag{B.15}$$

$$\bar{x}_2 = 0.178\left[\frac{\mu U}{W}\left(\frac{2a}{B}\right)^2\right]^{0.162} \tag{B.16}$$

$$f = 2.05\left[\frac{\left(\frac{\mu U}{W}\right)^{0.68}}{\left(\frac{B}{2a}\right)^2}\right] \tag{B.17}$$

Equation B.15 can be used to express the load, W in terms of the minimum film thickness, sliding speed, viscosity and skirt geometry. Equation B.17 can be used to express the friction coefficient in terms of the normal load, sliding speed, viscosity and skirt geometry.